Generation and Characterisation of Nanostructures from Single Adsorbed Polyelectrolyte Molecules

DISSERTATION

zur Erlangung des akademischen Grades

Doktor rerum naturalium
(Dr. rer. nat.)

vorgelegt

der Fakultät Mathematik und Naturwissenschaften
der Technischen Universität Dresden

von

Ganna Gorodyska

geboren am 7.03.1977 in Kiew, Ukraine

Gutachter: Prof. Dr. M. Stamm

Prof. Dr. H.-J. Adler

Prof. Dr. J.P. Rabe

Eingereicht am: 13.12.04

Tag der Verteidigung: 09.09.05

Table of Contents

List of Abbreviations and Symbols

Latin letters

a	monomer length
a_k	length of statistical segment
A	amplitude
AFM	Atomic Force Microscopy
b	average distance between two charged groups along the chain
c_0	salt concentration for vanishing potential
c^*	critical concentration of coil overlapping
CGT	coil-to-globule transition
cmc	Critical micelle concentration
d	cantilever thickness
d_{bead}	size of beads in a necklace globule
D	translational diffusion coefficient
D	width
DCM	dichloromethane
DH	Debey-Hückel
DMAB	Dimethylamine borane
DNA	deoxyribonucleic acid
DLS	Dynamic Light Scattering
DRO	Dobrynin, Rubinstein and Öbuhov theory
DVB	Divinylbenzene linkage
e	elementary charge
f	fraction of charged monomers
F	force applied to cantilever
FJC	freely jointed chain
FRC	freely rotating chain
g	scattering vector
$g^{(2)}(t)$	correlation function of scattering intensity
$g^{(1)}(t)$	correlation function of electric field
h	height
HCF	Hexacyanoferrate
I	ionic strength
I	scattering intensity
<I>	average value of the intensity
IC	intermittent contact
IEP	iso-electric point
k	spring constant of cantilever [N/m]
k_B	the Boltzmann's constant $k_B = 1.38065 \cdot 10^{-23}$ J/K
l_C	contour length
$l_{p,0}$	persistence length
$l_{p,eff}$	effective persistence length
$l_{p,OSF}$	electrostatic persistence length
l_{str}	length of strings in a necklace globule
L	length
L_n	number average molecular length
L_w	weight average molecular length

LS	Light Scattering
M	molecular mass of polymer chain
M_i	molar mass of species i
M_n	number average molecular mass
M_w	weight average molecular mass
n	refractive index
N	degree of polymerization
N	number of segments of a chain
N_A	Avogadro's number
N_{bead}	number of beads in a necklace globule
N_i	number concentration of species i
P2VP	Poly(2-vinylpyridine)
P2VP-co-PS	Poly(2-vinylpyridine-co-styrene), random copolymer
PA	Palladium acetate
PB	Poisson-Boltzmann
PB	Prussian Blue clusters
PC	polycation
PDI	polydispersity index
PE(s)	polyelectrolyte(s)
PMB	Poly(methacryloyloxyethyl dimethylbenzylammonium chloride)
PS	Polystyrene
PS_7-$P2VP_7$	Polystyrene/poly(2-vinylpyridine) heteroarm star copolymer
r	radius of the particle
r_i	distance of i monomer from the center of mass of the chain
R	tip radius
R	end-to-end distance
R_g	radius of gyration
R_h	hydrodynamic radius
R_F	Flory radius
RMS	root-mean-square amplitude of cantilever oscillation
RMS	root-mean-square roughness of the surface
S	center of mass of the chain
SEM	Scanning Electron Microscopy
SPM	Scanning Probe Microscopy
STM	Scanning Tunneling Microscopy
t	time
T	temperature in Kelvin
THF	Tetrahydrofuran
TM	Tapping Mode
V	volume
V_r	molar volume
W	width
WLC	worm-like chain model
XPS	X-ray Photoelectron Spectroscopy
z	cantilever deflection
Z	cantilever-base displacement
Z	total number of charged groups of the chain

Greek letters

α	expansion coefficient of a coil
β	coherence factor
δ	solubility parameter
Δ	difference (f. eg. $\Delta x = x2 - x1$)
ε	dielectric constant of the solution
η_0	viscosity of solvent
Θ	unperturbed state
θ	scattering angle
λ	Gouy-Chapman length
λ_0	laser wavelength in vacuum (HeNe laser, 632,8 nm)
λ_B	Bjerrum length
λ_D	Debey-Hückel screening length ($1/k$)
ξ_M	Manning parameter
ρ_m	immobilized charge density of macroion
$\rho(\vec{r})$	charge density
σ	charge density per unit area of the surface
τ	reduced temperature
τ	relaxation time
$\varphi(\vec{r})$	electrostatic potential
ϑ	valence angle
Φ	rotation angle

Introduction.

In the last two decades there has been a growing interest towards the nanoworld. Following the rapid evolution of technology in the direction of the fabrication of smaller and smaller devices, a number of methods aiming at the patterning of matter on the length scale of a few nanometres have been developed in recent years. Nanostructures can be fabricated via a top-down approach by means of novel techniques (such as, e.g., ultrafast imprinting[1]) or by a combination of traditional lithography and chemical etching or chemical vapour deposition techniques[2]. A wide range of bottom-up techniques based on the self-assembly of nanometre-sized structural units into complex fabrications have been also recently developed[3]. Particularly interesting is the possibility of using self-assembled biological structures as templates for the deposition of inorganic matter, in particular metals[4]. On the other hand, polymer chemistry offers a fascinating world of different architectures and structures of molecular entities: ranging from stars, rods to branched, hyper-branched or H-shaped polymer molecules nearly of all possible architectures. It would be a challenging task to utilize those structures for the generation of nanoparticles, which then could serve specific tasks controlled by topology. This concept might be a route to a nanomachine consisting of a single molecule with different functions at different locations.

Most of conventional methods available for polymer science provide information referring to the ensemble average over many polymer chains. On the other hand, the observation and manipulation of molecules would be the method to directly probe and modify local properties of polymer individual molecules. This approach opens a fascinating area of research – *single molecule experiment*. Polymer single molecules can be considered not only as representative of the ensemble molecules, but also as *individual nanoscale objects* which can be used for future nanotechnology for the fabrication of single molecule electronic devices. Single molecule experiments are also important from fundamental point of view, and can be successfully applied for direct and visual investigation of various "classical" problems in polymer science, such as polymer reconformation, interpolyelectrolyte complex formation, polymer diffusion, adsorption, etc.

Among the methods which can be used for visualization of polymer molecules, atomic force microscopy (AFM) certainly occupies a leading place. Most of synthetic polymers are invisible by optical microscopy because of a resolution limit. They also could not be resolved with High Resolution Transmission Electron Microscopy because of low density of polymer molecules (contrasting problems). Scanning tunneling microscopy, on the other hand, is

applicable only for conductive objects and therefore can not be used for visualization of usual non-conductive polymers. That is why the state-of-the-art of AFM mostly defines what kind of molecules can be used in the single molecule experiment. Before this work the experiments were performed mainly with relatively "thick" polymeric molecules if the diameter of the chain was well larger then 1 nm: dendronized polymers, "molecular brushes", and some naturally occurring polymers: viruses, proteins and duplex DNA. However, most of the synthetic polymers and many natural polymers have much thinner chains.

Aims & objectives. The goal of this thesis is to extend the range of the nanoscale objects which can be successfully involved in the single molecule experiment to single molecules of "normal sized" polymers. Particularly, polyelectrolytes of different architecture will be visualized and their reconformation will be studied. Finally, PEs single molecules will be utilized as a pattern for metallization to fabricate nanoparticles of different shape, size and composition.

Novelty. The thesis presents experiments with single molecules of the "normal sized" polymers like poly-2-vinylpyridine (P2VP) performed by AFM. This finding allowed to study largely discussed problem, a coil-to-globule transition of polyelectrolytes (PE), and for the first time, visualize a theoretically predicted, so-called, pearl-necklace conformation. We also visualized block copolymers of more complicated architectures and studied their reconformation. For the first time, it was unambiguously confirmed the star-shaped nature of PS_7-PVP_7 star block copolymer and the amount of PVP arms was directly counted. It was discovered that PE single molecules of various architectures can be mineralized in different conformations that constitutes the route to nanoparticles of desired shape (including wire-shaped and star-shaped), size, and composition (including metallic, magnetic and semiconductive nanoparticles). The simple contrasting procedure was developed to improve the AFM visualization of positively charged polymer chains deposited on the substrates of relatively high roughness via counterion exchange with bulky hexacyanoferrate (HCF) anions or negatively charged nanoclusters of Prussian blue. The reaction of HCF anion could be used for recognition of polycation molecules, when polycations, polyanions, and neutral molecules coexist on the surface. We believe that the presenting work is important for the development of single molecule experiments with polymer chains.

Outline of the thesis. The first chapter gives short review of the theoretical background often used for the interpretation of experimental data. The second chapter describes basics, scope and limitation of the main research techniques: Atomic Force Microscopy and Dynamic Light Scattering. The third chapter discuss the conformations of PE molecules deposited on

flat solid substrates from solutions with different conditions. The fourth chapter is dedicated to development of metallization procedure, in particular deposition of palladium clusters onto single polyelectolyte molecules. Diverse conformational transitions responding to external stimuli and metallization of $P2VP_7$-PS_7 star-like block copolymer are described in the fifth chapter. The sixth chapter deals with a contrasting of single polycation molecules with cyanide-bridged compounds.

The main results of the work were published in the following papers:

Chapter 3:

- Minko, S.; Kiriy, A.; Gorodyska, G.; Stamm, M.; Single Flexible Hydrophobic Polyelectrolyte Molecules Adsorbed on Solid Substrate: Transition between a Stretched Chain, Necklace-like Conformation and a Globule *J. Am. Chem. Soc.*, **2002**, *124(13),* 3218-3219.
- Minko, S., Gorodyska G., Kiriy, A.; W. Jaeger G., Stamm, M. Visualization of Single Polyelectrolyte Molecules. *Polym. Mater. Sci. Eng*, **2002**, *87*, 185-186.
- Kiriy, A.; Gorodyska, G.; Minko, S.; Jaeger, W.; Stepanek, P.; Stamm, M.; Cascade of Coil-Globule Conformational Transitions of Single Flexible Polyelectrolyte Molecules in Poor Solvent *J. Am. Chem. Soc.*, **2002**, *124(45),* 13454-13462. The paper have been highlighted as the "Editor's Choice" in 8/10/02 issue of *Science* (Washington): **2002**, *298*, 1139.

Chapret 4:

- Gorodyska G., Kiriy A., Minko S., Stamm M. Metallic Nanoparticles from Single Polyelectrolyte Molecules. Organic/Inorganic Hybrid Materials Q6.33 Editors: R.M. Laine, C. Sanchez, S. Yang, C.J. Brinker *MRS Proceedings*, V. 726, 187-192, **2002**.
- Kiriy, A.; Minko, S.; Gorodyska, G.; Stamm, M.; Jaeger, W.; Palladium Wire-Shaped Nanoparticles from Single Synthetic Polycation Molecules *NanoLett.*, **2002**, *2(8),* 881-885.
- Minko, S.; Kiriy, A.; Gorodyska, G.; Stamm, M.; Mineralization of Single Flexible Polyelectrolyte Molecules *J. Am. Chem. Soc*., **2002**, *124(34)*, 10192-10197.

Chapter 5:

- Gorodyska, G.; Kiriy, A.; Minko, S.; Tsitsilianis, C.; Stamm, M. Reconformation and Metallization of Unimolecular Micelles in Controlled Environment. *NanoLett.,* **2003**, *3(3),* 365-368.

- Kiriy, A.; Gorodyska, G.; Minko, S.; Tsitsilianis, C.; Stamm, M. Atomic force microscopy visualization of single star copolymer molecules. *Polym. Mater. Sci. Eng* **2003**, *88*, 233-234.
- Kiriy, A.; Gorodyska, G.; Minko, S.; Tsitsilianis, C.; Stamm, M. Single Molecules and Associates of Heteroarm Star Copolymer Visualised by Atomic Force Microscopy. *Macromolecules*. **2003**, *36*, 8704-8711.

Chapter 6:

- Kiriy, A.; Gorodyska, G.; Minko, S.; Tsitsilianis, C.; Jaeger, W., Stamm, M. Chemical Contrasting in a Single Polymer Molecule AFM Experiment. *J. Am. Chem. Soc*., **2003**, *125*, 11202 – 11203.
- Kiriy, A.; Gorodyska, G.; Minko, S.; Tsitsilianis, C.; Stamm, M. Cyanide-Bridged Compounds as Contrasting Agents for AFM Imaging of Single Polycation Molecules. *Macromolecules*. Submitted.
- Kiriy, A.; Bocharova ,V; Gorodyska, G.; Minko, S.; Stamm, M. Assembling of Prussian Blue Nanoclusters Along Single Polyelectrolyte Molecules, *Polym. Mater. Sci. Eng*, **2004.**
- Kiriy, A.; Gorodyska, G.; Minko, S.; Tsitsilianis, C.; Stamm, M. Cyanide-Bridged Compounds as Contrasting Agents for AFM Imaging of Single Polycation Molecules, *Polym. Mater. Sci. Eng,* **2004.**

Chapter 1.

Polyelectrolyte Models and Theoretical Predictions

Polyelectrolytes (PEs) are a special class of polymers containing electrostatic charges along their chains. Due to their charges, PEs are water soluble, therefore they are closely connected with processes of life and play an indispensable part in many branches of modern technology[5]. In contrast to the well-established state of the theory of uncharged polymers in solution, our understanding of the behavior of PEs is rather poor. PEs cannot be understood as a simple superposition of electrolyte and polymer properties. Whereas excluded volume effects are the only important interaction in uncharged polymers, the long-range Coulomb interaction in PEs give rise to new critical exponents. On the other hand, in contrast to simple electrolytes, one type of charge is bundled together along a chain, resulting in strong fields near the chain even in high dilution. Owing to this peculiarity of PEs, a basic idea concerning the behavior of charged chains is the expectation that they should show rodlike behavior at infinite dilution and without added salt. So, almost all theoretical models on PEs are based on the concept of semirigid chains that results, however, in predictions showing fundamental discrepancies for highly flexible chains. The aim of this subchapter is not to give a detailed description of various theoretical approaches for PEs, but to review the theoretical background often used for the interpretation of experimental data.

Averages[6]. Since a polymer chain with i repeat units has a degree of polymerization of i and a molar mass of M_i, it can also be defined using its contour length $\boldsymbol{l_{Ci}}$. The number of molecules of size $\boldsymbol{l_{Ci}}$ is denoted by N_i.

The number average molecular length $< L_n >$ is given by

$$\langle \boldsymbol{L_n} \rangle = \frac{\boldsymbol{\Sigma\ N_i l_{C_i}}}{\boldsymbol{\Sigma\ N_i}}, \tag{1.1}$$

whereas the weight(mass) average molecular length $< L_w >$ is defined by

$$\langle \boldsymbol{L_w} \rangle = \frac{\boldsymbol{\Sigma\ N_i l_{C_i}^2}}{\boldsymbol{\Sigma\ N_i l_{C_i}}}. \tag{1.2}$$

The polydispersity ***PDI*** is defined as

$$\boldsymbol{PDI} = \frac{\langle \boldsymbol{L_w} \rangle}{\langle \boldsymbol{L_n} \rangle}. \tag{1.3}$$

These length averages can now easily be transformed into weight averages using the molar Mass $\boldsymbol{M_i}$ and length of a repeat unit $\boldsymbol{a}$ of the polymer in order to get:

$$\boldsymbol{W_{w,n}} = \frac{\boldsymbol{L_{w,n}}}{\boldsymbol{a}} \boldsymbol{M_i}. \tag{1.4}$$

1.1. Fundamental Models for Description of Polymer Shape in Solution

Since flexible polymers in solution can take large number of different configurations, their shape and size can be understood and described only statistically. The quantities used to characterize the size of chain molecule are the mean square end-to-end distance $\boldsymbol{<R^2>}$, the mean square radius of gyration $\boldsymbol{<R_g^2>}$ and the contour length $\boldsymbol{l_C}$..

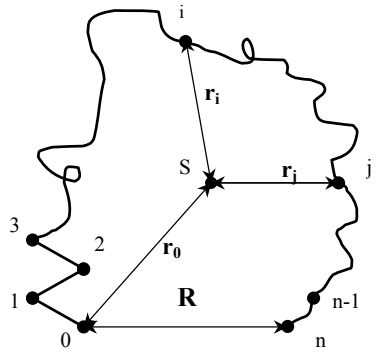

End-to-end distance is the distance between two end groups of the polymer. Its advantage is the obvious meaning, which is lost however for more complicated architectures, like star shaped molecules.

Figure 1.1 Sketch of a linear polymer chain. End-to-end distance R, the center of mass of the chain S and distance of i monomer from the center of mass r_i are indicated.

The mean square radius of gyration is a quantity that one can obtain experimentally (e.g. from light scattering):

$$\langle \boldsymbol{R_g^2} \rangle = \frac{\boldsymbol{1}}{\boldsymbol{N}} \sum_{\boldsymbol{i=1}}^{\boldsymbol{N}} \langle \boldsymbol{r_i^2} \rangle. \tag{1.5}$$

It is defined as a mean square distance of all segments r_i, here the monomers, from the center of mass of the chain. The contour length is defined as the entire length of the macromolecule.

The simplest model for the description of the shape of a macromolecule in solution is the Kuhn segment model[7] (**F**reely **J**ointed **C**hain, FJC[8]). The macromolecule is regarded thereby as a row of many, equivalent long and infinitely thin components. Any angle is acceptable between two segments. This model seems to be already too simplified, however it gives a good description of the reality on the condition that a segment consists of several monomers. The mean square end-to-end distance results for the FJC is

$$\left\langle \boldsymbol{R}^2 \right\rangle = \boldsymbol{N} \cdot \boldsymbol{a}_k^2 \tag{1.6}$$

with N being the number of statistical segment length a_k

$$\boldsymbol{a}_k = \frac{\left\langle \boldsymbol{R}^2 \right\rangle}{\boldsymbol{l}_C} \tag{1.7}$$

The mobility of the different segments of a macromolecule in solution due to the Brownian motion makes necessary an averaging over all conformations.

The extension of the FJC-model come out with consideration of fixed valence angle. Free rotating around the connection axles prevails in this case, that is why this model is called Freely Rotating Chain (FRC). The end-to-end distance becomes larger due to fixation of the connection angles

$$\left\langle \boldsymbol{R}^2 \right\rangle = \boldsymbol{N} \cdot \boldsymbol{a}^2 \frac{\boldsymbol{1} + \cos \boldsymbol{\vartheta}}{\boldsymbol{1} - \cos \boldsymbol{\vartheta}} \tag{1.8}$$

where ϑ is the valence angle and a is the monomer length.

The next refinement of the model takes into account of a hindered rotation around the connection axle, e.g. as it is caused by steric effects of the substituents (already by a hydrogen atom) at the backbone chain. Thus one or several rotation angles $\boldsymbol{\Phi}$ are energetically favorable. The hindered rotation means an additional expansion of the molecule in nearly all cases. The end-to-end distance results

$$\left\langle \boldsymbol{R}^2 \right\rangle = \boldsymbol{N} \cdot \boldsymbol{a}^2 \frac{\boldsymbol{1} + \cos \boldsymbol{\vartheta}}{\boldsymbol{1} - \cos \boldsymbol{\vartheta}} \cdot \frac{\boldsymbol{1} + \left\langle \cos \boldsymbol{\Phi} \right\rangle}{\boldsymbol{1} - \left\langle \cos \boldsymbol{\Phi} \right\rangle} \tag{1.9}$$

Excluded Volume Effect. Interactions between chain segments mentioned above are restricted to within a few neighbors along the chain. However, segments separated by many bonds along the chain will interact if they come close to each other. Since the segments have finite volume they push off each other and the chain will swell. Hence, the coil size of a chain with such with such an interaction is larger than that of an ideal chain. This effect is called the

excluded volume effect. In real polymer, the nature of excluded volume interaction is quite complex. Besides steric effects, the interaction also includes van der Waals attraction and not only between polymer segments but also between chain segments and solvent molecules as well as between solvent molecules.

One of the most important results first suggested by de Gennes[9] is the conclusion that the dependence of many physical quantities on the chain length N (as well as on several other parameters) can be represented as universal scaling laws. For the average size of the polamer one obtains

$$\left\langle R^2 \right\rangle^{1/2}, \left\langle R_g^2 \right\rangle^{1/2} \cong aN^{\nu} \tag{1.10}$$

with critical indexes

$$\nu = \begin{cases} 1/3, & T < \Theta \\ 1/2, & T = \Theta \\ 0.588 & T > \Theta. \end{cases} \tag{1.10a}$$

At the Θ-temperature the chain show ideal behavior, and relations derived before are valid. Above T= Θ the chain is swollen, while below the Θ-temperature the chain undergoes a coil-to-globule transition into a collapsed state.

The swelling of the coil due to the excluded volume interaction is often represented in terms of so-called expansion factors α^2

$$\left\langle R^2 \right\rangle = \alpha^2 \left\langle R^2 \right\rangle_{\theta} \tag{1.11}$$

Persistence Length. A model suggested by Kratky and Porod[10] for stiff or semiflexible polymers in solution is the so-called worm-like chain (WLC) model. A characteristic quantity in this model is the persistence length. It determines the stiffness of the chain and is defined as the distance over which the memory of the initial orientation of the polymer persists. The bare or intrinsic persistence length ($l_{p,0}$) due to monomer structure and non-electrostatic interactions of the polymer is defined as:

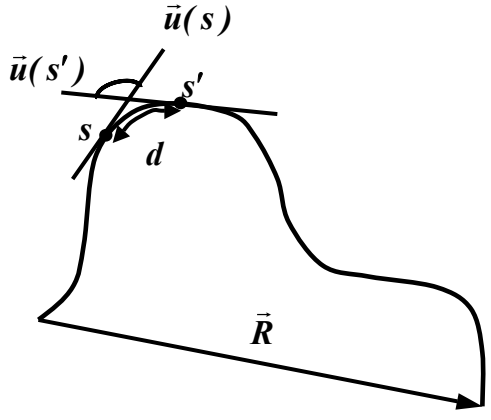

$$l_{p,0} = \frac{d}{1 + \cos\theta} \tag{1.12}$$

d is the segment length between s and s', θ the angle between two adjacent unit vectors tangential to the chain at position s and s' (see Figure 1.2).

Figure 1.2 Sketch of a worm-like chain. Unit vectors $\vec{u}(s)$, $\vec{u}(s')$ tangental to the chain at position s, s', bend angle θ between unit vectors $\vec{u}(s)$, $\vec{u}(s')$, and end-to-end vector $\vec{R}$ are indicated.

The wormlike chain relations can be written as

$$\left\langle R^2 \right\rangle = 2l_{p,eff}l_C - 2l_{p,eff}^2\left(1 - e^{-l_C/l_{p,eff}}\right) \tag{1.13}$$

$$\left\langle R_g^2 \right\rangle = \frac{1}{3}l_{p,eff}l_C - l_{p,eff}^2 + \frac{2l_{p,eff}^3}{l_C}\left[1 - \frac{l_{p,eff}}{l_C}\left(1 - e^{-l_C/l_{p,eff}}\right)\right] \tag{1.14}$$

where the effective persistence length $l_{p,eff}$ is discussed below.

The two limiting cases are:

1. $l_C/l_{p,eff} >> 1$ (Gaussian coil limit)

$$\left\langle R^2 \right\rangle = 6\left\langle R_g^2 \right\rangle = 2l_{p,eff}l_C \tag{1.15}$$

2. $l_C/l_{p,eff} << 1$ (rigid rod limit)

$$\left\langle R^2 \right\rangle = 12\left\langle R_g^2 \right\rangle = l_C^2 \tag{1.16}$$

Comparing Eq. (1.15) with corresponding expression of a Kuhn chain given in Eq. (1.7) the following relation can be established

$$a_k = 2\, l_{p,eff.} \tag{1.17}$$

However, in the case of PEs, the persistence length is increased due to electrostatic repulsion between monomers. Thus, the theoretical description of the persistence length should include this effect. This leads to an additional contribution to the persistence length, the electrostatic persistence length $l_{p,OFS}$ due to intrachain repulsion[11]. Thus, the effective persistence length $l_{p,eff}$ is given by

$$l_{p,eff} \cong l_{p,0} + l_{p,OFS} \tag{1.18}$$

The index OSF stands for the theoreticians Odijk, Skolnick, Fixman who derived the electrostatic persistence length $l_{p,OFS}$ for a monovalent salt[11,12]

$$l_{p,OSF} = \frac{\lambda_B}{4}\left(\frac{\lambda_D}{b}\right)^2 \tag{1.19}$$

with the average distance between two charged groups along the chain b, the Debye screening length λ_D, and the Bjerrum length λ_B. The latter parameters are discussed later in subsection 1.2.2. For high salt concentration the bare or intrinsic persistence length $l_{p,0}$ dominates, because $l_{p,OFS}$ decreases with increasing ionic strength $l_{p,OFS} \propto \lambda_D^2 \propto I^{-1}$. However, serious objection arose to the application of the OSF model for intrinsically flexible polyelectrolytes (most experiments[13] suggested a square-root relation $l_{p,OFS} \propto I^{-1/2}$) and multivalent ions.

Polymer Solutions with Finite Concentration. The whole concentration region can be divided into tree parts: dilute, semidilute, and concentrated. The experimental results presented in this work was collected mostly in a dilute solution. In a dilute solution the concentration is sufficiently low that the polymer coils are well separated from each other. Thus characterization of single polymer chains is possible. Each polymer occupies a region with a radius of order of $R_F \propto \langle R^2 \rangle^{1/2}$, the so-called Flory radius. The intermolecular interaction between coils are weak and the polymer solution can be described as nonideal gas of polymer coils. With increasing concentration the polymer coils come closer and start to hinder each other (Figure 1.3).

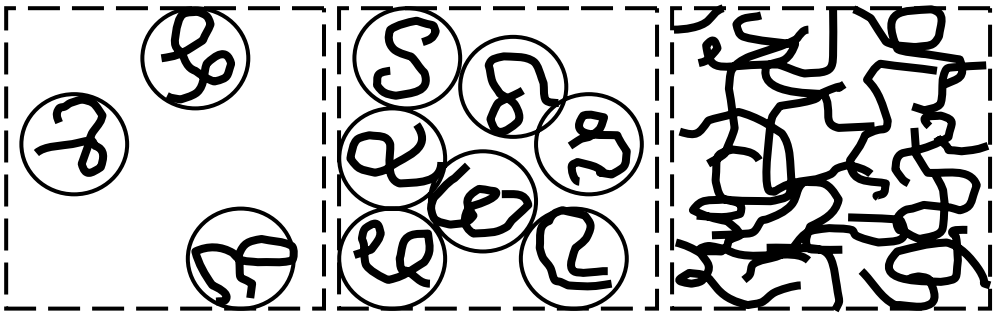

Figure 1.3 Schematic presentation of dilute solution (a), solution at overlap concentration (b), semidilute solution (c) by de Gennes[9].

The concentration c^*, at which polymer coils come into contact, called overlap concentration. The most common definition of c^* is

$$c^* = \frac{3 \cdot M}{4\pi R_g^2 \cdot N_A} \tag{1.20}$$

where M is the molecular weight and N_A is Avogadro's number.

1.2. Polyelectrolytes in Solution

The electrostatic interaction of macroions in aqueous monovalent salt solutions can be described by the classical mean-field treatment of electrostatic interaction, the Poisson-Boltzmann (PB) equation, that is discussed in the following.

1.2.1. Poisson-Boltzmann (PB) Equation

The Poisson-Boltzmann (PB) equation can be derived from the Poisson equation, where the electrostatic potential $\varphi(\vec{r})$ is connected with the charge density $\rho(\vec{r})$ as:

$$\nabla^2 \varphi(\vec{r}) = -\frac{1}{\varepsilon} \rho(\vec{r}) \,. \tag{1.21}$$

Here, ε is the dielectric constant of the solution (e.g. water). At any point within the potential $\varphi(\vec{r})$ the electrostatic energy of an ion is determined by $eZ\varphi(\vec{r})$. The probability to find an ion within this potential is proportional to the Boltzmann factor $exp(-eZ\varphi(\vec{r})/k_BT)$. Therefore the charge density $\rho(\vec{r})$ in Eq. (1.21) can be written as:

$$\begin{aligned}\rho(\vec{r}) &= \rho_m(\vec{r}) + eZc_0 e^{-eZ\varphi(\vec{r})/k_BT} - eZc_0 e^{eZ\varphi(\vec{r})/k_BT} \\ &= \rho_m(\vec{r}) - 2eZc_0 \sinh\left(\frac{eZ\varphi(\vec{r})}{k_BT}\right)\end{aligned} \quad , \tag{1.22}$$

where ρ_m is the immobilized charge density of the macroion, Ze is the charge of the ions and c_0 the salt concentration for vanishing potential. Eqs. (1.21) and (1.22) lead directly to the classical non-linear Poisson-Boltzmann equation:

$$\nabla^2\varphi(\vec{r}) = \frac{2eZc_0}{\varepsilon}\sinh\left(\frac{eZ\varphi(\vec{r})}{k_BT}\right) - \frac{1}{\varepsilon}\rho_m(\vec{r}). \tag{1.23}$$

The mean field approximation assumes pointlike ions in thermodynamic equilibrium and ignores contributions from fluctuations as well as ion correlation effects. The PB equation (1.23) can only be solved exactly in the case of a charged planar surface. For other geometries this equation can be solved directly within the Debye-Hückel approximation.

1.2.2. Debye-Hückel (DH) Approximation

In the Debye-Hückel (DH) regime the electrostatic interaction energy is much smaller than the thermal energy. Thus, for these low potentials, $eZ\varphi(\vec{r}) < k_BT$, the charge density $\rho(\vec{r})$ in Eq. (1.22) can be Taylor expanded

$$\begin{aligned}\rho(\vec{r}) &= \sum_i c_{o_i} eZ_i \exp(-Z_i e\varphi(\vec{r})/k_BT) + \rho_m(\vec{r}) \\ &= \sum_{i=0, n_+=n_-} c_{o_i} eZ_i - \sum_i c_{o_i} e^2 Z_i^2 \frac{\varphi(\vec{r})}{k_BT} + \rho_m(\vec{r})\end{aligned} \tag{1.24}$$

such that the Poisson-Boltzmann Eq. (1.23) can be linearized and reduces to the Debye-Hückel equation:

$$\begin{aligned}\nabla^2\varphi(r) &= \frac{e^2}{\varepsilon k_BT}\sum_i c_{0_i} Z_i^2 \varphi(\vec{r}) - \frac{1}{\varepsilon}\rho(\vec{r}) \\ &= k^2\varphi(\vec{r}) - \frac{1}{\varepsilon}\rho(\vec{r})\end{aligned} \tag{1.25}$$

where the Debye screening length $k^{-1} = \lambda_D$ appears as the characteristic decay length of the potential. It is defined by

$$\lambda_D = k^{-1} = \left(\frac{\varepsilon k_BT}{2e^2 I}\right)^{1/2} = (8\pi\lambda_B I)^{-1/2} \tag{1.26}$$

Here, $I = 1/2\Sigma_i c_{0i} Z^2_i = Z^2 c_0$ is the ionic strength and $\lambda_B = e^2/(4\pi\varepsilon k_B T)$ is the Bjerrum length. The Bjerrum length is defined as the distance at which the electrostatic interaction between elementary charges e equals the thermal energy $k_B T$. In water $\lambda_B \approx 0.7$ nm. In Table 1.1 the screening length λ_D is given for different salt concentrations. Under physiological conditions, i.e. at about 100 mM, the Debye screening length amounts to $\lambda_D \approx 1$ nm.

Table 1.1 Screening length λ_D for different NaCl solutions.

[NaCl] (mM)	k (nm^{-1})	λ_D (nm)
5	0,23	4,34
50	0,73	1,37
100	1,03	0,97
600	2,52	0,40
1000	3,25	0,31
2000	4,59	0,22

If the electrostatic potential becomes larger than $k_B T$, in principle one has to solve the full non-linear PB equation (1.23). On the other hand, it has been shown that there is a wide range of salt concentrations where the DH approximation is valid. It is therefore applied to the systems discussed in this thesis.

1.2.3. Manning Condensation

In the presence of a solution of mobile monovalent salt ions, the situation of a macroion containing a charge Ze can be described as follows: Let the number of ions that lie at a certain distance from the macroion be Z'. In this region the DH approximation is still valid. However, the remaining ions ($Z - Z'$) are condensed on the macroion having a local concentration that is higher than in the surrounding salt concentration. Thus, the effective charge of the macroion becomes screened to $Z'e$ [14].

In the case of a cylindrical geometry with a charge per unit length of $\tau_C = e/b$, where b is the spacing per elementary charge, also a certain amount of ions condense on the charged cylinder. Thus, the effective charge per unit length becomes

$$\tau'_C \equiv e / \lambda_B \tag{1.27}$$

in the region $|\tau_C| > |\tau'_C|$ [15]. This region corresponds to the region in which the dimensionless charge density (also known as the *Manning Parameter* ξ_M) becomes larger than 1. The Manning Parameter is defined as

$$\xi_M \equiv \frac{\lambda_B |\tau_C|}{e} = \frac{\lambda_B}{b} . \tag{1.28}$$

It defines the ratio of the electrostatic energy $eZ\varphi$ to the thermal energy k_BT. Thus, the counterion condensation threshold is given by $\xi_M \approx 1$. In the region $\xi_M > 1$, the electrostatic energy dominates over the thermal energy and the DH approximation fails (see section 1.2.2).

However, far from the cylinder surface, the potential decreases and the electrostatic energy is small compared to the thermal energy. Thus, the DH equation (1.25) becomes valid again, but the macroion charge is screened by the counterions. Using the effective charge τ'_C instead of τ_C, the electrostatic interaction at large separations can be calculated within the DH approximation.

If two oppositely charged macroions are brought into close contact with each other, their condensed counterions can be released into the solution. The released counterions will gain entropy that will favor the formation of the complex. This release is referred to as the entropic counterion effect.

1.3. Polyelectrolyte Chain in Poor Solvent

The overall shape of a charged polymer in a poor solvent is determined by the balance of the electrostatic repulsion and the surface tension. Consider a dilute polyelectrolyte solution of chains with degree of polymerization N, monomer size a, and fraction f of charged monomers in a poor solvent with dielectric constant ε. An uncharged chain in a poor solvent forms a globule.[5,9] The monomer density $\rho_{gl} \approx \tau/a^3$ inside this globule is defined by the balance of the two-body attraction ($v N\rho$) and the three-body repulsion ($a^6 N\rho^2$) between the monomers of the chain. Here $v \approx -\tau a^3$ is the second virial coefficient, with the reduced temperature given by $\tau = (\Theta - T)/\Theta$. The size R of the globule with density ρ_{gl} is equal to

$$R_{gl} \approx (N/\rho_{gl})^{1/3} \approx a\,\tau^{-1/3} N^{1/3} \qquad (1.29)$$

There is one important length in the globule - the size ξ_T of the density fluctuations (thermal blob size[9]). On length scales smaller than ξ_T, the chain statistics are unperturbed by the volume interactions and are that of a random walk of g_T monomers ($\xi_T \approx a g_T^{1/2}$). On length scales larger than the correlation length ξ_T, the attraction between monomers wins and thermal blobs in the globule are space-filling, $\rho \approx g_T/\xi_T^3$. The number of monomers in a thermal blob is $g_T \approx 1/\tau^2$ and its size is $\xi_T \approx a/\tau$. The surface tension γ of the globule is of the order of k_BT per thermal blob at the globular surface, $\gamma \approx k_BT/\xi_T^2$.

1.3.1. Cylindrical Globule.

With increasing fraction of charged monomers or increasing solvent strength, the balance between the interfacial and the Coulomb energies is violated. It was suggested by Khokhlov[16] that, in order to optimize its energy, the polyelectrolyte chain takes the shape of an elongated

cylindrical globule with length L_{cyl} and width D. The theory of Khokhlov was extended by Raphael and Joanny[17] to the case of "mobile" charges on the chain and by Higgs and Raphael[18] to the case of screening of electrostatic interactions by added salt. The size of the cylinder can be found by optimizing the sum of the surface energy and Coulomb energy at fixed volume determined by the solvent quality. This minimization of the free energy $F_{cyl} = F_{sur} + F_{Coul}$ leads to the cylinder length

$$L_{cyl} \approx aN\tau^{-1}(uf^2)^{2/3} \tag{1.30}$$

and width

$$D \approx a(uf^2)^{-1/3} \tag{1.31}$$

Here $u \approx \lambda_B / a$ is the ratio of the Bjerrum length λ_B and the bond length a, f is the fraction of charged monomers, N is the degree of polymerization, and τ is the reduced temperature given by $\tau = (\Theta - T)/\Theta$. It is important to note that the width D of the cylinder is the length scale at which the Coulomb repulsion between charges becomes of the order of the surface energy (electrostatic blob in a poor solvent).

1.3.2. Necklace Globule

However, the cylindrical globule is not the free energy minimum of a polyelectrolyte chain in a poor solvent. Kantor and Kardar[19] have recently proposed that a polymer with short-range attraction and long-range repulsion may form a necklace with compact beads joined by narrow strings. Dobrynin, Rubinstein and Obuhov[20] (DRO) extend this idea and develop a scaling theory that describes how, with varying solvent quality or charge on the chain, the polyelectrolyte in a poor solvent undergoes a cascade of abrupt transitions between necklace-like configurations with different numbers of beads. They found that the length of the necklace globule is proportional to the total polymer charge and is larger than the length of the cylindrical globule. Consequently, the free energy of the necklace globule is lower than that of the cylindrical one.

DRO theory consider a necklace globule, as sketched in Figure 1.4, with N_{bead} beads of size d_{bead} joined by $N_{bead} - 1$ cylindrical strings of length l_{str} and width d_{str}. $L_{nec} = (N_{bead} - 1)\, l_{str} + N_{bead}\, d_{bead}$ is the total length of the necklace.

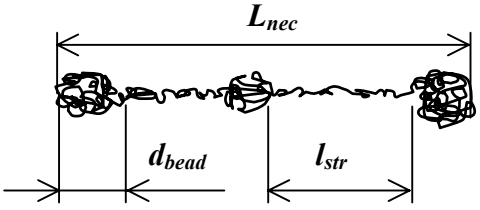

Figure 1.4 A necklace globule of the length L_{nec} with N_{bead} beads and N_{bead}-1 strings. Beads are spherical with diameter $d_{bead.}$. Strings are cylindrical with length l_{str} and diameter $d_{str.}$

The details of the necklace configuration described in such a way. The total length of the necklace

$$L_{nec} \approx a\left(\frac{u}{\tau}\right)^{1/2} fN \qquad (1.32)$$

is proportional to the total charge on the chain fN and is longer than that of a cylinder, $L_{nec}/L_{cyl} \approx (D/\xi_T)^{1/2}$. This longer length allows the polyelectrolyte to have lower energy because the charges are separated by larger distances. The diameter of the beads is of the order of the electrostatic blob size D - the same as the diameter of the cylinder (Eq. (1.31))

$$d_{bead} \approx D \approx a(uf^2)^{-1/3} \qquad (1.33)$$

The length of the string

$$l_{str} \approx a\left(\frac{\tau}{uf^2}\right)^{1/2} \qquad (1.34)$$

is larger than the diameter of the beads d_{bead} by the factor $(D/\xi_T)^{1/2}$.

The number of beads N_{bead} of the necklace can only be an integer

$$f \approx \left(\frac{\tau}{u}\frac{N_{bead}}{N}\right)^{1/2} \qquad \text{where } N_{bead} = 1, 2, 3, \ldots \qquad (1.35)$$

between the states of the necklace globule with different numbers of beads. Upon changing the valence f or solvent quality τ, the globule undergoes a cascade of transitions between states with different integer numbers of beads N_{bead} on the necklace.

1.3.3. Diagram of States of Polyelectrolyte in a Poor Solvent

In Figure 1.5 it is sketched a diagram of states of a polyelectrolyte chain (with $N = 100$ monomers and $u = 2$) in a poor solvent as a function of valence f and solvent quality τ. In region I close to the Θ-temperature ($\tau < N^{-1/2}$) and for lower valence ($f < u^{-1/2}N^{-3/4}$), the short-range attraction between monomers and the electrostatic repulsion between charges are too weak to deform the chain and it behaves like a Gaussian coil. In a poor solvent (further below the Θ -temperature: at effective temperatures $\tau > N^{-1/2}$) and at low charge density f (in region II of the phase diagram), the size of the thermal blob ξ_T is smaller than the Gaussian chain size $R \approx aN^{1/2}$, and the short-range attraction results in a collapse of the chain into a spherical globule. This globule is stable at lower charge density $f < (\tau/uN)^{1/2}$ as long as its surface energy is larger than the electrostatic energy (see Eq. (1.35) for $N_{bead} = 1$).

At higher valence $f > (\tau/uN)^{1/2}$, the spherical globule is unstable with respect to capillary waves and first splits into a dumbbell with two smaller globules joined by a string of thermal blob width ξ_T($N_{bead} = 2$ part of region III - see also insert in Figure 1.5). As the charge density

f increases further, the necklace with two globules (dumbbell) splits into one with three smaller globules connected by two strings of diameter ξ_T. At still higher valence f, it splits again into a necklace with $N_{bead} = 4$ globules and so on. This cascade of abrupt transitions between the necklaces with different numbers of globules occurs at the boundaries given by Eq. (1.35) and is shown in region III of the diagram. At the upper boundary $f \approx \tau^{3/2}u^{-1/2}$ of this region, the size of the globules (beads) D is comparable to the width of the strings ξ_T.

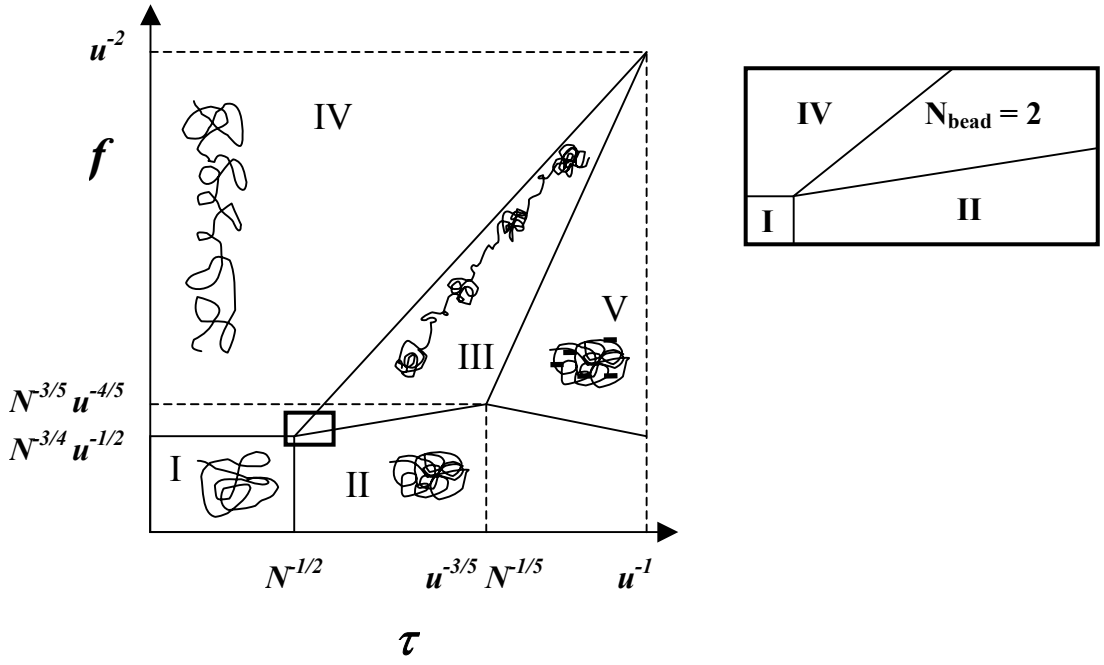

Figure 1.5 Diagram of states of a polyelectrolyte chain in a poor solvent. Regime I, unperturbed Gaussian coil; regime II, spherical globule; regime III, cascade of abrupt transitions between necklace configurations with different number of beads; regime IV, Θ-solvent-like cylindrical configuration. In regime V a single glouble with condensed counterions is expected.

Region IV of the diagram above the cascade zone at higher valence f and smaller effective temperature τ corresponds to the $\boldsymbol{\Theta}$ -like state of a polyelectrolyte with the chain in the shape of a cylinder. The electrostatic blob in this regime is the length scale at which electrostatic repulsion is of the order of thermal energy kT (but is still given by Eq. (1.31).[9] On length scales smaller than the electrostatic blob size D, the chain is Gaussian. On larger length scales, the electrostatic repulsion forces the polyelectrolyte into a linear array of electrostatic blobs. The length of the polyelectrolyte in this regime (region IV) is $L \approx bN(uf^2)^{1/3}$. Note that at the boundary of regions I and IV (at $f \approx u^{-1/2}N^{3/4}$), the length L of the chain crosses over to its Gaussian size. At higher valence f we expect Manning condensation[14] to define the upper boundary of region IV. This condensation of counterions occurs at a linear charge density along the cylinder axis higher than λ_B^{-1}: $f > u^{-2}$.[14]

In region V of the diagram, the strong electrostatic attraction between counterions and charged groups on the polymer chain also results in counterion condensation. The crossover

condition between condensed and free states of counterions can be found by comparing the thermal energy kT with the electrostatic interaction between a bead and a counterion for the necklace globule in regime III ($E_{III} \approx e\, m_{bead} f/\varepsilon D$) and between the globule and a counterion for a spherical globule in regime II ($E_{II} \approx e^2 Nf/\varepsilon R$). These conditions give the upper, $f \approx \tau^3 u$, and lower, $f \approx \tau^{-1/3} u^{-1} N^{-2/3}$, boundaries of regime V in the diagram of states.

The most striking part of the diagram is region III with the "necklace" cascade of transitions.

1.4. Computer Simulations

Simulation studies have provided to be very important tool in polymer science. General discussions of the two methods used in simulation studies, the Monte Carlo and the molecular dynamics method, can be found in several books and review.[21] Our discussion is limited to the simulations of a polyelectrolyte in a poor solvent.

Dobrynin et.al.[20] have carried out a Monte Carlo simulation of a single weakly charged chain under a poor solvent conditions to check out their theoretical predictions. They consider a freely jointed uniformly charged chain consisting of N monomers with charge fe on each.[22] The monomers interact with each other through a Coulomb potential

$$\frac{U_{Coul}(r_{ij})}{k_B T} = \frac{uaf^2}{r_{ij}}$$

and a Lennard-Jones potential

$$\frac{U_{LJ}(r_{ij})}{k_B T} = \varepsilon_{LJ}\left[\left(\frac{r_0}{r_{ij}}\right)^{12} - 2\left(\frac{r_0}{r_{ij}}\right)^{6}\right]$$

where r_{ij} is the distance between the ith and jth monomers. The Lennard-Jones potential has its minimum value $-k_B T\varepsilon_{LJ}$ at distance $r_{ij} = r_0$ (in the model r_0 has been chosen to be equal to the bond length a).

At lower valence $f < 1.7/N^{1/2}$, the chain forms a spherical globule (Figure 1.6a) with a size proportional to $N^{1/3}$. When the charge density becomes larger than the critical value $f \approx 1.7/N^{1/2}$, the polyelectrolyte takes a dumbbell configuration (Figure 1.6b). At still higher charge density, the polymer can form a necklace configuration of three beads joined by two strings (Figure 1.6c). These results of the Monte Carlo simulations support scaling prediction of the "necklace cascade" of transitions of a polyelectrolyte chain in a poor solvent.

A structural transition with a sharp increase of chain size at some value of charge density was observed in earlier Monte Carlo simulations of a polyelectrolyte chain in a poor solvent,[23] but the authors did not analyze the corresponding changes of the chain conformation.

In a nondynamical Monte Carlo simulation, Higgs and Orland[24] also observed a sharp increase of chain size with increasing coupling constant u, but they interpreted it as confirming Khokhlov's elongated globule picture. The conformation of a polyelectrolyte in a poor solvent regime was not studied in ref 24.

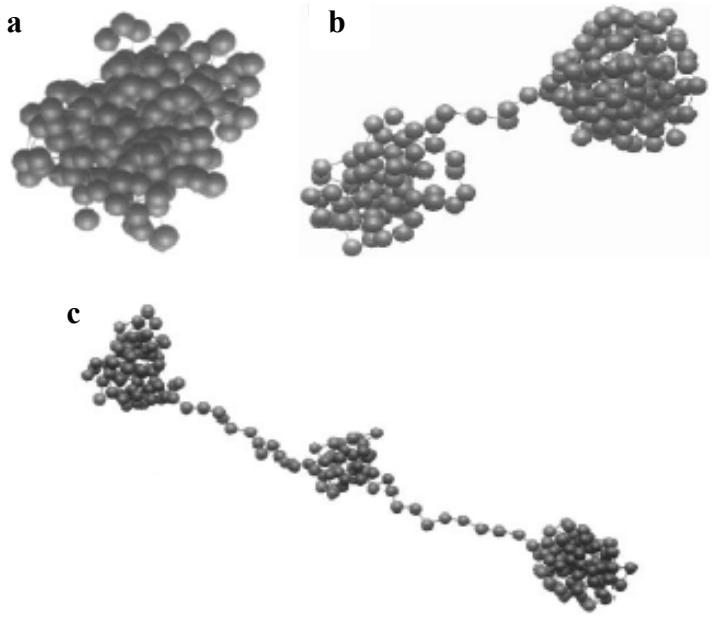

Figure 1.6 Typical configurations of a freely jointed uniformly charged chain with N = 200 monomers interacting via Coulomb and Lennard-Jones potentials (with $\varepsilon_{LJ} = 1.5$ and $u = 2$) at three different charge densities: (a) spherical globule for $f = 0$; (b) dumbbell for $f = 0.125$; (c) necklace with three beads for $f = 0.15$.

Micka et.al.[25] reproduced the picture of DRO for the strongly charged polyelectrolytes in poor solvents by molecular dynamics simulations. They showed typical pearl-necklace-like conformations, where small globules are connected by thin bridges. The globules are much smaller than in their weakly charged case, but clearly detectable.

1.5. Adsorption of hydrophobic polyelectrolytes onto oppositely charged surfaces

The adsorption of flexible PEs onto oppositely charged surfaces driven by the Coulomb attractive forces has been a classical problem in polymer physics over two decades.[26, 27, 28,29] In addition to its pure academic interest, PE adsorption has numerous important technological applications, *e.g.* for colloid stabilization.[30, 31]

In the pioneering paper of Wiegel,[26] the adsorption of an individual chain was considered in the absence of any interactions other than the electrostatic attraction of the charged monomers to the surface described by a screened Coulomb or Debye-Hückel potential. In real solutions, in addition to the polyelectrolyte-surface attraction there is a hierarchy of interactions (intra- and interchain) that affect significantly the adsorption. Attempts to take

these interactions into account were made in subsequent papers.[27,29] There are both short-range interactions (van der Waals or hydrophobic interactions) between uncharged monomers (which are a majority in weakly charged polyelectrolytes) and long-range Coulomb repulsive interactions between charged monomers. The short-range interactions are usually described in terms of the solvent strength and are repulsive or attractive under good or poor solvent conditions, respectively. The intrachain non-electrostatic interactions are dominated by the long-range Coulombic interactions under good or *Θ*-solvent conditions except when the density of adsorbed chains is high[32]. Short-range interactions are important under poor solvent conditions, when the attractions between uncharged monomers may induce a partial collapse of the polymer. This situation is very typical of many synthetic polyelectrolytes.

In the present subchapter, a simple scaling theory of adsorption of an individual polyelectrolyte chain under poor-solvent conditions developed by Borisov et.al.[33] would be given. This theory is based on the combination of i) the scaling approach developed in references 29 for the adsorption of polyelectrolytes from good and *Θ*-solvents; ii) the necklace model for polyelectrolyte globules suggested by Dobrynin *et al.*[20](see also subchapter 1.3); iii) the theory of adsorption of neutral polymers in poor solvent[34].

1.5.1. Adsorption of a polyelectrolyte chain in a *Θ*-solvent

We now give a brief summary of the scaling theory[28] describing the adsorption of an individual polyelectrolyte chain tethered onto an oppositely charged surface under *Θ* -solvent conditions*.

The grafting surface is uniformly negatively charged. The charge density per unit area of the surface (measured in elementary charges e) is denoted by σ. As a measure of the charge of the surface is introduced the Gouy-Chapman length

$$\lambda = 1/2\pi\lambda_B\sigma \qquad (1.36)$$

If the charged surface is in contact with a salt-free solution, the Gouy-Chapman length gives the range of spreading of the counterion cloud above the surface[35]. If the solution contains salt, the interaction is screened over the Debye length λ_D.

The chain conformation is determined by a balance between the attractive Coulombic energy of the charged monomers to the oppositely charged surface and the conformational entropy penalty for chain confinement. The confinement free energy of a Gaussian chain in an adsorbed layer of thickness D_{ads} is given by[9]

* The constraint that one of the chain end points is grafted on the surface insures that the chain remains actually bound to the surface. It does not influence the chain conformation.

$$F_{conf} \Big/ k_B T \cong \frac{N}{\left(D_{ads}/a\right)^2} \tag{1.37}$$

In a salt-free solution, the attraction between charged monomers and the surface is partially screened by the counterions ensuring neutralization of the overall surface charge. When salt is added to the solution, an additional screening is provided by the co- and counterions of the salt.

Depending on the salt concentration there are 2 asymptotic behaviors for the electrostatic potential. At low salt concentration, $\lambda << \lambda_D$, the reduced electrostatic potential near the surface is given by

$$\psi(z) \cong 2\, ln\left(\frac{\lambda}{2\lambda_D} + tanh\frac{z}{2\lambda_D}\right) \tag{1.38}$$

$\psi(z)$ is the dimensionless electrostatic potential; it depends only on the distance z to the negatively charged surface and can be calculated from the one-dimensional Poisson-Boltzmann equation.[35]

If the adsorbed layer thickness D_{ads} is still much smaller than the Debye length λ_D the attraction energy of the polyelectrolyte chain to the surface is given by

$$\frac{F_{Coulomb}}{k_B T} \cong fN\psi(D_{ads}) \cong \begin{cases} fND_{ads}\lambda^{-1} + F_0, & D_{ads} << \lambda, \\ fN\, ln(D_{ads}/\lambda) + F_0, & \lambda << D_{ads}, \end{cases} \tag{1.39}$$

where F_0 is a constant independent of the layer thickness. The minimization of the overall free energy, $F_{\text{conf}} + F_{\text{Coulomb}}$ with respect to D_{ads} gives the equilibrium thickness of the adsorbed layer

$$D_e / a \cong \begin{cases} (\lambda/af)^{1/3}, & D_{ads} << \lambda, \\ f^{-1/2}, & D_{ads} >> \lambda. \end{cases} \tag{1.40}$$

Similar scaling laws (with a slightly different exponent) obtained for polyelectrolytes in a good solvent. The results are in good agreement with the simulations of reference 29b.

In the limit of strongly charged surfaces, $D_{ads} >> \lambda$, the adsorbed layer thickness D_{ads} is independent of the surface charge density.

In the high salt limit, $\lambda >> \lambda_D$, the potential in the vicinity of the adsorbing surface can be approximated as

$$\psi(z) \cong -\frac{2e^{-z/\lambda_D}}{\lambda/\lambda_D}. \tag{1.41}$$

In the strong-screening limit, $D_{ads} >> \lambda_D$, the electrostatic field due to the charged surface is screened at distances $z > \lambda_D$ and only the charged monomers within a layer of thickness λ_D experience the Coulomb attraction of the surface. The problem is therefore very similar to the

adsorption of a polymer in a short-range attractive surface potential and arguments suggested by deGennes can be used.[9, 36]

If we assume a roughly uniform distribution of fN charged monomers in the layer, the Coulombic attractive energy of the chain by the surface is given by

$$\frac{F_{Coulomb}}{k_B T} \cong \frac{fN\lambda_D^2}{\lambda D_{ads}} . \qquad (1.42)$$

Minimizing the total free energy $F_{\mathrm{Coulomb}} + F_{\mathrm{conf}}$, we obtain the adsorbed layer thickness in the high salt limit:

$$D_e(\lambda_D) \cong (\lambda a / f\lambda_D^2) a . \qquad (1.43)$$

An adsorbed polyelectrolyte coil can be viewed as a monolayer of "adsorption electrostatic blobs" with a size given by equations (1.40) or (1.43) in the regimes of low and strong ionic strengths, respectively. The chain sequence inside a blob retains unperturbed Gaussian statistics. The Coulombic attraction energy of the charged monomers of a blob to the surface is of the order of the thermal energy $k_{\mathrm{B}}T$. As for neutral polymer adsorption, the size D_{e} of the electrostatic adsorption blob (or, more exactly, the inverse value, $(D_e/a)^{-1}$) measures the adsorption strength.

So far, the wall has been implicitly considered as penetrable to the monomers; this corresponds to the case where a short-range attraction of the monomers exactly counterbalances the hard-wall constraint. It seems more natural to consider an impenetrable hard wall. As usual, this entails an adsorption threshold. The chain can be decomposed into effective monomers of size λ_D; each of these units loses an energy of order $k_{\mathrm{B}}T$ upon adsorption and gains an electrostatic energy $(\lambda_D/a)^2 f(\lambda_D / \lambda)$. This sets the desorption threshold at $D_{\mathrm{e}} \sim \lambda_D$ and the strong screening regime where $D_{\mathrm{ads}} > \lambda_D$ does not exist. The same reasoning shows that in the absence of salt, the screened regime ($D_{ads} >> \lambda_D$) described by equation (1.40) also has a very small range of validity.

All these adsorption regimes correspond to the case where the interaction of the polyelectrolyte with the surface is stronger than the intra-chain Coulombic repulsions. The strength of the intra-chain repulsions is characterized by the electrostatic blob size or correlation length ξ_{e}. An electrostatic blob is the largest chain section that remains virtually unperturbed by intra-chain Coulombic repulsions and obeys Gaussian statistics.[37] The number of monomers in the electrostatic blob g_{e} is related to ξ_{e} as $g_{\mathrm{e}} \cong (\xi_e/a)^2$. The electrostatic free energy of an electrostatic blob is of order k_BT and

$$\xi_e \cong a(f^2\lambda_B/a)^{-1/3}. \qquad (1.44)$$

An isolated polyelectrolyte chain can then be pictured as a string of electrostatic blobs with a radius

$$R_e \cong N \xi_e / g_e \cong N a(f^2\lambda_B/a)^{1/3}. \quad (1.45)$$

The chain is stretched by the electrostatic repulsions in a Θ-solvent whenever $\xi_e << N^{1/2}a$. We only consider this case in the following.

Description of an adsorbed chain is valid if the chain thickness D_e is smaller than the Gaussian radius of the chains $R_0 \cong N^{1/2}a$, *i.e.* at high enough surface charge density. At lower surface charge density, a tethered polyion gets inclined by the Coulomb attractive force without any perturbation of the structure of the chain of electrostatic blobs. In this regime the average distance of the chain monomers from the surface decreases with increasing surface charge as[28a]

$$D_{ads} \cong \lambda/fN. \quad (1.46)$$

For polyelectrolyte chains in good or Θ -solvents, equation (1.46) has also been compared to Monte Carlo simulations in reference 29.

In many instances, the solvent (water) has a much higher dielectric constant than the substrate. The image charge of a test charge has the same sign as the test charge and almost the same value. The image charge repulsion dominates over the attraction of the wall if the attraction is weaker than the total direct electrostatic interaction between the monomers, *i.e.* if $D_e >> \xi_e$. When the surface charge is too weak, the chain is anchored normal to the surface.

1.5.2. Adsorption of a polyelectrolyte globule

A very weakly charged polyelectrolyte adopts a compact spherical globule shape in the absence of interaction with the surface because the intra-chain Coulomb repulsion is dominated by the interfacial free energy. This is the case if $\tau >> f^2N\lambda_B/a$.

No strong short-range attraction between the monomers and the surface except for the electrostatic attraction is assumed. More quantitatively, if γ_{ws} is the interfacial tensions between water and the bare surface and γ_{ps} between polymer and the bare surface, the difference γ_{ws} - γ_{ps} is small compared to the interfacial tension of the globule water interface γ. This is true for moderately hydrophobic surfaces. Otherwise, the globule adsorbs and spreads on the surface due to the hydrophobic attraction. This situation is not considered here.

Following 34, the strength of the short-range attraction between the monomers and the surface is characterized by the adsorption length $\xi_{ad} \sim \delta^{-1}a$, where $-k_BT\,\delta$ is the monomer-surface contact energy. Then γ_{ws} - $\gamma_{ps} \cong k_BT/\xi_t\xi_{ad}$ and the contact angle between the globule and the surface is given by Young's law, $\cos\theta \cong \xi_t/\xi_{ad}$. If we assume that $\xi_t << \xi_{ad}$, the

contact angle is $\theta \cong \pi/2$. In the absence of long-range Coulombic attraction, the weakly charged globule adopts on the surface a hemi-spherical shape.

The attraction of the charged monomers to the oppositely charged surface induces a compression of the globule in the z-direction at constant volume $V_{gl} \cong Na^3/\tau$. The globule is equivalent to an incompressible liquid droplet. The globule deformation leads to an increase in its surface area and thus to an increase of the interfacial free energy opposing the deformation. At small deformation, $D_{ads} \leq R_{gl}$ where D_{ads} is the globule thickness, the globule is deformed into an oblate ellipsoid, with an increase in interfacial area $\Delta A \cong (R_{gl} - D_{ads})^2$. The corresponding increase in the free energy is $F_{surf}/k_BT \cong \gamma(R_{gl} - D_{ads})^2$. When D_{ads} is much smaller than the unperturbed globule radius R_{gl}, the strongly confined globule has a pancake shape. The dominant contribution to the surface area of the globule is $\Delta A \cong V_{gl}/D_{ads}$. The associated free-energy penalty is

$$\boldsymbol{F_{surf}/k_BT \cong \gamma V_{gl}/D_{ads} \cong N\tau/D_{ads},\ \xi_t << D_{ads} << R_{gl}}. \qquad \textbf{(1.47)}$$

The elastic response of the confined globule is due to an increase in interfacial energy when the confinement occurs without deformation of the thermal blobs ($D_{ads} \geq \xi_t$). At stronger compression, $D_{ads} \leq \xi_t$, the thermal blobs are confined and the elastic response is the same as that of a confined Gaussian coil.

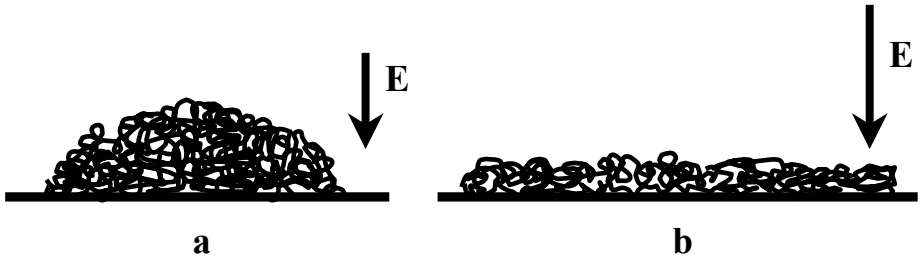

Figure 1.7 Adsorption of a weakly charged polyelectrolyte globule: weakly perturbed conformation at low surface charge density (a) and pancake conformation at high surface charge (b).

1.5.2.1.Adsorption from a salt-free solution

We consider first the low salt limit, $\lambda >> \lambda_D$. The Coulombic attraction energy of the globule by the surface is given by equation (1.35). At low surface charge density (*i.e.* at large λ) the charged monomers experience a linear attractive potential from the charged surface. This is equivalent to a gravitational field for an oil-in-water droplet on a weakly hydrophobic substrate. When the surface charge increases, the globule is progressively compressed in the z-direction and forms a flat pancake, with a contact angle $\theta \cong \pi/2$.

The globule is weakly compressed and its maximum thickness on the surface varies as

$$\boldsymbol{D_{ads} \cong R_{gl}\left(1 - \left(\frac{fN^{2/3}a}{\lambda\tau^{5/3}}\right)^{1/2}\right)} \qquad \textbf{(1.48)}$$

if $\lambda >> fN^{2/3}\tau^{-5/3}a$. This situation is illustrated in Figure 1.7a. In this weak-interaction regime, image charge effects may become important in the usual situation where the dielectric constant of the substrate is much lower than that of the solvent. The optimal position of the globule then shifts away from the wall or even disappears. The onset of strong perturbation (compression) of the globule by the Coulomb force occurs at $\lambda \cong fN^{2/3}\tau^{-5/3}a$. In the strong-deformation limit, $\lambda << fN^{2/3}\tau^{-5/3}a$, the globule is strongly compressed. The minimization of the total free energy $F_{surf} + F_{Coulomb}$ gives then

$$D_{ads} \cong \left(\frac{\lambda\tau}{fa}\right)^{1/2} a, \quad D_{ads} << \lambda, \tag{1.49}$$

while the lateral dimension of the compressed globule scales as

$$R_{II} \cong N^{1/2} a \left(\frac{\lambda\tau^3}{fa}\right)^{-1/4}, \quad D_{ads} << \lambda, \tag{1.50}$$

Equations (1.49) and (1.50) are valid if $D_{ads} << \lambda$, when there is no screening of the attractive interaction between the charged monomers and the surface. When the surface charge density increases ($\lambda \leq \tau a/f$), the counterions are localized close to the surface and screen the attraction between the charged monomers and the surface. The attractive electrostatic free energy is in this case given by equation (1.39) at $D_{ads} >> \lambda$ and the pancake thickness is

$$D_{ads} \cong \frac{\tau a}{f}, \quad D_{ads} >> \lambda, \tag{1.51}$$

$$R_{II} \cong N^{1/2} a \left(\frac{\tau^2}{f}\right)^{-1/2}, \quad D_{ads} << \lambda, \tag{1.52}$$

In the scaling approximation D_{ads} is then independent of the surface charge density.

This last regime exists only if the pancake thickness is larger than the thermal blob size, $\xi_t << f^{1/2}a$. This condition implies that the solvent is poor enough to induce a collapse of a chain sequence containing less than one charged monomer. In the opposite case, $\xi_t >> f^{1/2}a$, the crossover between equation (1.49) and equation (1.40) occurs with decreasing λ at $D_{ads} \cong \xi_t$, *i.e.* at $\lambda \cong fa/\tau^3$. Upon further increase in the surface charge density, the pancake thickness D_{ads} becomes smaller than ξ_t, and the elastic response of the polymer to compression is the same as that of a Gaussian coil. The adsorbed polyelectrolyte in this regime forms a flat layer of Gaussian "electrostatic adsorption blobs" of size $D_e \cong (\lambda/af)^{1/3}a$.

These results on flat pancakes are consistent if the thickness D_{ads} of the pancake is smaller than the globule size. The consistency condition is obtained by comparing D_{ads} given by equation (1.51) to the collapsed chain radius given by (1.29). This requires that $\tau \leq$

$(f^2\lambda_B/a)^{3/8}N^{1/4}$. This condition must be combined with the condition for existence of the globule $\tau >> f^2N\lambda_B/a$ that insures that the polymer is not in a necklace conformation. The strongly compressed regimes for adsorbed globules only exist at small enough charge ($f<<(a/\lambda_B)^{1/2}N^{-3/5}$). The region in the ($\tau$,$f$)-plane where a globular polyelectrolyte forms a flat pancake upon adsorption is displayed in Figure 1.8.

1.5.2.2. Adsorption at high ionic strength

Upon addition of salt the attractive interaction with the surface is screened and gets weaker. The effect of salt is negligible at weak ionic strength if the Debye screening length is larger than both the Gouy-Chapman length λ and the adsorbed layer thickness D_{ads}. We consider here the strong-screening limit where the screening is dominated by salt. It is convenient to treat the adsorbed polymer as a thin film and to use the language of thin-film physics.[38] The electrostatic free energy per unit area of a film of thickness D_{ads} is $F_{\text{Coulomb}}(D_{ads}) = \rho_{gl} \int_o^{D_{ads}} \psi(z)\mathrm{d}z$ and the disjoining pressure is $\Pi = -\frac{\partial F_{Colulomb}}{\partial D_{ads}} = -\rho_{gl}\,\psi(D_{ads})$.

The minimization of the total globule free energy at constant volume leads to $-\gamma = F_{\text{Coulomb}}(D_{ads}) + D_{ads}\,\Pi(D_{ads}) = \rho_{gl}\,[\int_o^{D_{ads}} \psi(z)\mathrm{d}z - D_{ads}\,\psi(D_{ads})]$.

If the surface is weakly charged, $\lambda >> \tau a/f$, the Gouy-Chapman potential given by equation (1.41) must be used and the adsorbed globule thickness is given by

$$\left(\frac{D_{ads}}{\lambda_D} + 1\right) exp\left(-\frac{D_{ads}}{\lambda_D}\right) = 1 - \frac{\lambda\tau a}{2\lambda_D^2 f}. \qquad \textbf{(1.53)}$$

When $\lambda >> \lambda_D > D_{ads}$, the thickness is the same as in the absence of added salt (D_{ads} (λ_D = 0) $\cong$ $(\lambda\tau/fa)^{1/2}$), as given by equation (1.49). When $(\lambda\tau/fa\ \lambda_D^2)^{1/2}a$ approaches $\sqrt{2}$, the thickness of the adsorbed globule diverges

$$D_{ads} \cong \lambda_D \left| ln\left(1 - \frac{\lambda\tau a}{2\lambda_D^2 f}\right)\right|$$

This means that when the Debye screening length becomes of the order of or smaller than the adsorbed globule thickness in the absence of salt, the globule is no longer confined and retains its hemispherical shape upon adsorption.

In the opposite limit where the surface is strongly charged $\lambda << \tau a/f$, the relevant electrostatic potential is given by (1.38). When the screening length is larger than the adsorbed globule thickness, the thickness is given by the result at zero ionic strength of equation (1.51) D_{ads} (λ_D = 0) $\cong$ aτ/f. When the screening length is smaller than the adsorbed globule thickness ($D_{ads} > > \lambda_D$), the adsorbed globule thickness is given by

$$\left(\frac{D_{ads}}{\lambda_D}+1\right)exp\left(-\frac{D_{ads}}{\lambda_D}\right)=\frac{\pi^2}{8}-\frac{\tau a}{4\lambda_D f}. \qquad (1.54)$$

When the Debye length approaches the thickness of the adsorbed layer in the absence of salt, the thickness of the adsorbed globule diverges as $D_{ads} \cong \lambda_D \left| ln\left(1-\frac{2\tau a}{\pi^2 \lambda_D f}\right)\right|$. As for a weakly charged surface, the adsorption becomes very weak when the screening length becomes equal to the thickness of the adsorbed globule at low ionic strength. This result is similar to the adsorption behavior of a polyelectrolyte chain in a Θ-solvent that "desorbs" when the screening length is of the order of the adsorbed chain thickness.

1.5.3. Adsorption of a polyelectrolyte necklace

In this section we consider the interaction of a polyelectrolyte chain in a necklace conformation with an oppositely charged surface. Both the intra-molecular Coulombic repulsions and the Coulombic attraction of the chain to the interface are important. We assume that the necklace contains many collapsed beads ($N_{bead} >> 1$); its dimensions are then given by equations (1.32,1.33).

We consider first the salt-free case and discuss the effect of increasing surface charge on the necklace conformation. At low surface charge density the electrostatic attraction between the chain and the surface is weak and induces only an inclination of the necklace towards the surface. As discussed in subchapter 1.5.1, the average distance D_{ads} of the chain monomers to the surface is then given by equation (1.46) irrespective of the solvent quality. This inclination occurs as long as $D_{ads} \geq d_{bead}$, which is the case if $\lambda \geq N^{3/2} f^{4/3} \tau^{-1/2} u^{1/6} a$.

At higher surface charge density the necklace is confined in the transverse z-direction. The confinement free energy is that of a Gaussian chain, $F_{conf}/k_BT \cong d_{bead}^2/D_{ads}^2$. The balance with the electrostatic attraction to the surface gives the thickness of the adsorbed necklace

$$D_{ads} \cong \left(\frac{\lambda \lambda_B^{1/2} a^{3/2}}{\tau^{3/2}}\right)^{1/3}. \qquad (1.55)$$

The thickness of the adsorbed necklace as given by equation (1.55) does not depend on N, which is the signature of an initial stage of adsorption. Obviously, equation (1.55) can only be valid if the thickness is larger than the globule size $D \geq \xi_e$, or $\lambda \geq (a\tau/\lambda_B)^{3/2} f^2 a$.

Upon further increase of the surface charge, the thickness of the adsorbed necklace remains constant until the beads get confined. According to the results of the previous section, this occurs if $\lambda \cong f\, g_{bead}^{2/3} \tau^{5/3} a$, or $\lambda \leq (\tau^{-1} f^{-1/3} \lambda_B^{-2/3} a^{5/3})$. The conformation of the chain is then a two-dimensional necklace of pancakes (the confined beads). The Rayleigh instability also

exists in two dimensions in the absence of salt when the local screening length close to the surface (λ) is larger than the size of the two-dimensional beads.[33] The thickness of the compressed beads, D_{ads}, is given by equation (1.49). The lateral size of the pancake beads and the number of monomers in one bead are obtained from the calculation on the two-dimensional Rayleigh instability.[33] The line tension is here $\gamma_s = \gamma D_{ads}$ and the surface charge density $q_s = f\tau D/a^3$. One obtains a number of monomers in the beads $g_{bead}^{2d} \cong \tau a^{-3} d_{||}^2 D_{ads} \cong g_{bead}$, where $d_{||}$ is the in-plane radius of each bead. The number of monomers in a bead and the number of beads therefore remain constant upon adsorption (at least at the scaling level). The in-plane size of the beads is then

$$d_{||} \cong (f^{3/2} \lambda_B \lambda \tau / a^3)^{-1/4} a. \qquad (1.56)$$

With increasing surface charge density, the concentration of counterions in the vicinity of the surface progressively increases; this enhances the screening of the interbead Coulombic repulsion. The local screening length in the vicinity of the surface is roughly equal to the Gouy-Chapman length λ. The screening is not however exponential. Therefore, when $\lambda \le d_{||}$, the Coulomb repulsion between beads is screened at scales larger than λ and an adsorbed necklace assumes a uniform pancake conformation, similar to that described in subchapter 1.5.2.1 and shown in Figure 1.7b. This happens when $\lambda \le f^{3/5} \lambda_B^{-2/5} \tau^{-1/5} a^{7/5}$.

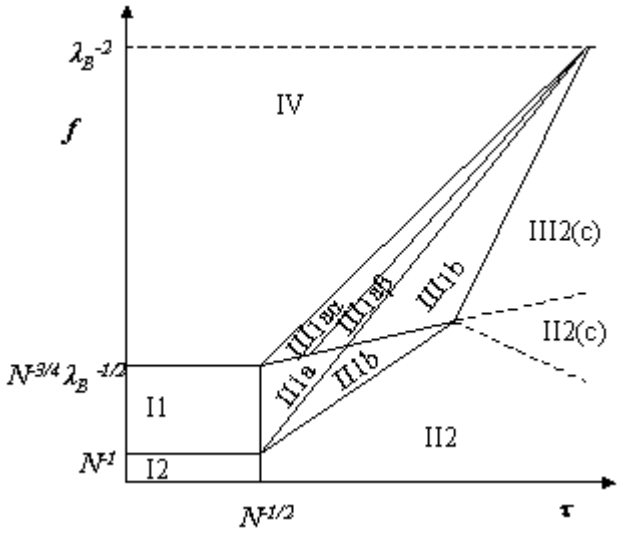

Figure 1.8 Adsorption of a polyelectrolyte in poor solvent. Notations are as in Figure 1.5. Index 2 means that the globule/pearls are not compressed. Index 1 indicates regions with confined globules/pearls. Index "a" denotes regimes where the polymer becomes first Gaussian at all scales when the surface charge is increased. (Index "b" corresponds to regimes where the interaction with the wall becomes short-ranged first.) In regime III1-aα no lateral collapse is predicted upon increase of the surface charge (in contrast to regime III1-aβ). (c) denotes regions where counterion condensation takes place in the bulk.

As long as the adsorbed globule retains the necklace structure, the strings between beads are also confined by the attraction to the surface. The confinement of the strings is described by the results for polyelectrolyte chains in a Θ solvent given by equation (1.40); it is expected when $\lambda \le f^{-1/2} \lambda_B^{-3/4} \tau^{-3/4} a^{7/4}$.

The change of conformation of a charged necklace adsorbed on an oppositely charged surface when the surface charge increases (or the Gouy-Chapman length decreases) depends

on the relative values of the solvent quality and the fraction of charged monomers. The various possible regimes are represented in a τ-f diagram in Figure 1.8:

i) If $\tau \leq f^{1/2}$, or $\xi_t \geq f^{1/2}a$, there are 2 options:

– if $f^{4/7}(\lambda_B/a)^{1/7} \geq \tau \geq f^{2/3}(\lambda_B/a)^{1/3}$ (region III-1- aα in Figure 1.8), both the thickness of the beads and that of the strings decrease with the surface charge and become equal to ξ_t when $\lambda \cong fa/\tau^3$; at this point the beads are completely unfolded into a monolayer of thermal blobs and the lateral dimension of a bead $\sim \xi_t \sqrt{g_{bead} / g_t}$ coincides with the length of a string; at higher surface charge (smaller λ), the necklace behaves as a polyelectrolyte in a Θ solvent and the adsorption occurs according to the same scenario as for the Gaussian chain;

– if $f^{1/2} \geq \tau \geq f^{4/7}(\lambda_B/a)^{1/7}$, in region III-1-aβ, the coalescence of the beads into a uniform pancake when $\lambda \cong f^{3/5}\lambda_B^{-2/5}\tau^{-1/5}a^{7/5}$ is followed by an unfolding of the two-dimensional globule into a monolayer of thermal blobs when $\lambda \cong f\tau^{-3}$. At smaller values of λ, the scenario of regime III-1- aα is recovered.

ii) If $\tau \geq f^{1/2}$, *i.e.* $\xi_t \leq f^{1/2}a$, two regions must be distinguished:

– if $\tau \leq f^{1/3}\lambda_B^{-1/3}a^{1/3}$, in region III-1-b, the coalescence of the beads in a laterally uniform pancake occurs when $\lambda \leq f^{3/5}\lambda_B^{-2/5}\tau^{-1/5}a^{7/5}$. Upon further increase of the surface charge, the thickness of the pancake decreases as $D_{ads} \cong (\lambda\tau/af)^{1/2}a$ and then levels off at $D_{ads} \cong a\tau/f$ when $\lambda \leq \tau a/f$;

– if $\tau \geq f^{1/3}\lambda_B^{-1/3}a^{1/3}$, in region III-2-(c), the solvent quality is poor enough to prevent compression of the beads by the Coulombic attraction of the oppositely charged surface. In this regime the counterions condensate on the beads stabilizing the single globule against the necklace as in the bulk.

The effect of added salt on the adsorption of a necklace is very similar to that described above for a globule and will not be described in detail: if the salt concentration increases so that the screening length λ_B becomes smaller than the thickness D_{ads} in the absence of salt, the chain desorbs. However, in case of a necklace the addition of salt also influences the intra-molecular interactions. If $\lambda_B \leq \xi_e$, the inter-bead Coulomb repulsions are screened and the necklace in the bulk collapses into a spherical globule. For an adsorbed necklace, we expect lateral coalescence of confined beads to occur at even lower salt concentration, when the screening length becomes comparable to the lateral dimensions of the compressed beads.

In summary, the conformation of a polyelectrolyte in a poor solvent adsorbed onto an oppositely charged interface is determined by the balance of i) the electrostatic attraction of the charged monomers to the surface; ii) intra-chain Coulombic repulsion between charged monomers and iii) the surface free energy of the deformed globule interface. Both the

Coulombic interaction between the chain and the interface and the intra-chain Coulombic repulsion are screened by addition of salt in the solution and by the localization of the counterions near the strongly charged surface. Adsorption can be induced either by increasing the surface charge density or by decreasing the ionic strength of the solution.

The conformation of an adsorbed chain in the globular state leads to flat pancakes on the surface. This is very similar to the flattening of a liquid drop on a solid surface under the influence of gravity.

For an adsorbed polyelectrolyte necklace, an increase of the ionic strength of the solution results first in the coalescence of compressed beads into a uniform pancake and then to a desorption. An increase in the surface charge density at low ionic strength results in the compression of adsorbed globular beads and (at sufficiently low ionic strength) in the coalescence of the beads to form a uniform pancake.

The main limitation of discribed approach is that the local charge density of the polymer had been always considered as weak. Even when f is small, when the polymer collapses, the local charge density may become large and induce counterion condensation. Note however that even in the bulk, when the counterions condense on the beads of a necklace polyelectrolyte, the necklace structure does not remain stable and collapses to a globule. This must be taken into account in region III-2-(c) of Figure 1.8.

Chapter 2.

Research Methodology

2.1. Atomic Force Microscopy (AFM)

AFM belong to a family of Scanning Probe Microscopy (SPM) instruments that are used to measure properties of surfaces. The development of the AFM was preceded by the development of the Scanning Tunneling Microscope (STM) in 1981 at IBM Zurich Research Laboratory by Binnig and Rohrer.[39] Its ability to view the atomic lattice of a sample surface earned the inventors the Nobel Prize in Physics in 1986. Although the STM provides subangstrom resolution in all three dimensions, it is limited to conductive and semiconductive samples. To image insulators as well as conductors, the Atomic Force Microscope (AFM) soon renamed as Scanning Force Microscopy (SFM) was developed in 1986.[40] AFM involves scanning a sharp tip across the sample surface while monitoring the tip-sample interaction to form three-dimensional surface topography image of nanometer lateral and subangstrom vertical resolution. In addition to the favourable imaging conditions and the high resolution, AFM offers a variety of new contrast mechanisms which provide information on differences in friction, adhesion, elasticity, hardness, electric fields, magnetic fields, carrier concentration, temperature distribution, spreading resistance, and conductivity.

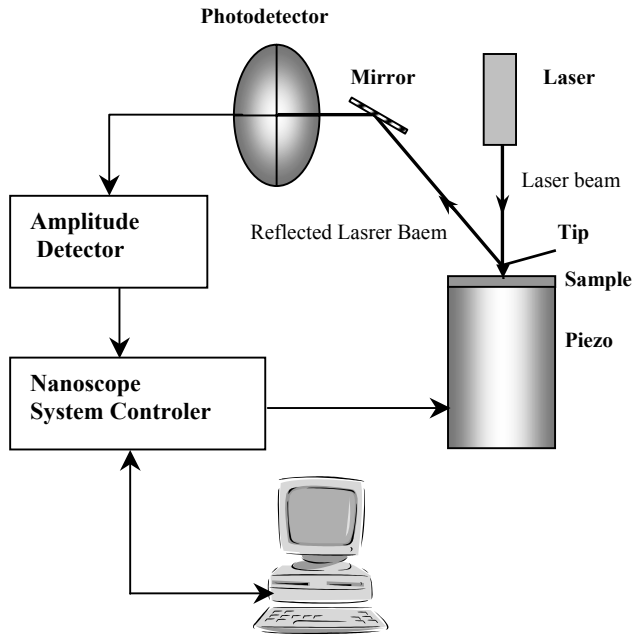

Figure 2.1 Scheme of AFM microscope.

A principle schematic of AFM is shown in Figure 2.1. A sharp tip on the end of a flexible cantilever moves across a sample surface. The scanning motion is conducted by a piezoelectric tube scanner which scans the sample in a raster pattern with respect to the tip (or scans to the tip with respect to the sample). The tip-sample interaction is monitored by reflecting a laser off the back of the cantilever into a split photodiode detector. By detecting the difference in the photodetector output voltages, changes in the cantilever deflection or oscillation amplitude are determined. A feedback loop maintains a constant tip-surface interaction force by vertically moving the scanner to maintain a constant photodetector difference signal. The distance the scanner

moves vertically at each x,y data point is stored by the computer to form the topographic image of the sample surface.[41]

2.1.1. Operating and Imaging Modes

In general, physical nature and character of tip-sample interaction are quite complicated, since they are defined by tip characteristics, surface properties and surrounding medium. For investigation of not charged surfaces under ambient condition the main forces which contribute to exert the tip are: repulsive force coming from mechanical contact of tip end atoms with sample, van der Waals force and capillary force arising from condensation of water vapour in the contact area.

Scanning force microscopes can be operated in many ways measuring different interactions between the probe tip and sample and using different types of detection schemes.

Operating modes can be roughly classified as "contact", "non-contact", and "intermittent contact" modes depending on the sign of the forces exerted on the tip[42] (Figure 2.2). When the AFM is operating in the attractive region, it is called "non-contact". In this region, the cantilever is bent toward the sample, since it is being pulled by attractive forces. Operation in the repulsive region is called "contact" imaging. Here, the cantilever is bent away from the sample due to the sample deformation. If an oscillatory tip displacement is sufficiently large to pass through both regions, the probe experiences both attractive and repulsive forces. These modes are called "intermittent contact" or tapping mode.

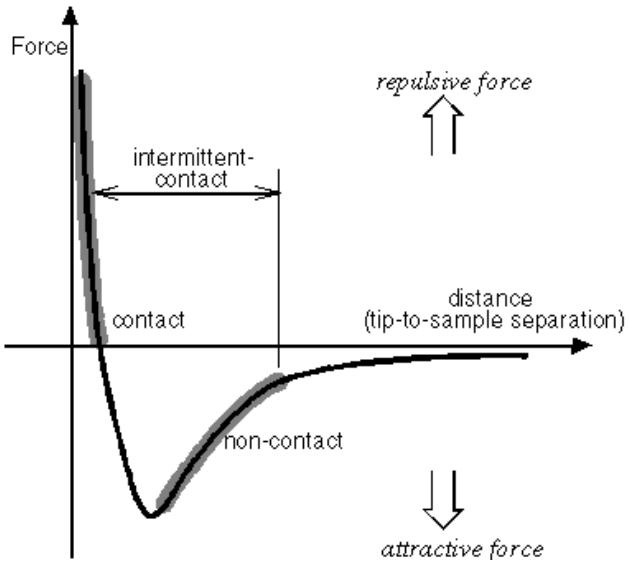

Figure 2.2 Force interactions between the sample surface and the probing tip.

The two most commonly used modes of operation are contact mode AFM and TappingMode™ AFM, which are conducted in air or liquid environments. In contact mode the scanning probe is essentially dragged across a sample surface while monitoring the change in cantilever deflection with the photodiode detector. The tip interacts with the sample, and the cantilever bends according to the Hooke's law: $F = kz$, where F, k, and z are the applied force, the cantilever spring constant, and cantilever deflection, respectively. The feedback loop maintains a constant force during imaging, which typically ranges between 0.1

to 100nN. Low spring constant (k < 0,1 N/m) probes are typically used to minimize the value of the applied force. Contact mode works well for hard surfaces in ambient conditions and in liquid. In the case of scanning soft polymeric materials the tip penetrates into the material and damages it upon movement in lateral directions.[43] This happens on soft materials even at negative deflection set-points.

Tapping Mode (TM) AFM was developed for investigation of soft materials.[44, 45] In this mode, the cantilever oscillates near its resonant frequency f_0 and lightly "tapping" on the surface during scanning. The tip rapidly moves in and out of the sample surface with an amplitude which is sufficiently high to overcome adhesion forces[44] so that it stays in contact only for a short fraction of the oscillation period. Depending on the cantilever type, the frequency typically varies from 50 to 500 kHz, and the amplitude changes up to 100 nm. The laser deflection method is used to detect the root-mean-square (RMS) amplitude of cantilever oscillation. A feedback loop maintains a constant oscillation amplitude at a certain value (amplitude set-point A_{sp}) by moving the scanner vertically at every x,y data point. Recording this movement forms the topographical image.

In order to understand the origin of the images in taping mode AFM, it is instructive to examine the cantilever response as a function of the distance at a fixed lateral position. Figure 2.3 depicts variation of the tip amplitude, A, as a function of the cantilever-base displacement Z. At large distances, the cantilever oscillates with a constant amplitude which is determined by viscous damping of the cantilever body in air. When approaching the surface, the tip starts to interact with the surface. Eventually, the oscillations become unstable and the tip jumps into contact. Still the energy of the cantilever is high enough to overcome adhesion forces and to be detached from the surface. When the tip enters the intermittent contact range ($Z<Z_0$), the amplitude of oscillation linearly reduces and the contact duration increase with decreasing the distance between the surface and the cantilever base. At some point, the amplitude drops rapidly and the tip become trapped by the sample. Beyond this point, the tip stays permanently in contact with the surface.

The deviation of the amplitude signal from a certain set-point value A_{sp} is used by a feedback loop to maintain the separation Z between the tip and sample constant, and hereby visualize the surface structure. The lower is the set-point (or the amplitude set-point ratio A_{sp}/A_0, where A_0 is the amplitude of free oscillations), the closer the tip can come to the sample. When the surface composition is uniform, the amplitude variation is mainly caused by the surface topography. However, if the surface is heterogeneous, the variation in the

amplitude can be affected by local differences in viscoelasticity[46,47,43] and adhesion[48] of the sample.

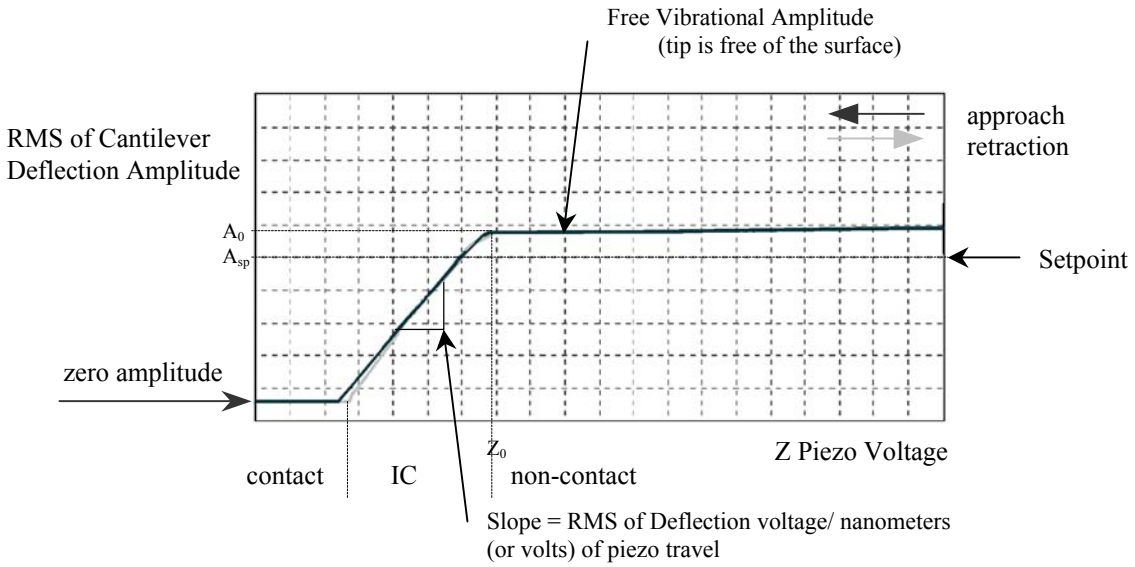

Figure 2.3 Typical amplitude-distance curve.

The advantage of tapping mode with respect to contact mode is that it eliminates the lateral, shear forces present in contact mode. The time of contact of the tip with the surface and the friction energy are from one to two orders smaller in the tapping mode than in the contact mode.[49] This enables TM to image soft, fragile, and adhesive surfaces without damaging them, which can be a drawback of contact mode AFM. TM is now the scanning mode of choice for most applications, particularly for soft surfaces like polymers.

2.1.2. Measurements in Liquid

AFM applications can be carried out in a variety of environments. One of the main advantages of scanning force microscopy is its ability to perform in situ imaging in liquids, something not possible with electron microscopy. Morphology variation and interfacial forces at the liquid/solid interface can be investigated as a function of the solvent quality, the ionic strength, and pH.[50,51,52,53,54] In addition, the immersion of the tip into the liquid prevents capillary condensation and may cause disjoining pressure. Consequently, the repulsive force exerted on the sample can be set lower than in air, so that soft polymers and biological samples can be imaged without distortion of their native structure.[55]

The surface deformation could be reduced even further with intermittent contact AFM. Tapping mode imaging in liquids has been used mainly for biological systems such as DNA,[56] cells,[57] chromosomes and proteins.[58] However, it turned out to be rather tricky to perform the measurements. The resonant frequencies were usually 2–5 times lower than in air and the

resonant peak gets strongly dampened and broadened.[59,60] The preferred probes for TappingMode in fluid are the short V-shaped silicon nitride cantilevers with low stiffness.[61] For this probes the resonant frequency in fluid is a broad peak between 7-12kHz.

Imaging samples in a hydrated state with an AFM is commonly performed by enclosing the sample and probe in a fluid environment, as shown in Figure 2.4. The fluid cell consists of a small glass assembly with a wire clip for holding an AFM probe. The glass surfaces provide a flat, beveled interface so that the AFM laser beam may pass into the fluid without being distorted by an unstable fluid surface. It must be noted that not only the tip choice but also the design and operation of a fluid cell is of great importance. The cell should be inert against the liquid and sealed in order to avoid leakage or evaporation of the liquid. Any variation of the total mass changes the resonant properties of the cantilever assembly. It can disturb the measurements or even result in unstable imaging conditions. The use of an o-ring is recommended when fluid exchange in the cell is desired or when evaporation is an issue (e.g., working with heated fluids or solvents). Otherwise, capillary forces are strong enough to ensure that the fluid remains in between the substrate and the fluid cell and does not overflow onto the scanner. A small amount of fluid should be used in that case (typically ~100μL), which also presents the advantage of limiting thermal drift problems.[62] Both the liquid and the sample surface should be of maximum purity. Adsorption of some contaminant on the surface of the cantilever or the probe tip has to be taken into account as it can result in imaging artefacts and even destruction of the force sensor. The description of different designs of fluid cells can be found elsewhere.[63]

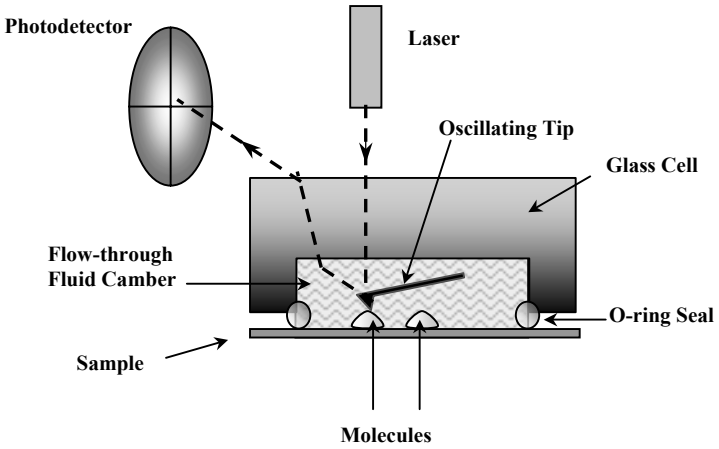

Figure 2.4 Fluid cell for an AFM which allows imaging in an enclosed, liquid environment.

2.1.3. Calibration of the Tip Shape

One of the key component in the AFM system is the probe, or tip, since AFM image is always a result of the interaction of the tip shape with the surface topography. With today's sophisticated technology, tip/cantilever assemblies (Figure 2.5a) can be mass-produced with consistently-shaped, very sharp tips. These tips are secured on the end of cantilevers which have a wide range of properties designed for a variety of scanning technologies. The tips are

micro-fabricated from silicon or silicon nitride and they are usually either conic or pyramidal in shape. Although the shape of the tip does have some effect on its imaging properties, the critical part of the tip is the absolute apex, which typically has an end radius of 2 nm to 20 nm, depending on the tip type.

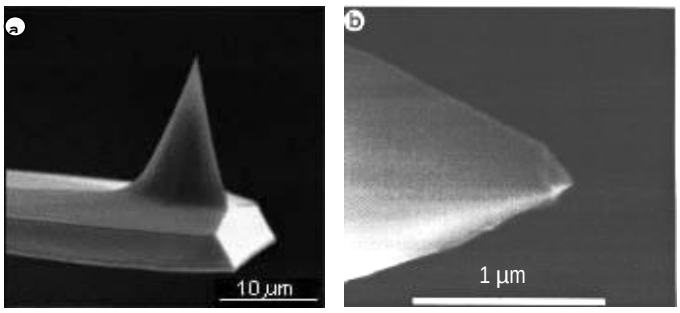

Figure 2.5 SEM image of an integrated single crystal silicon tip/cantilever assembly (a) and tip[64] (b) used in non-contact atomic force microscopy.

The tip geometry is crucial for imaging of surface structures which are commensurate with the tip shape. The finite size of the AFM tip does not allow the tip to accurately probe narrow or sharp features on a sample, resulting in underestimation of surface roughness and rounding/broadening of sharp surface features. Additionally, blunt tip is unable to reach down into narrow valleys. This can be seen in the example below (Figure 2.6). These and other artefacts originating from convolution of the tip shape with the surface topography have been discussed elsewhere.[65, 66, 67]

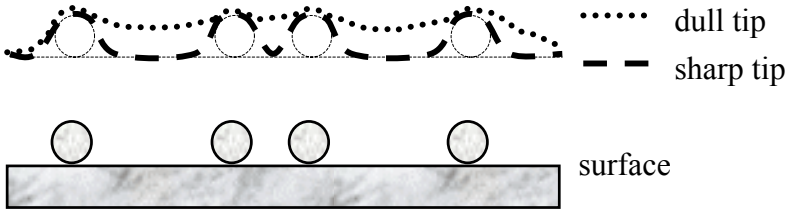

Figure 2.6 Schematics and topographic profiles of spheres recorded with sharp and dull probe.

Since tips with an infinite aspect ratio do not exist,[68, 69] they require a special procedure to calibrate their unknown geometry. Electron microscopy provides valuable information on the overall shape of the tip[67] (Figure 2.5b), however it is less suitable for characterization of the nanometer sized probe apex.

Calibration method of the tip shape bases on extraction of the tip geometry from the topographic profile of the specially designed substrate. This procedure can be done before, during of or immediately after the experiment in order to monitor the degradation of the tip over extended use. Depending on the substrate structure, this approach can be used for microscopic characterization of the overall shape of the tip as well as nanoscopic characterization of the probe apex. In order to measure the radius of the probe apex and identify atomic scale asperities on it, one has to use native structures whose geometry is

strictly defined. Figure 2.7 shows different substrates which can be used for calibration of probe apex.

1. Spherical particles of gold with a diameter below 100 nm were used to calibrate the tip shape and evaluate the lateral dimensions of biomolecules.[70] When the particle is smaller than the tip curvature ($r<R$), the tip radius can be determined directly from the SFM profile as $\boldsymbol{R=L^2/4r}$ (Figure 2.7a). This calibration method works rather well if the particle has perfect spherical shape, is rigid, and do not move during the scanning process.

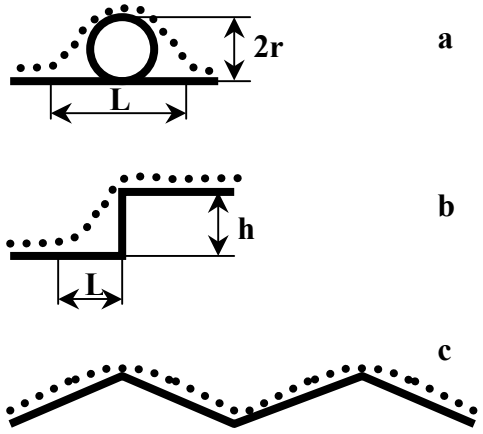

Figure 2.7 Different methods for the shape calibration of the probe apex using: small sphere ($r<R$) (a); a terrace of height h (b); a saw tooth surface of a single crystal formed of alternating crystalline planes (c).

2. Crystalline steps enable very easy measurement the tip radius using the equation $\boldsymbol{R=L^2/2h}$, where h is the step height (Figure 2.7b). This calibration method requires a rigid substrate with many steps which are uniform in height in a range of 1–10 nm.
3. Single crystals with a stepped surface structure prepared by cutting a crystal at a certain angle relatively to the main crystallographic planes represent one of the most accurate calibration techniques (Figure 2.7c). This calibration method can be used to quantify the contact area required for characterization of micromechanical surface properties such as friction[71] and hardness.[72]

2.1.4. AFM Experimental Setup

Multimode™ Nanoscope IIIa and Dimension™ 3100 Nanoscope IIIa (or Nanoscope IV) Atomic Force Microscopes (AFM) produced by Digital Instruments, Santa Barbara, USA was used for sample characterization.

The usual settings for *tapping mode* were as follows: scan rate 0.4-1.2 Hz, the proportional and internal gains 1.0-3.0 and 0.1-0.3, respectively, with ratio of the first to the second close to 10. The amplitude set-point ratio (A_{sp}/A_0) was in the range of 0.99-0.85 for the "light" tapping mode. All measurements were done at ambient conditions (temperature 21 ± 20^0 C; relative humidity 50-70 %). We observed no effect of humidity on the visualized conformations of PE molecules.

AFM in fluid. Fluid cells consist of a glass cantilever holder and silicon o-ring to form an enclosed fluid environment with the ability to exchange liquids was used for measurements in

fluid. Tapping mode in fluid was conducted by oscillating the cantilever acoustically (traditional).

Types of cantilevers and tips:

Si cantilevers for intermittent contact (tapping) mode AFM with ultrasharp tips type NSC16/Al BS from *MikroMasch*,[73] Estonia. Radius of curvature <10 nm, tip height (H) 15-20 μm, full tip cone angle 30º. Typical cantilever length (L) 230±5 μm, cantilever width (W) 40±3 μm, cantilever thickness (d) 7.0±0.5 μm. Resonant frequency 170±20 kHz, average spring constant (k) 40 (min 25, max 60) N/m. The reflective side coated with Al.

n^+-Si cantilevers for non-contact/tapping™ mode AFM type A-NCH from *Nanosensors,*[74] *Switzerland.* Resistivity (Ω´) 0.01-0.025 Ohm·cm, H = 10-15 μm, L = 117 μm, W = 28-30 μm, d = 3.7-4.5 μm. Resonant frequency 348-424 kHz, k = 39-72 N/m.

n^+-Si cantilevers for non-contact/tapping™ mode AFM type FM from Nanosensors. Resistivity (Ω´) 0.01-0.025 Ohm·cm, L = 219 μm, W = 21-23 μm, d = 2.5-3.4 μm. Resonant frequency 67-87 kHz, k = 1.3-3.6 N/m.

Silicon probes for tapping/intermittent contact mode AFM model BS-Tap300 from BudgetSensors,[75] *Bulgaria*. Tip radius <10 nm, H = 17±2 μm, L = 125±10 μm, W = 30±5 μm, d = 4±1 μm. Resonant frequency 300±100 kHz, k = 40 N/m (min 20 N/m, max 75 N/m).

Oxide-sharpened silicon nitride probes for contact mode AFM and for TappingMode AFM in liquid with acoustic drive type DPN from Veeco Instuments Inc.,[76] *USA.* V-shaped cantilever configuration, spring constants 0.32 N/m, nominal tip radius of curvature 5 - 40nm, cantilever thickness 0.6 μm (min 0.4 μm, max 0.7 μm), cantilever lengths 100 μm, tip half angle 35°, gold reflective coating.

In single molecule experiments tips were used after the calibration with gold nanoparticles (diameter 5.22 nm, Pelco™ AFM Gold Standard Kit) to evaluate the tip radius. Most measurements were done with the tip radius 14.9 ± 1.9 nm. The dimensions of structures obtained from AFM images were corrected (decreased) by the tip radius according to the standard procedure [77] (see section 2.1.3).

2.2. Dynamic Light Scattering (DLS)

2.2.1. Fundamentals of the Method

Dynamic light scattering (DLS) provide structural information of polymer in solution, e.g., the translational diffusion coefficient and the hydrodynamic radius of the scattering particles.[78] With this method particle sizes within a range from nm up to several μm can be determined. The theory of DLS or photon correlation spectroscopy is described in details in several classical textbooks.[79] We will limit ourselves to a few brief points relevant to our discussion.

Due to the Brownian motion of the scattering particles in solution, a shift of the frequency of the scattered light occurs in analogy to the well-known Doppler effect of acoustic waves. The diffusion coefficient of the particles can be obtained from the analysis of the line with of the spectral density profile of the scattered light. However, the slow motion of the particles leads to very small frequency shift, which cannot be measured with sufficient accuracy by optical methods. Fortunately, the spectral density profile is physically equivalent and related by a Fourier transformation to a time-dependent autocorrelation function of the photon current, which can be computed by a digital correlator.

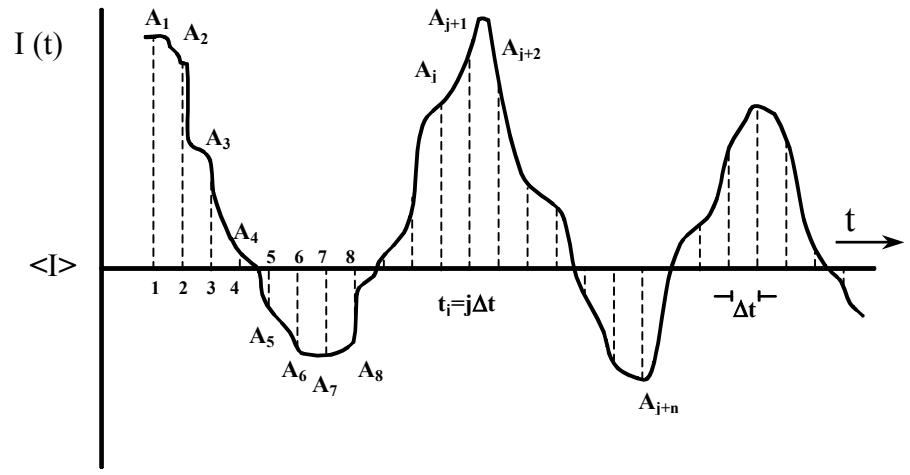

Figure 2.8 Schematic representation of the fluctuations in the scattered intensity as a function of time. <I> is the average value of the scattered intensity, Δt is an observation time interval and determines the temporal resolution of the DLS experiment.

The correlation function of scattered intensity is given by

$$G^{(2)}(t) = \langle I(t)I(0)\rangle = \lim_{T\to\infty} \frac{1}{T}\int_0^T I(t)\cdot I(t+\tau)dt\,. \qquad (2.1)$$

Division by mean square of intensity results in normalized intensity correlation function:

$$g^{(2)}(\tau) = \frac{\langle I(t) \cdot I(t+\tau) \rangle}{\langle I(t) \rangle^2} \tag{2.2}$$

Typical autocorrelation function of polyelectrolyte in water solution is shown on Figure 2.9.

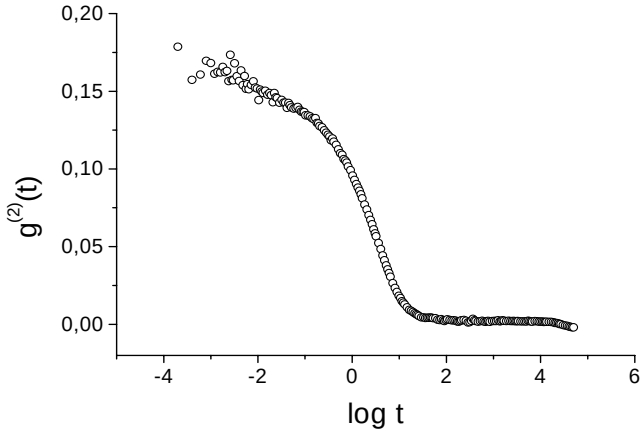

Figure 2.9 Autocorrelation function of polyelectrolyte in water solution

Profile of scattered light $g^{(2)}(t)$ is related to the correlation function $g^{(1)}(t)$ of the electric field by the Siegert relation

$$g^{(2)}(t) = (1 + \beta \cdot |g^{(1)}(t)|^2) \tag{2.3}$$

The factor β in front of the dynamic part of the autocorrelation function is called the coherence factor, $0 \leq \beta \leq 1$. It is constant that depends on the number of coherence areas that generates the signal.

For monodisperse system of particles, the simple expression is valid:

$$g^{(1)}(t) = exp(-t/\tau) \tag{2.4}$$

where τ is the relaxation time $1/\tau = D \cdot g^2$, D is the translational diffusion coefficient and g is the scattering vector.

Length of the scattering vector $g = \frac{4\pi \cdot n}{\lambda_0} sin(\theta/2)$, λ_0 is the laser wavelength in vacuum (HeNe laser, 632,8 nm), n – refractive index of the medium (water), θ is the scattering angle (90°).

Using Einstein-Stokes equation $D = \frac{k_B T}{6\pi \cdot \eta_0 \cdot R_h}$, the hydrodynamic radius R_h can be calculated from the diffusion coefficient D

$$R_h = \frac{k_B T}{6\pi \cdot \eta_0 \cdot D} = \frac{k_B T}{6\pi \cdot \eta_0} \cdot \tau \cdot g^2 \qquad (2.5)$$

where η_0 is the viscosity of the solvent, T the temperature in Kelvin and k_B the Boltzmann's constant.

For polydisperse system $g^{(1)}(t)$ is given by an integral equation:

$$g^{(1)}(t) = \int_0^\infty A(\tau) e^{-t/\tau} d\tau \qquad (2.6)$$

where $A(\tau)$ is the normalized distribution function of the relaxation time.

2.2.2. Experimental Setup

The dynamic light-scattering instrument schematically represented on Figure 2.10. It employs an ALV5000/E correlator. The source of light is Spectra Physics 125A HeNe laser operated at 632,8 nm. The correletor was operated in the autocorrelation mode, which enable to have still strong enough scattering signal for the photomultiplier and detection electronics while working with solutions of very low concentration. The measured intensity correlation functions $g^{(2)}(t)$ were analyzed using nonlinear inverse Laplace transformation to obtain the distributions of relaxation times $A(\tau)$, which can be easily recalculated to the distributions of hydrodynamic radius of the scattering particles $A(R_h)$ using the Stokes-Einstein relation.

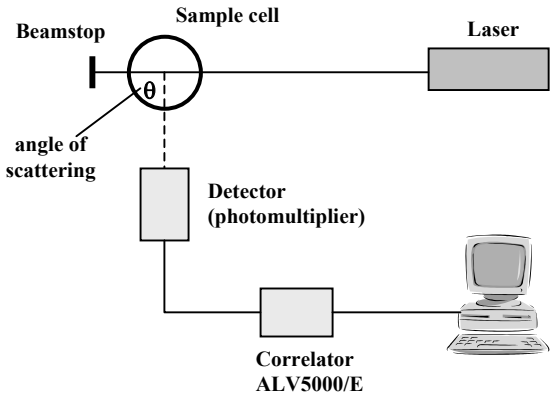

Figure 2.10 Scheme of experimental setup of dynamic light-scattering instrument.

Chapter 3.

Conformational Transitions of Polyelectrolytes

In this chapter we show that hydrophobic flexible polyelectrolyte molecules of poly(2-vinylpyridine) and poly(methacryloyloxyethyl dimethylbenzyl ammonium chloride) are trapped and frozen due to adsorption on the mica surface and that the single molecule structures observed with AFM reflect the molecular conformation in solution. Increase of ionic strength of the solution induces a cascade of abrupt conformational transitions due to the intra-chain segregation ranging from elongated coil to compact globule conformations through intermediate pearl necklace globule conformations with different amount of beads per chain. Length of the necklaces and number of beads decreases, while diameter of beads increases with the increase of ionic strength. Co-existence of extended coils, necklaces with different amount of beads and compact globules at the same time indicates a cascade of first-order-type phase transitions.

3.1. Introduction

PE macromolecules undergo diverse conformational transitions responding to change of environment (ionic strength, pH, condensation agents, temperature, concentration) driven by interplay between attractive short range van der Waals and repulsive long range Coulomb interactions. A change of PE conformations in controlled environment and, particularly, coil-to-globule transition (CGT) phenomena attracts continuously enhanced interest due to their importance in industry and nature.[5] For example, gelation of PE in water and reversible swelling or shrinking of PE gels responding to external stimuli is considered to be one of the most promising properties of PE[80] based on CGT phenomenon.

CGT is considered to be a complicated process when the transition character depends on chain stiffness and specific interactions in the system.[81] Traditionally polymer science considers CGT for flexible polymer chains as a gradual process which is associated with the second-order phase transition[9] (Figure 3.1A), while for stiff polymers the theory suggests[9,82] the sharp first-order phase transition (Figure 3.1C). In contrast to the theoretical predictions many experimental results have indicated continuos character of CGT for different flexible and stiff polymer chains.[83] Single molecule experiments with stiff DNA molecules[84] and brush molecules[85] have shown that an individual chain exhibits a first-order phase transition between an elongated coil and an spherical or *ordered* toroidal[86] globule while this transition appears continuous in the ensemble.

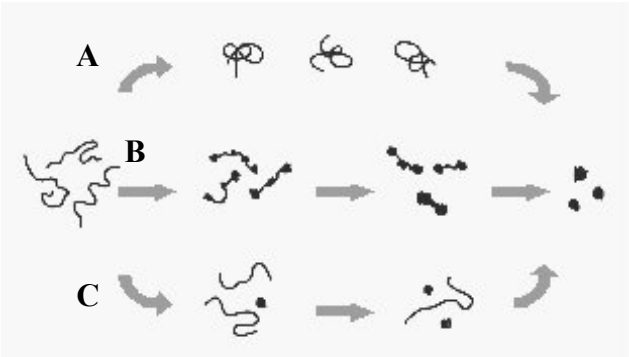

Figure 3.1 Outline of different CGT mechanisms for PE in poor solvent: continuous second order phase transition (A); cascade of first order transitions between necklaces, assumed for flexible PE (B), abrupt two-state first order transition, found for stiff PE (C).

In contrast, DNA modified by synthetic polymers undergo continuous second-order phase transition through the set of partially collapsed *disordered* intra-segregated conformations.[87] That displays the general tendency for polymers when highly cooperative all-or-non character of collapse transitions usually is realized for ordered folding reactions[88] or very stiff molecules,[82] if in both cases the density of the compact state is much lower than the density of

coil.[89] The mechanism of CGT for synthetic flexible PE on the single molecule level is still intensively discussing.

CGT for PE has a specific character due to the additional free energy component introduced by the Coulomb interaction, which, first of all, causes the influence of charge density on conformations of PE coil and globule. This effect is much more pronounced in the case of flexible PE as compared to stiff DNA molecules characterized with intrinsic stiffness introduced by intramolecular hydrogen bonds. Electrostatic repulsion affects elongated conformations of PE coils. Khokhlov has proposed a cylindrical conformation for the deformed weakly charged flexible PE globule in poor solvent.[90] Recent theoretical analysis predict intermediate necklace-like conformations of weakly charged flexible PE chains (DRO model), when the chains adopt conformations resembling a sequence of polymer beads interconnected by narrow strings.[91] The theory suggests that a decrease of the charge density leads to a cascade of abrupt transitions between necklaces with different numbers of beads. Consequently, such a transition is an alternative to a continuous transition pass from coil to globule conformation of PE molecules and may be considered as a sequence of intrinsic first-order transitions between necklaces (Figure 3.1B). There are several experimental reports confirming these theoretical predictions.[92] However, it has been difficult to obtain fully conclusive results about mechanism of CGT in a single PE chain, because the competition between single-chain events and an aggregation of several chains was always present under experimental conditions. In addition, conventional methods, such as laser light and neutron scattering, NMR-spectroscopy, sedimentation and conductivity provide information referring to the ensemble average over many polymer chains. In the case of the highly fluctuating necklace conformations one may assume that scattering experiments show an averaged picture of CGT. In this case single molecule experiments is a powerful tool to clarify the mechanism of CGT via direct visualization of morphology of single molecules.

In this chapter we show that addition of salt effects the PE globule conformation in the same fashion as decrease of charge density. We present the direct evidence of the stepwise transitions between different necklace globules with the increased screening of electrostatic interactions and ion condensation effect[91c,d] induced by addition of mono- and three-valence ions.

3.2. Experimental Part

3.2.1. Materials

Poly(2-vinylpyridine) (P2VP) of molecular weight ranging from 50 kg/mol to 800 kg/mol was purchased from Polymer Sources Inc. (synthesized by anionic polymerization, polydispersity index of about 1.1).

Polycation poly(methacryloyloxyethyl dimethylbenzylammonium chloride) (PMB) (below) was obtained from Dr. Jaeger and was synthesized by free radical polymerisation in aqueous solution. Synthesis and methods of PMB characterization were described elsewhere.[93]

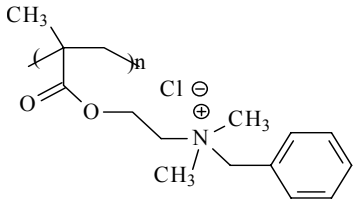

Methacryloyloxyethyl dimethylbenzyl ammonium chloride (MB-Cl) from ATOCHEM and water soluble initiator 2,2'-azobis (2-amidinepropane) hydrochloride (AAP) from WAKO were used without further purification. Polymerization of MB-Cl was carried out in aqueous solution using AAP as a cationic water soluble initiator in a stirred tank reactor. The monomer solution was purged with nitrogen for 16 h at room temperature and than thermostated at reaction temperature. Polymerizations run after injection of the solution of initiator in oxygen-free water under nitrogen at reaction temperature ± 0.5 K. Further experimental conditions for the synthesis of polymers with different molecular weight are derived from kinetic data of the polymerization process.[93] In order to exclude side reactions and to follow the kinetics precisely the polymerization was stopped at law conversion (10%) by rapid cooling and dilution in water. The polymers were purified by ultrafiltration (Minisette, Pall-Filtron, cut off 10000 Dalton) and isolated by freeze drying (Christ Beta 1/16).

For this study, two samples of PMB with different molecular weights PMB-1 with M_n = 480 kg/mol, M_w = 720 kg/mol, M_w/M_n = 1.5, and PMB-2 with M_n = 3880 kg/mol, M_w = 6130 kg/mol, M_w/M_n= 1.58 (GPC data) were used.

Random copolymer poly(2-vinylpyridine-co-styrene) (P2VP-co-PS) (styrene content 30%), M_w= 220 kg/mol, M_n = 130 kg/mol) was purchased from Aldrich.

3.2.2. Sample Preparation

Sample preparation. Solutions of PMB or P2VP (0.0005 mg/ml) were prepared in Milipore water (18 MΩm × cm), pH 3 (HCl, Aldrich). A corresponding amount of concentrated salt (NaCl or Na_3PO_4, Aldrich) solution was added and the mixture was allowed to equilibrate at room temperature for 2 h. The mica was cut and gently pressed onto a sticky tab on a 15-mm diameter metal disk. Then we set a drop of the examining solution on the surface of the freshly cleaved mica for 60 seconds and afterwards we removed the rest of the drop either with centrifugal force or with nitrogen flux. We did not observe any difference in conformations of the visualized single molecules on the samples prepared with these two different procedures. Finally samples were rinsed with water and dried with nitrogen flux.

Most of adsorption experiments were done at pH 3 near the iso-electric point (IEP) of mica substrate (see Appendix 4). The IEP of the freshly cleaved mica was determined by streaming potential measurements with an electrokinetic analyzer (EKA, Anton Paar, Austria). The electric potential was measured as a function of pressure loss in a streaming channel between two mica plates. ζ-Potential was calculated from the streaming potential as described elsewhere.[94] Debye length (λ_D) was calculated as $\lambda_D=(8\pi\lambda_B I)^{-1/2}$, where $\lambda_B \approx 0.7$ nm is the Bjerrum length (an aqueous medium and room temperature), $I= 1/2\ \Sigma\ c_i Z_i^2$ is the ionic strength, Z_i and c_i are the valence and concentration of ions.

AFM in fluid. Freshly cleaved mica was placed into the aqueous solution of PMB-2 (0.0005 mg/ml) with added salt (Na_3PO_4, 8.7 mM; pH 3, HCl) for 1 minute and then rinsed in salt aqueous solution with the same salt concentration (Na_3PO_4, 8.7 mM; pH 3, HCl) to remove the excess of unadsorbed PMB-2. Afterwards the mica plate was dried only from bottom side (the top side was retained wet), gently pressed onto a sticky tab on a 15-mm diameter metal disk and mounted in the microscope. The measurements were performed in the tapping mode in a sealed fluid cell which was filled with aqueous solution of Na_3PO_4 (8.7 mM; pH 3, HCl).

Dynamic light scattering. The measurements were performed at the concentration regime[95] of PE (c_p = 0.01 mg/ml) much below the overlap concentration c_p^* = 0.46 mg/ml (for PMB-1). The concentration satisfied the condition for the ratio between the molar PE monomer concentration ($c_p^m \approx 4 \times 10^{-4}$ mol/l) and the salt (NaCl) concentration (c_s ranging from 0.004 M to 2 M) to be $c_p^m / c_s < 0.1$ to avoid the slow diffusive mode occurring in PE solutions and falsifying dynamic light scattering measurements. All measurements were performed in aqueous solution at pH 2.0 (HCl). At the salt concentration above 0.2 M we observed on $A(R_h)$ a pronounced peak corresponding to aggregated PE molecules. Above this

concentration we used only the peak which corresponded to the faster diffusive mode assuming that this peak originates from single molecule globules, but not from their aggregates. Normally, this procedure is not very reliable. Very good agreement between DLS and AFM data supports that such a procedure in this particular case was reasonable.

3.3. Results and Discussion

According to DRO model we consider PE chain (Figure 3.2) with the *f* fraction of charged monomers in poor solvent as a necklace globule of the total length L with N_{bead} beads of the size d_{bead} joined by N_{bead} -1 cylindrical strings of the length l_{str}. In our discussion we associate with L the apparent long axis length measured in similar way as for stiff DNA molecules as the longest distance in the outline of the polymer globule in AFM images[84]. Within an ensemble of molecules we calculate the number average (L_n) and the weight average (L_w) necklace length. We should distinguish L from contour lengths l_C of PE chains obtained from the length of a curve line drown along the contour of chain backbone. Always L is smaller than l_C, only in the case of rod-like chain $L \approx l_C$. For convenience in our discussion we consider an extended polymer coil and a compact globule as two limiting cases of necklace conformation which dimensions are characterized by L. It is clear that L is not strictly defined parameter for PE in a coil conformation. Therefore, we use L to introduce dimensions of necklace globules, while this value for PE solutions with a small screening effect serves for very rough estimations of molecular dimensions.

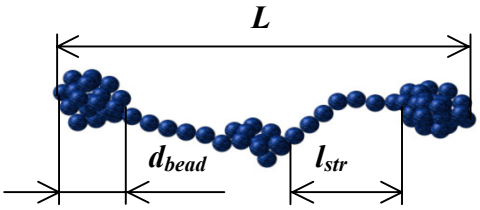

Figure 3.2 Schematic presentation of pearl necklace globule of the length L, with the diameter of beads d_{bead} and the distance between beads l_{str}.

3.3.1. Conformations of PVP at Different Ionic Strength and pH

Being a typical weak polyelectrolyte, P2VP is hydrophobic polymer at pH higher than 4 and display PE behavior in the protonated state in acidic conditions. Therefore, the conformation of P2VP chains can be, in principle, effected by both, the ionic strength of solution and pH.

At pH 2.0 in aqueous solution P2VP (pK_α=2.3) is highly charged[96] and adsorbed molecules appear in AFM images as worm-like chains with the average thickness of about 0.2 nm (Figure 3.3). The number-average contour lengths of the chains obtained from AFM images are slightly smaller than values calculated from molecular weight (Table 3.1). That difference can be explained by error in the evaluation of the experimental contour length

caused by bends and knots on the chain. The number of bends increases with molecular weight of P2VP (Figure 3.5a).

Since identification of the chain ends is possible for chains adsorbed in extended conformation, statistical treatment of end-to-end distance for P2VP of different molecular weight was performed to prove single molecule origin of observed structures. Mean-square end-to-end distance was found to be proportional to the molecular weight of P2VP (Figure 3.4). The error of the measured end-to-end distance increases with molecular weight of the polymers because of difficulty to identify ends of the coiled chains. These results suggest that we observe unfolded adsorbed single P2VP chains.

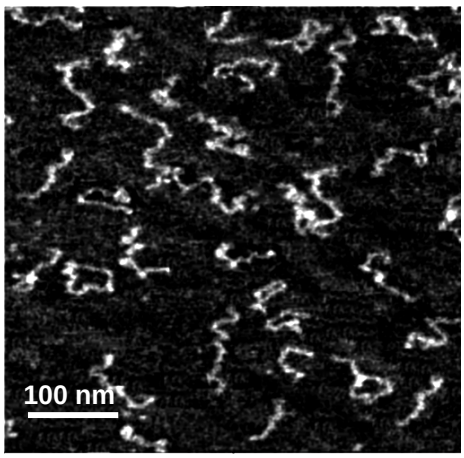

Figure 3.3 AFM image (500 × 500 nm^2; Z range 2 nm) of P2VP, M_n= 59 000 g/mol adsorbed on mica at pH 2.

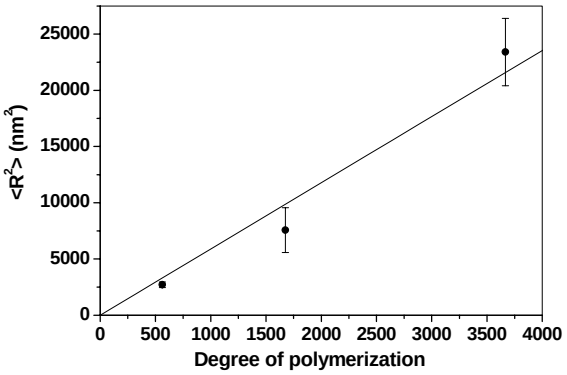

Figure 3.4 Mean-square end-to-end distance $<R^2>$ for the adsorbed P2VP molecules at pH=2.0 plotted as a function of the degree of polymerization.

Table 3.1 Molecular dimensions of adsorbed P2VP chains at pH=2.0

M_n (kg/mol)/ polydispersity index	calculated number-average contour length , nm	experimental number-average contour length (nm)/ polydispersity index	experimental end-to-end distance, R, nm
59/ 1.05	143	130/1.04	52±5
176/ 1.2	425	325/1.10	78±28
385/1.08	931	845/1.05	153±35

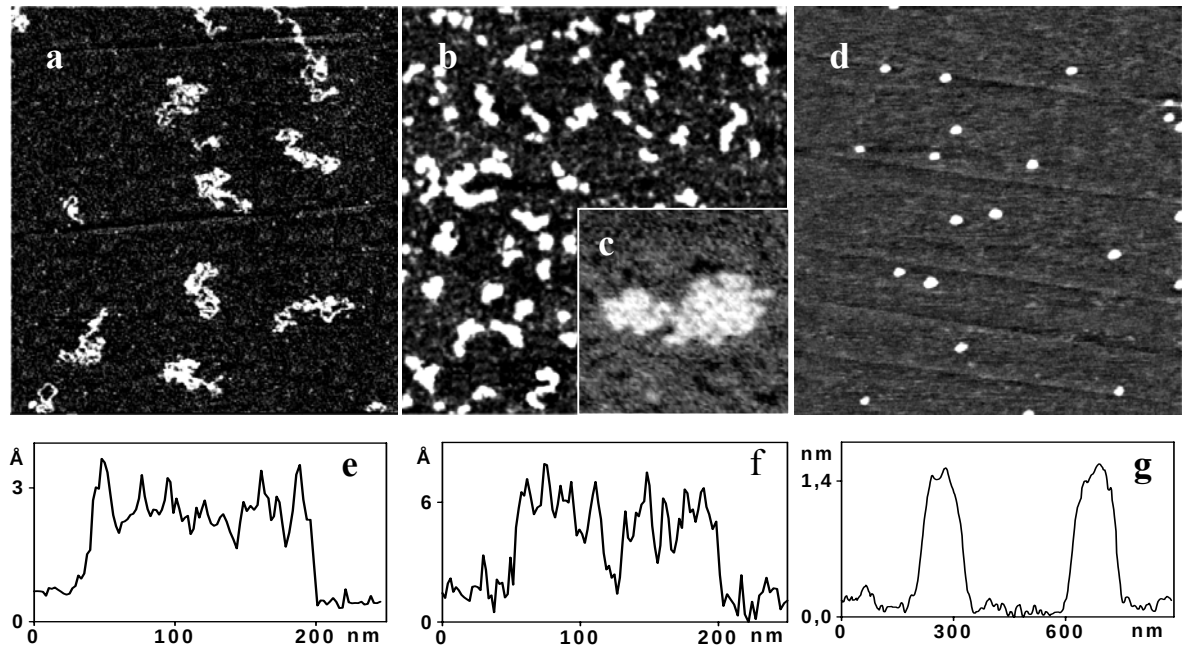

Figure 3.5 AFM images of P2VP, M_n= 385 000 g/mol adsorbed on mica (Z- range 2 nm): (a) 1×1 μm^2 at pH=2.0; (b) 500 × 500 nm^2 at pH=3.5 and NaCl 0.02 mol/l; (c) inset 100x100 nm^2- zoom of the image B; (d) 1×1 μm^2 at pH=3.5, NaCl 1.0 mol/l; (e), (f), (g) – cross-sections along single molecule from (a), (c), (d), respectively.

At pH=3.5 P2VP (NaCl 0.02 mol/l) molecules appear to be much more strongly coiled chains resembling a deformed globule (Figure 3.5b) with average height of 0.35 nm. Here and below the structures formed by P2VP of M_n=385 kg/mol. are considered, as a most representative example. The data suggest that a decrease of the fraction of charged monomers affects the transition to necklace-like globular conformation. These globule conformations resemble dumbbell (Figure 3.5c) and trimbell structures predicted from theory and simulations.[91]

At pH=3.5 and a NaCl concentration 1.0 mol/l the chains undergo a transition to the still more compact globule conformation (Figure 3.5d) with the average height of the structures of 1.4 nm. The average volume of the globule calculated from AFM data is 680 nm^3, which is comparable with the volume of the single P2VP molecule equal to 660 nm^3.

The AFM images obtained for P2VP of M_n=735 kg/mol show very coiled conformations and were not used for statistical analysis of structures in the whole range of pH.

Thus we showed that AFM investigations allow to observe unfolded adsorbed *single* P2VP chains, to visualize details of the chain conformation and to extract quantitative statistics of the molecular dimensions. Single PE flexible molecules of poly(2-vinylpyridine) undergo conformational transition from stretched worm-like coil and to compact globule via necklace-like globules, as a fraction of charged monomers decreases, that is in good agreement with DRO theory for weakly charged flexible PEs in poor solvent.

3.3.2. Collapse of PMB induced by adding Na_3PO_4

Further advance in the study of necklace-like conformations can be achieved by using relatively "thick" PE molecules of PMB which allowed to obtain much better resolution for AFM investigation as compared to P2VP and to identify some particular details of deposited-on-mica necklace structures in the dry state as well as under salt aqueous solution.

In Figure 3.6 the series of experiments of the stepwise CGT study of PMB-2 molecules in aqueous solutions by adding Na_3PO_4 are presented. Similar experimental data for PMB-1 molecules with added NaCl are available as Appendix 2. In salt free solutions both polymers appear as extended coils (Figure 3.6a). Dimensions of the PE molecules such as number average (l_n) and weight average (l_w) contour length, polydispersity index (PDI = l_w / l_n), height and width obtained from statistical analysis of 150 structures on 18 AFM images are presented in Table 3.2. It was not possible to measure contour length of PMB-2 molecules because they appeared in more coiled conformations and we met the problem to identify ends of the coils. The height of the structures is consistent with the size of monomer.

Table 3.2 Average sizes of PMB molecules as appeared in AFM images.

PE	Contour length, nm l_n / l_w / PDI	Height, nm	Width, nm
PMB-1	319 / 454 / 1.42	0.75 ± 0.15	2.4 ± 0.6
PMB-2		0.72 ± 0.18	2.3± 0.8

Added salt dramatically changes molecular conformations and the fine morphology of PE chains. Images in Figure 3.6 (b-m) clearly show intra-molecular segregated areas. Two pronounced differences from salt free solution can be found on the images: the polymer coil start to segregate into small beads nicely observed on zoom image in Figure 3.6e, g; the beads segregate in big clusters. Height of the beads is several times larger than the height of the backbone. According to DRO model, the beads are formed due to the PE intra-chain segregation induced by screening effect of the added salt and due to the enhanced attraction induced by condensed salt ions. Larger clusters are structures resulting from the deposition of PE globules on the substrate. The latter can be understood if we compare Figure 3.6a and Figure 3.6c. The intrinsic beads and apparent cluster of beads can be distinguished due to the alternating thickness of the structures on cross-section of images (Figure 3.6g, h, m, l and o). Clusters of the beads have very rough surface formed by closely packed sequence of beads while beads itself appear on the cross-section as smooth bumps.

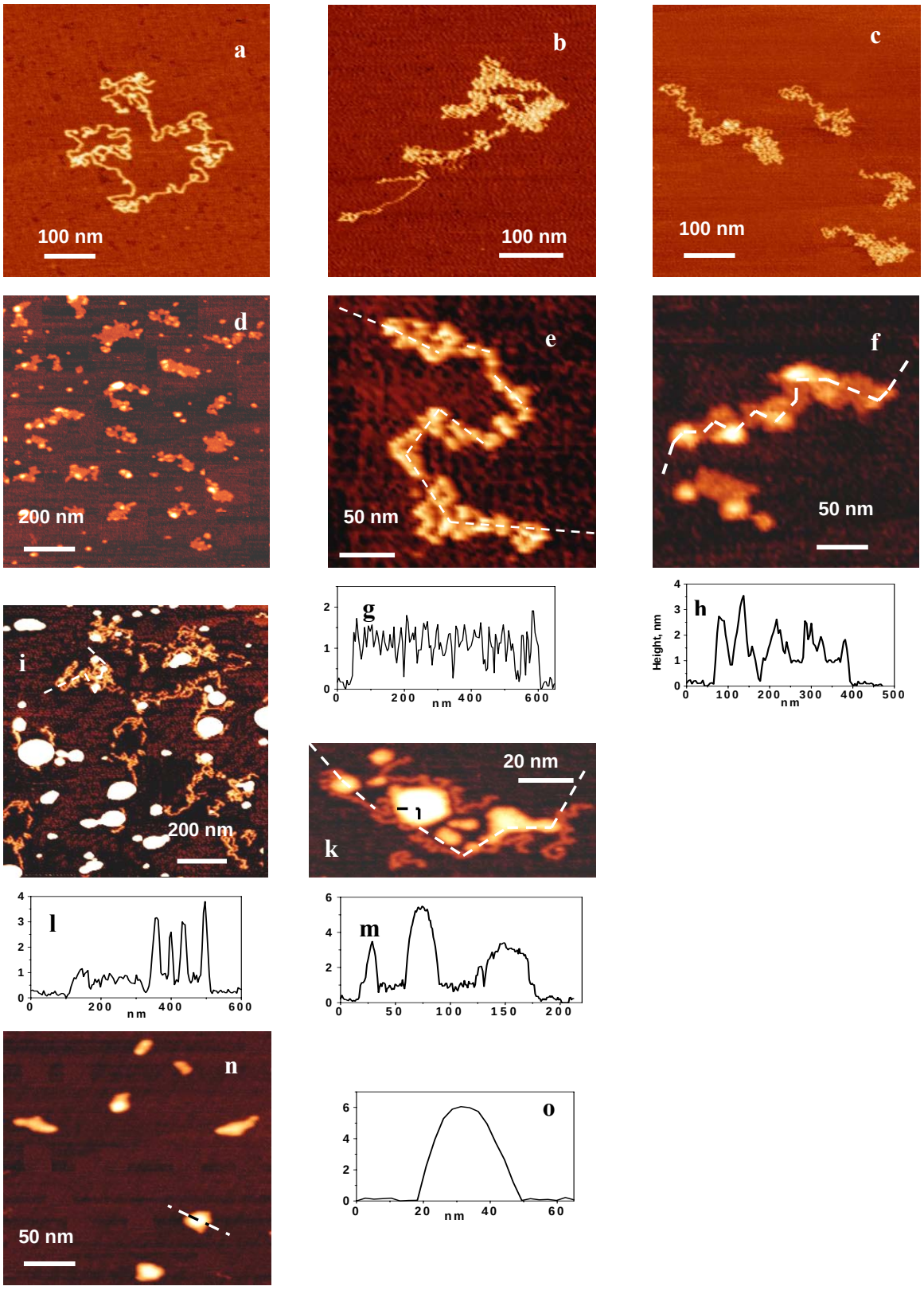

Figure 3.6 AFM images of PMB-2 single molecules deposited from aqueous solutions: reference, no salt (a) and with added Na_3PO_4: 4.2 mM (b); 6 mM (c and e); 8.4 mM (d and f); 8.7 mM (i); 12 mM (k); 18 M (n). Cross-sections from AFM images: (g) - corresponds to (e); (h) - corresponds to (f); (l) - corresponds to (i); (m) - corresponds to (k); (o) - corresponds to (n); We present cross-section from original (no deconvolution) AFM images. The dimensions corrected by the tip radius are presented in Figure 3.7 and in Table 3.3.

Each step of adding of salt results in the increase of the size of beads and the decrease of their number as well as the decrease of the necklace length as it is shown in Figure 3.7. Additionally, the characteristics of molecular dimensions are presented in Table 3.3.

These results are in good qualitative agreement with DRO theory which suggest the effect of charge density f on chains that $L \sim f$; $d_{bead} \sim f^{(-2/3)}$; $N_{bead} \sim f^2$. In our experiments we increase ionic strength of the solution which show similar to charge density but inverse influence on PE molecular conformations due to the screening of the Coulomb interaction and due to the enhanced attraction induced by condensed salt ions. l_{str} can not be calculated directly from AFM images. The evaluation of this value as $l_{str} = (L - N_{\text{bead}} d_{\text{bead}})/(N_{\text{bead}}-1)$ results in a large error, but, nevertheless, it shows that changes in globule conformations occurs at $\lambda_D \leq l_{str}$. Therefore, the local conformation of the necklace is perturbed when the screening length becomes comparable to the distance between beads. In the range of the ionic strength of the solutions the screening length changes by only factor 2.

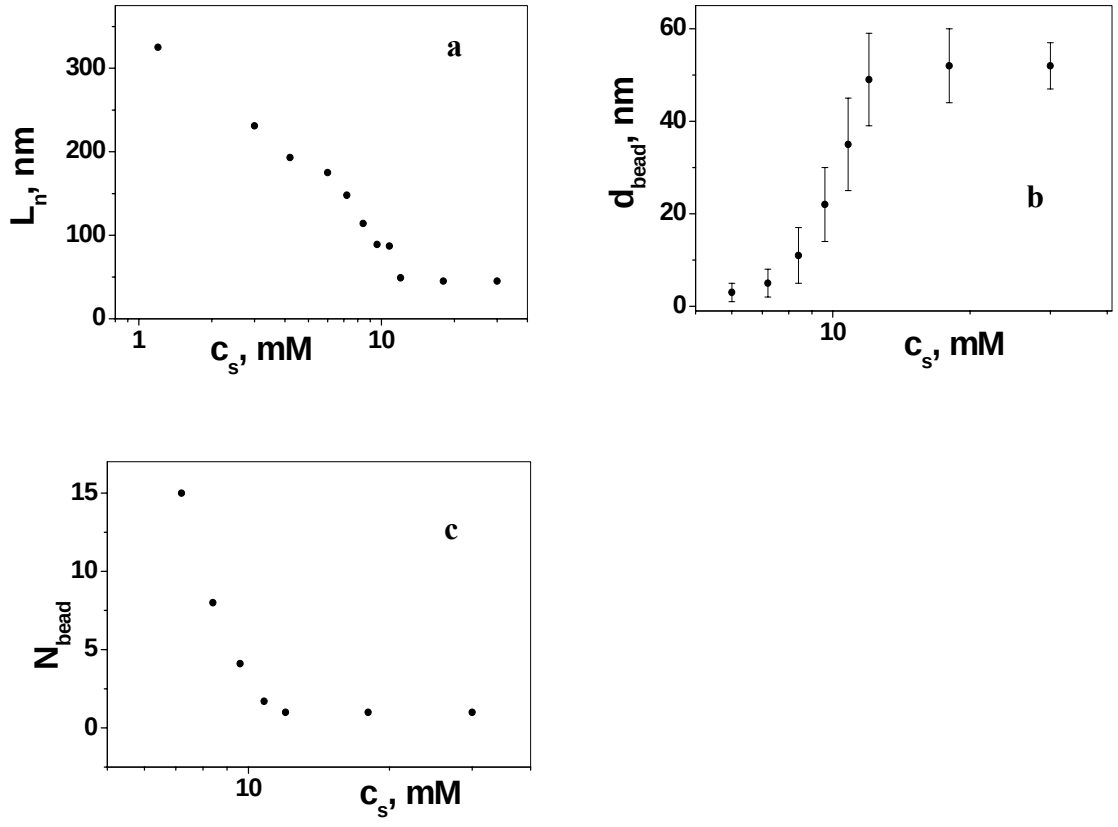

Figure 3.7 Ionic strength dependence of average quantitative characteristics of pearl necklaces: length on necklace globule (a); diameter of beads (b); number of beads per globule(c).

Table 3.3 Molecular dimensions of PMB-2 globules deposited on mica from Na_3PO_4 solutions at pH 3

Ionic strength, M	Debye length, λ_D, nm	Size of necklace L_w / L_n / PDI (L_w and L_n ± 10 nm)	Average diameter of beads, d_{bead}, nm	Average number of beads, N_{bead}	Distance between beads, l_{str} ± 3 nm	Average height of structure, nm
0	9.7	334 / 248 / 1.34				0.8±0.2
0.007	3.4	325 / 201 / 1.61				0.8±0.2
0.018	2.2	231 / 177 / 1.42				0.8±0.2
0.025	1.9	193 /163 / 1.19				0.8±0.2
0.036	1.6	175 / 140 / 1.25	3±2	28±10	3	0.8±0.2
0.043	1.5	148 / 103 / 1.44	5±3	15±5	5	1.2±0.3
0.050	1.4	114 / 99 / 1.16	11±6	8±3	3	2.5±0.5
0.058	1.3	89 / 65 / 1.37	22±8	4±2	0.3	4.1±0.8
0.065	1.2	87 / 56 / 1.56	35±10	2±1		4.9±1
0.072	1.1	49 / 61 / 1.25	49±10	1		5.5±1
0.108	0.9	45 / 51 / 1.14	45±8	1		5.5±1
0.180	0.72	45 /55 / 1.21	45±5	1		5.5±1

Consequently, the observed dramatic conformation change of the necklace globules is mainly effected by the enhanced attraction introduced by added counterions. It is remarkable, that at ionic strength larger than 6 mM we observe a sharp transition of necklaces to dumbbell conformations or single globule with loops and tails (Figure 3.6i and Figure 3.6k). Also, this abrupt transition can be explained by the contribution of the ion condensation effect. The increase of the necklace density with the increase of ionic strength promotes the ion condensation.[91] This effect leads to counterion-induced attraction between different parts of the chain and due to a feed-back type mechanism it amplifies the collapse.[97] This mechanism can be enhanced by polyvalent ions in the case of Na_3PO_4. It is noteworthy, that the formation of globule conformation by PMB-1 molecules in NaCl solution was observed at ionic strength three time larger than for the case of Na_3PO_4 solution.

Finally, we prove that the observed necklace structures are not introduced by drying of the samples. Figure 3.8 present the AFM image of the necklace morphology obtained by scanning

under water solution. Despite a poorer resolution the intra-molecular segregated beads are clearly pronounced on the image and the cross-section.

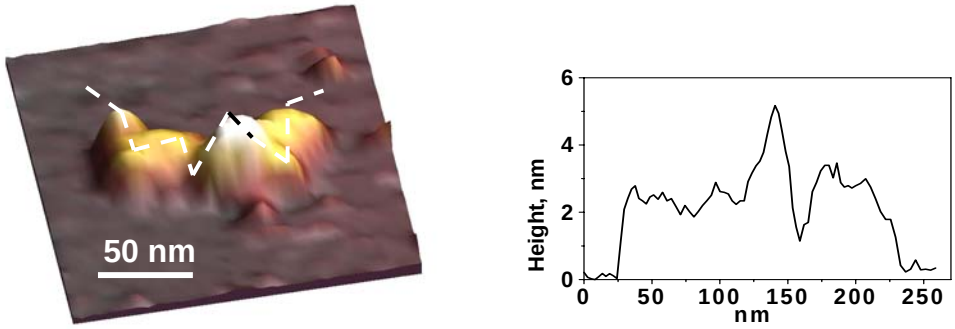

Figure 3.8 AFM image of PMB-2 under aqueous solution with added 8.4 mM of Na_3PO_4

The sample of P2VP-co-PS was studied to demonstrate the role of hydrophobic interactions in formation of the intra-molecular segregated structures. As it was demonstrated in section 3.3.1 P2VP adopts extended coil conformation in aqueous solution at pH 2 and necklaces are formed with increase of pH values. Figure 3.9 indicates that P2VP-co-PS copolymer shows the necklace-like morphology at pH 2. In this copolymer the balance between hydrophobic and Coulomb interactions is shifted due to the introduction of styrene monomers.

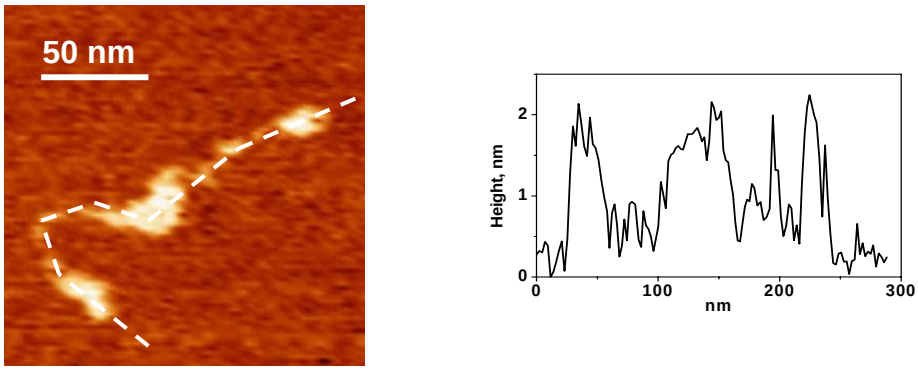

Figure 3.9 AFM image of P2VP-co-PS single molecules deposited from aqueous solution at pH 2.

3.3.3. What do we observe with AFM: Comparison of PE Conformation of Adsorbed PE Chains with Solution Conformation

Since PEs molecules was immobilized onto the solid support prior the AFM experiments, it is always a reasonable and important question, to ask how the conformation of adsorbed molecules reflects the solution conformation. To clarify this point, we studied a model PE solutions by both AFM and LS methods.

Polymer adsorption appears in literature as a two-step process. The first step is the diffusion to and adsorption onto an initially bare surface (rapid). The second step is the

ensuing surface rearrangements, when the adsorbed chains reconformate (slow and history dependent).[98] Changes occurring during long period of time of equilibration in adsorbed layers were found to have a complicated nonequilibrium character[99] sometime resulting even in oscillation of adsorbed amount caused by interplay between adsorption, reconformation and desorption kinetics.[100] Generally, we may expect various possibilities from no change to large changes in conformation of PE chains after they approach solid substrate surface. Even in the case of large changes the reconformation kinetics can be very different. Reconformation characteristic time of the adsorbed chains differs from seconds to hours depending on interactions in particular system.

Nevertheless, following conformation changes during transition from three to two dimensions can be described:

1) The molecules freely equilibrate on the surface before they are captured in particular conformation and can be described as ideal worm-like chain in 2D solution

$$\left\langle R^2 \right\rangle_{2D} = 4 l_p l_C - 8 l_p^2 \left(1 - e^{-l_C / 2 l_p}\right) \tag{3.1}$$

for $l_C \to \infty, \left\langle R^2 \right\rangle_{2D} = 4 l_p l_C$ or

$$\left\langle R^2 \right\rangle_{2D} = 2 \left\langle R^2 \right\rangle_{3D} \tag{3.2}$$

2) The molecules adhere without having equilibrated on the substrate, and the resulting conformation resembles a projection of a three-dimensional chain with $\left\langle R^2 \right\rangle_{3D}$ (eq. 1.13) onto *x-y* plane. The mean-square of the projected end-to-end distance becomes:

$$\left\langle R^2 \right\rangle_{proj.} = \left\langle R_x^2 \right\rangle + \left\langle R_y^2 \right\rangle = \frac{2}{3} \left\langle R^2 \right\rangle_{3D} \tag{3.3}$$

In this case polymer molecules are kinetically trapped by the substrate and changes in conformation can be detected after a long period of time. The polymer chain is adsorbed on the substrate surface retaining the memory about their solution conformation and its two dimensional (2D) size correlates with dimensions of the chain in solvent.

3) The molecular conformations can be strongly effected by screening interaction with charged surface.[33]

4) Capillary forces and stresses appearing in the chains during drying can also effect chain conformation violently and unpredictably that results in buckling and twisting of chains[101].

Clear, that the first two cases seems to be optimal since the solution conformation of PE molecules can be unambiguously reconstructed using the equations 3.1-3.3. Much more difficulties one can meet trying to describe strictly surface screening influence on the PE

conformations (the case 3). Finally, to the best of our knowledge, there is no any mathematical description of conformational changes occurred upon drying.

Rivetti et. al.[102] studied the deposition process of DNA molecules onto a mica surface by AFM imaging. They found, that DNA molecules deposited onto pristine mica are able to equilibrate on the surface as in an ideal two-dimensional solution, since the surface and DNA are similarly charged and there is no strong adhering interactions (case 1). In contrast, DNA molecules deposited onto glow-discharged mica or H^+-exchanged mica do not equilibrate on the surface. These molecules adopt conformations similar to those expected for a simple projection onto the surface plane, suggesting a process of kinetic trapping (case 2).

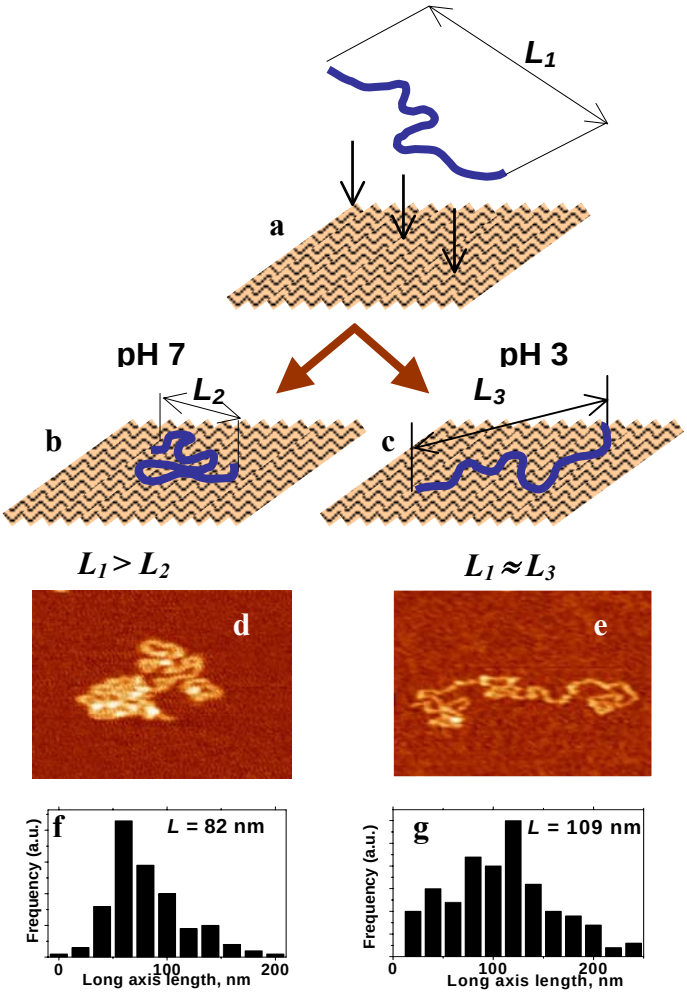

Figure 3.10 Adsorption of PMB-1 molecules on solid substrate: outline of two possible cases when molecule (a) with the characteristic size *L* adsorbed and trapped with dramatic change of conformation (b) or with very small change of dimensions (c) and experimental representative AFM images of the conformations on negatively charged (ζ potential -28 mV) (d) and at ISP of mica (e), respectively; histograms showing the differences of the average *L* after adsorption for both cases (f) and (g), respectively.

In Figure 3.10 the experimental illustration of two different cases of a change of the molecular conformation is outlined, which was founded for PMB-1 chains adsorbed on mica

substrate. The PMB-1 chain of characteristic dimension L_1 approaches the mica surface and appears in the dry state as a worm like coil with the size L_2 or L_3 when adsorbed at pH 3 and pH 7, respectively. Figure 3.10d and Figure 3.10e show representative AFM images of the adsorbed chains, while in Figure 3.10f and Figure 3.10g we present corresponding histograms obtained from measurements of 150 molecules (from about 15 different images). We may conclude that $L_2 < L_3$ which is in good agreement with the theoretical prediction for adsorption of hydrophobic polyelectrolytes on strongly oppositely charged surfaces.[33] At pH 3 the mica surface is only slightly negatively charged while much larger negative charge at pH 7 enhances screening of the intra-chain Coulombic repulsion in PMB-1 which appears in the more coiled conformation. Consequently, adsorption of PE chains onto the mica at pH 7 corresponds to the situation when molecular conformations are strongly effected by interaction with charged surface and dimensions of adsorbed molecules do not reflect their solution conformation (case 3).*

Now the difference in the $\langle R^2 \rangle_{2D}$ and $\langle R^2 \rangle_{proj.}$ values will be used in the analysis of the data to distinguish to which molecular conformation correspond value L_3, equilibrated or kinetically trapped. For that reason we compare results of light scattering experiments with AFM data for PE molecules of different length and for different ionic strength of PE solutions (Figure 3.11 and Figure 3.12).

First of all $\langle R^2 \rangle_{AFM}$ values obtained from AFM images for P2VP adsorbed on mica at pH 2 (HCl 0.01 M) of different molecular weights (Table 3.2) were compared with values of gyration radius (R_g) of protonated P2VP (HBr 0.01 M) published elsewhere.[b] The mean-square end-to-end distance $\langle R^2 \rangle_{3D}$ of the chain in solution was calculated from radius of gyration[b] R_g for two theoretical models: well-known limiting behavior for Guassian coil (eq. 1.15) and for rigid rod (eq. 1.16) (Figure 3.11 dotted and dasher line, respectively).

If the deposited molecules with mean-square end-to end distance $\langle R^2 \rangle_{AFM}$ are able to equilibrate onto the surface, their solution mean-square end-to-end distance $\langle R^2 \rangle_{3D}$ can be recovered by utilization of equation 3.2, assuming $\langle R^2 \rangle_{AFM} \equiv \langle R^2 \rangle_{2D}$ (Figure 3.11 squares ■). Whereas molecules are trapped immediately upon contact with surface ($\langle R^2 \rangle_{AFM} \equiv \langle R^2 \rangle_{proj.}$),

* Most of the experiments described above were performed near IEP of mica at pH ranging from 2 to 3 assuming that in this case the surface introduces minimal changes in PE molecular conformations and we are close to the case 2.

mean-square end-to-end distance $\langle R^2 \rangle_{3D}$ in solution can be found using equation 3.3 (Figure 3.11 circles ●)

One can see that in the first case ($\langle R^2 \rangle_{AFM} \equiv \langle R^2 \rangle_{2D}$) end-to-end distance in solution is derived to be too small to conform to the chains in extended conformation expected at pH 2 (values lying under Gaussian limit). One can see from the Figure 3.11 that the line corresponded to the case 2 (trapped conformation, $\langle R^2 \rangle_{AFM} \equiv \langle R^2 \rangle_{proj.}$) lies between two lines evaluated from light scattering data for Gaussian coil and rod models. Therefore, we may conclude that values obtained from AFM images fit better to the model assuming the projection of the three-dimensional chain onto the plane or, in another words, correspond to kinetically trapped chains.

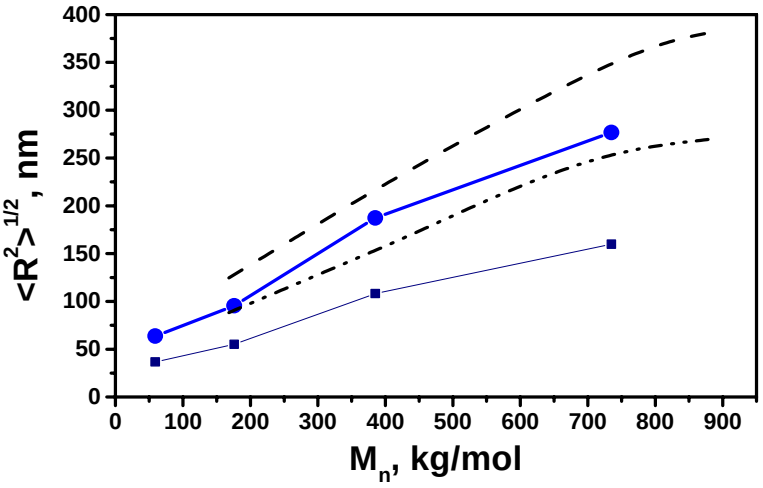

Figure 3.11 Comparison of the molecular weight dependence of $<R^2>^{1/2}$ obtained from AFM data assuming: $<R^2>_{AFM}=<R^2>_{2D}$ (squares ■); $<R^2>_{AFM}=<R^2>_{proj.}$ (circles ●); and $<R^2>^{1/2}$ evaluated from R_g: Gaussian limit (dotted curve); rod limit (dash curve), where R_g was used from static light scattering data (published by Beer, Schmidt and Muthukumar[b]) for protonated P2VP.

In Figure 3.12 we compare L measured from AFM images as long-axis length of the adsorbed chain with the dynamic light scattering hydrodynamic radius (R_h) for PMB-1 molecules at different ionic strength of PE solutions.

Both series of experimental data clearly show the good correlation between molecular dimensions in solution and deposited on mica substrate at IEP.

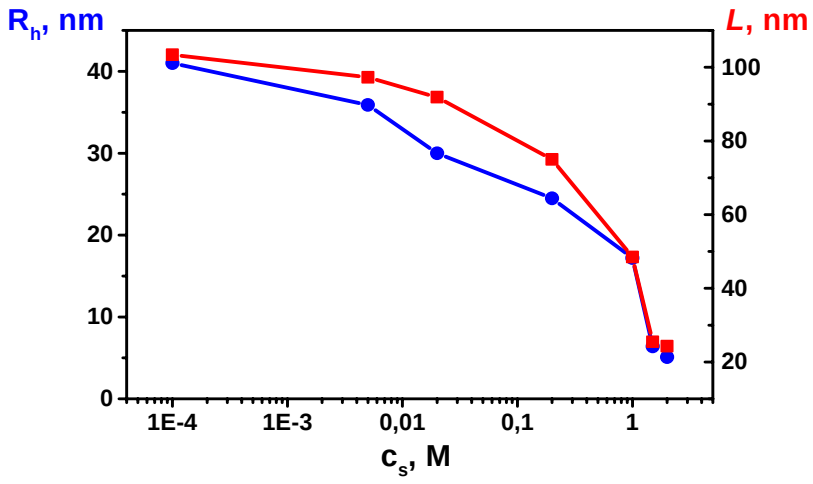

Figure 3.12 Comparison of the ionic strength dependence of L obtained from AFM data (squares ■) with the hydrodynamic radius R_h obtained from DLS experiment (circles ●) for PMB-1 in NaCl solutions.

To address a question how the post-adsorption events affect the conformations of adsorbed chains, i.e. to estimate how strong attraction forces between PE chains and surface are, several control experiments were performed. It was previously shown that addition of poor solvents such as acetone into PE solutions induce their collapse. Our experiments confirm this observation.

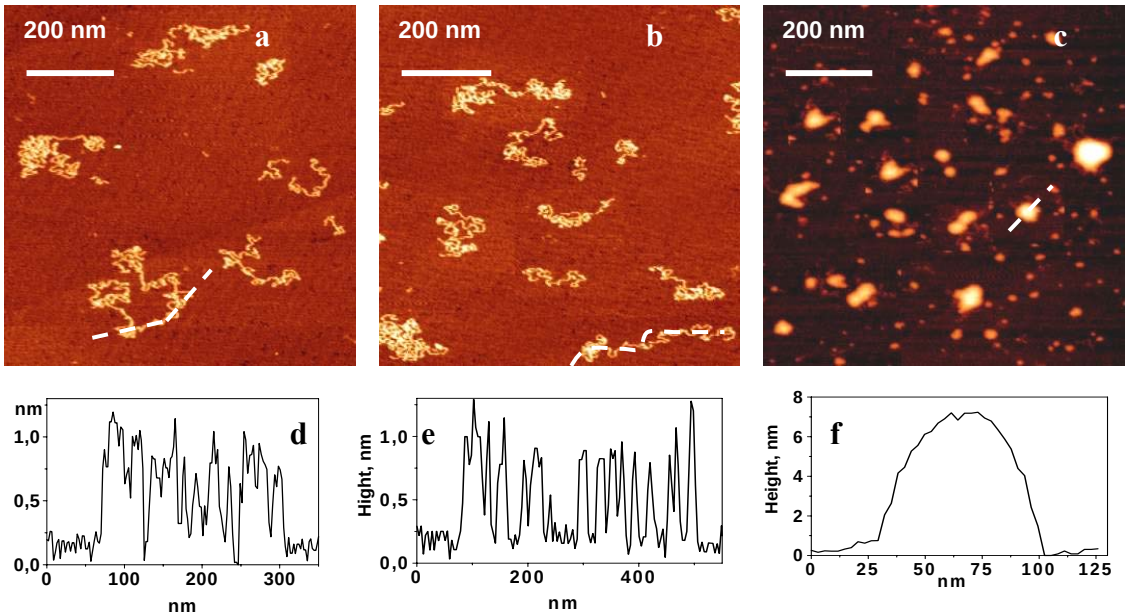

Figure 3.13 AFM images (800 × 800 nm^2) of PMB-2 single molecules deposited onto mica: in extended conformations (Z-range 2nm) from pH 3 aqueous solution and dried (a); similar experiment, but after deposition sample was introduced into acetone for 5 min and dried (Z-range 2nm), because of the strong interaction with the substrate no change was detected in 5 minutes of exposure (b); in globular conformation from solution in 9:1 acetone: water (pH 3) mixture (c). (d), (e), (f) – cross-sections along single molecule from (a), (b), (c), respectively.

Figure 3.13d, f show PMB-2 molecules adsorbed onto the mica from 90% acetone aqueous solution as globule structures. In the second experiment we adsorbed PMB-2 molecules in extended conformation from salt-free aqueous solution. Afterward it was dried and then placed in the acetone, or aqueous acetone (90%) or concentrated (18 mM) solution of Na_3PO_4. In all cases we compared conformations of the adsorbed PE molecules (reference) (Figure 3.13a, d) with those after the treatment with the condensation agents (Figure 3.13b, e). No changes in molecular conformations during exposure of the sample in the poor solvent (acetone) during 5 minutes was found, i.e. before and after the treatment PMB single molecules appear on AFM images in extended conformation. Comparing these data we may conclude that adsorbed conformations of PE molecules are frozen by the strong nonelectrostatic interaction with mica and short-time treatment with collapsing agent do not change their extended conformations.

In the second set of experiments we investigated how drying of the sample may change a conformation of adsorbed PE molecules. We deposited PE molecules in necklace globule conformations and then, before drying, we replaced with help of a syringe the PE solution with water and then with condensation agents. The experiments had the same results: no changes in the frozen necklace conformations were observed with AFM and mainly Z-collapse is observed. Thus experiments described above additionally proves that the adsorbed PE chains are kinetically trapped on the surface and the molecular conformations are frozen.

However, it should be mentioned that long time effects influence the conformation of adsorbed molecules comparatively strong. Two series of experiments have been carried out. In the first series we let P2VP chains to adsorb onto mica in globular conformation from pH 4 aqueous solution for 1 min (Figure 3.14a).

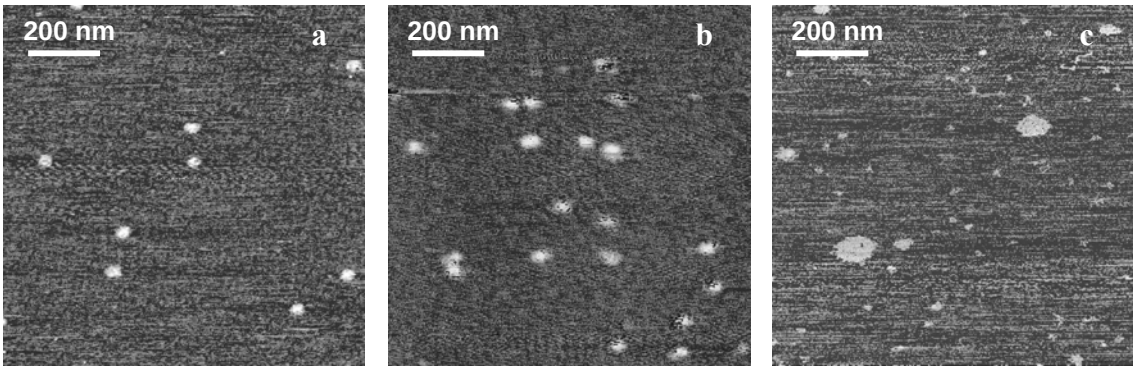

Figure 3.14 AFM images (1 × 1 μm^2, Z-range 5 nm) of P2VP single molecules deposited onto mica: in globular conformations from pH 4 aqueous solution and dried (a); similar experiment, but after deposition sample was introduced pH 2 aqueous solution: for 5 h and dried (b); for 14 h and dried (Z-range 2 nm) (c).

Afterward PE solution was replaced with P2VP-free pH 4 aqueous solution and then with pH 2 solution and left the sample in pH 2 solution for 5 h, or 14 h, correspondingly (Figure 3.14b, c). Initial structures appears on AFM image as a hemisphere with the height more than 1.3 nm. After 5 h staining with pH 2 solution molecules scarcely changed their shape and resemble core-shell structures, but the average height decreased down to 0.8 nm. Further transformations of the structures took place in 14 h of the staining. All features reassembling pancake became not higher the 0.4 nm and average diameter around 50 nm. Thus molecule adsorbed in collapsed state can equilibrate their conformation according to environment during 14 hours or more.

Complementary to the experiment described above we tried to reconformate adsorbed chains in the opposite direction. Initially, P2VP chains have been adsorbed onto mica in extended conformation from acid water (pH 2) (Figure 3.15a) and then stained with condensation agent (1M NaCl aqueous solution at pH 7). In this case AFM images shows a lot of relatively high (1.5-2 nm) spherical structures already after 5 h of staining (Figure 3.15b), but these structures could not correspond to P2VP molecules, because of their large number. They originate probably from damaging of mica by concentrated NaCl solution. On the Figure 3.15c one can also discern another kind of structures, which have the same height as initial (about 0.3 nm) but slightly contracted shape. Despite of poor resolution, we believe that the latter is P2VP molecules which slow reconformate upon exposure in poor solvent.

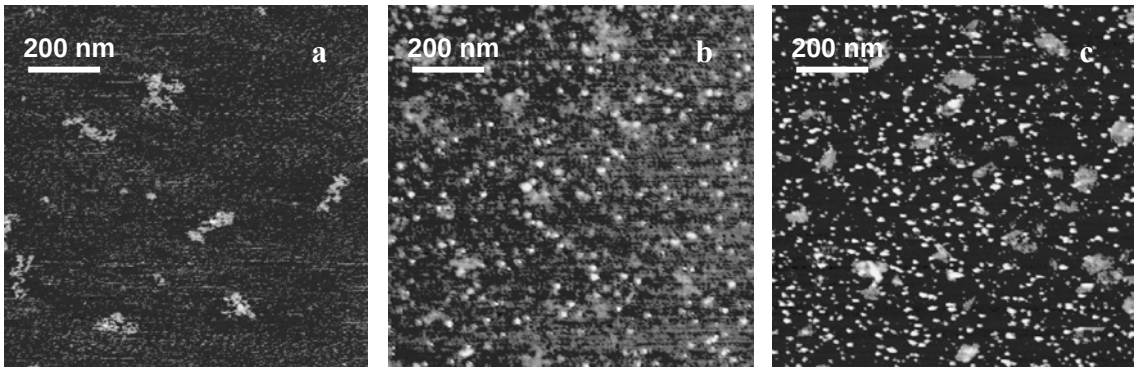

Figure 3.15 AFM images (1 × 1 μm^2, Z-range 2nm) of P2VP single molecules deposited onto mica: in extended conformations from pH 2 aqueous solution and dried (a); similar experiment, but after deposition sample was introduced 1M NaCl pH 7 aqueous solution: for 5 h and dried (b); for 14 h and dried (c).

Thus the rate of reconformation from globule to coil is higher than opposite transformation. This difference could be explained by difference in contacting areas of initially adsorbed structure with surface of mica which are different for coils and globules. The larger is the contact area, the stronger initial conformation is fixed by the surface interactions.

Additional facts also support our conclusions about frozen conformations. We found no effect of humidity on the molecular conformations. Even ion exchange of adsorbed PMB with polyvalent ions effected no large change in molecular conformations, that allowed us to overcome the X-Y collapse and metallize the single molecules in different conformations. (see Chapter 4 - 6)

3.3.4. Character of CGT.

The plots of molecular dimensions vs. ionic strength (Figure 3.7) show the narrow but continuous CGT region. At the same time we identified on AFM images co-existence of extended coils, necklace-like and compact globules with loops and tails of nonsegregated segments (Figure 3.6i and Figure 3.6k). Such a coexistence is considered as sign of the first order phase transition. This picture is very similar to those observed for the first-order transition of rigid DNA molecules when the discontinuous process on the level of single molecules appears as continuous transition within finite assemble of molecules.[84] This result is a very nice example demonstrating similarity in nature. In the case of flexible hydrophobic PE the superposition of the first-order transitions between necklaces with different amount of beads results in the apparent smooth character of the process for assemble of PE molecules. As it was mentioned above the ion condensation mechanism can even enhance the sharp transition.

Histograms of size distribution (Appendix 1, 3) also indicate the co-existence of coil and globule conformations in each step of the transition although the bimodal character of the histograms is not always very well pronounced because of the superposition of the cascade of CGT.

Therefore, PE molecules occupy an intermediate place between stiff chains collapsing by the first-order-type phase transition and flexible polymers collapsing by the second-order-type phase transition. This intermediate place is caused by the abrupt splitting of the PE globule into charged beads when the necklace globule jumps from one to another conformation with different amount of collapsed beads as effective repulsion decreases.

3.4. Conclusions.

In conclusion, the first direct observation of the polyelectrolyte chain conformations representing the transition between different conformations of single flexible PE molecules adsorbed on solid substrates from aqueous solution affected by different environment is described in this chapter.

The *weak* PE - P2VP - undergoes conformational transitions from stretched worm-like coil to compact globule via necklace-like globules as the fraction of charged monomers decreases with an *increase of pH*. These results are in good agreement with recently developed DRO theory for weakly charged flexible polyelectrolytes in poor solvent.

The *strong* PE - PMB - undergoes transition from extended coil and compact globule conformations through the cascade of intermediate necklace-like globules with decreasing amount of beads upon *increase of ionic strength* of solution. Size of the beads increases with increase of ionic strength. Co-existence of extended coils, necklace-like globules and compact globules indicates the cascade of the first-order CGT.

For both PEs studied, the size of the deposited single molecules measured by AFM correlates very well with molecular dimensions in solution obtained in LS experiments.

Chapter 4.

Generation of Nanostructures by Templating of Single Adsorbed Polyelectrolyte Molecules

In this chapter we describe a simple chemical route to fabricate wire-shaped metallic nanoparticles of about 2-5 nm in a diameter and 50-1000 nm in length from single synthetic polycations. The preparation is based on the generation of Pd-clusters on templates of single molecules of poly(2-vinylpyridine) or poly(methacryloyloxyethyl dimethylbenzylammonium chloride) adsorbed from aqueous solution on the surface of Si-wafer or mica in different conformations ranging from an elongated wormlike coil to compact globule. Pd(+2) ions was adsorbed and coordinated by these single molecule templates via an ion exchange reaction exposing the samples to palladium acetate acidic aqueous solution. In the next step, Pd(+2) was reduced by dimethylamine borane. The dimensions of formed nanoparticles are determined by the conformation and size of the underlaying polyelectrolyte chains.

4.1. Introduction

Due to the considerable success in modern supramolecular[103] and polymer[104] chemistry various molecular objects of different shapes and functionalities are available now. Using complimentary building blocks and employing chemical reactions or self-assembling methodology[105] it is possible to design complicated structures at molecular level. These approaches provide the development of the modern field of molecular electronics.[106] For the further miniaturization of electronic devices it would be a challenging task to develop simple methods to fabricate nanoparticles of dedicated shape and desired properties incorporated in a supermolecular construction assembled from single functional molecules.

Nanoparticles of a various shape from spherical clusters to nanowires attract great interest because of their importance for the further miniaturization of electronic devices.[107,108,109] One-dimensional (1D) sequences of nanoparticles (nanowires) are important elements of the nanotechnology toolbox because they provide interconnects between functional devices and even can be used as elementary units of optoelectronic devices. They also have been attracting increasing attention due to unique optical,[110] magnetic,[111] and catalytic[112] properties. Several routes have been developed for the synthesis of metallic nanowires, including the template synthesis,[113] step-edge decoration,[114] vapor-liquid-solid condensation,[115] as well as several other wet chemical techniques based on reduction of metals in the presence of protecting polymers or surfactants.[116] Template-based methods involve deposition of metals into cylindrical pores of a host material, so-called 1D nanotemplates, e.g., carbon nanotubes,[117] rod-like micelles,[118] etc. The ultimate limit of the fabrication of nanoparticles via the template synthesis is determined by the use of polymer micelles,[119] microphases in block copolymers,[120] and single molecules as templates.[121] Recently, DNA molecules has been successfully used as biotemplates for the deposition of metal clusters and fabrication of nanowires from single molecules.'' The synthesis is based on a two-step procedure that involves binding of metals (Pd or Ag) to DNA followed by chemical reduction. This procedure results in 20-100 nm thick metallic wire-shaped particles, which are, however, much larger than 2 nm assumed for the diameter of a single DNA molecule. Vacuum evaporation was used to deposit gold on single extended DNA strands to produce wires of width <10 nm and of length up to 60 nm.[121]

Here, we further advanced in the miniaturization of nanowires by templating single synthetic flexible polyelectrolyte molecules of a diameter which is substantially smaller than the diameter of DNA molecules.

DNA represents semiflexible polyelectrolytes (PE), the rigidity of which is affected by both bare and effective electrostatic persistent length. The bare rigidity originates from secondary structures stabilized by hydrogen bonds, while electrostatic rigidity is affected by the Coulomb repulsion, which gives the sum of the persistent length of 50 nm in aqueous environment.[122] Because of this rigidity, DNA exhibits a highly elongated coil conformation in the absence of condensation agents. Polymers, surfactants, metal ions, and organic solvents may cause a firstorder coil-compact globule transition of DNA molecules. Nevertheless, the bare rigidity predominates the shape persistence of DNA molecules to the condensation agents to some extent. Particularly, this stability allows one to template DNA in salt solution and obtain wire-shaped metallic nanoparticles.[123, 124, 125]

Flexible synthetic PE molecules express rather different behavior. A flexible backbone rapidly responds to the change of a charge density resulting in a continuous cascade of coil globule transitions in the presence of condensation agents (see Chapter 3). In Chapter 3 we reported the visualization of different conformations of single flexible PE molecules of P2VP and PMB with atomic force microscopy and conditions to deposit fully stretched PE chains on the mica substrate. Solid substrates trap the PE molecules in elongated conformations which appear to be kinetically stable for a relatively long period of time even in the presence of condensation agents. In this chapter, we employ this possibility to fix the conformation of flexible PE deposited onto solid substrate and perform metallization of PE in the frozen conformation.

4.2. Experimental part

4.2.1. Materials

Two types of polycations (PC) were used:

1. P2VP of molecular weight ranging from 50 to 800 kg/mol was purchased from Polymer Sources Inc. (synthesized by anionic polymerization, polydispersity index of about 1.1).
2. PMB-1 with molecular weights M_n = 480 kg/mol, M_w = 720 kg/mol, M_w/M_n = 1.5, and PMB-2 with M_n = 3880 kg/mol, M_w = 6130 kg/mol, M_w/M_n = 1.58 (GPC data), obtained from Dr. Jaeger, were used (see also chapter 3.2.1)

$Pd(OAc)_2$ (PA), dimethylamine borane (DMAB), and DCM were used as received from Aldrich.

Highly polished silicon (Si) wafers (obtained from Wacker-Chemitronics) were first cleaned three times in a ultrasonic bath for 5 min with dichloromethane (DCM), placed in the

cleaning solution (prepared from NH_4OH and H_2O_2) at 60 °C for 1 h (*Note: NH_4OH:H_2O_2 solution reacts violently with organic compounds. Caution should be used when handling this solution*). Samples were finally exposed to 50% sulfuric acid for 15 min and then rinsed several times with Millipore water (18 MΩm × cm).

The mica was cut and used freshly cleaved from both sides, after metallization procedure it was gently pressed onto a sticky tab on a 15-mm diameter metal disk.

4.2.2. Sample preparation

We used three different procedures for mineralization of PE molecules.

Procedure 1. We use after Braun et.al.[123] and Richter et.al.[124] the procedure developed for metalization of DNA. 10 mg of $Pd(CH_3COO)_2$ in 25 ml of deionized water was placed in ultrasonic bath for 30 min and then the mixture was centrifuged for 5 min at 2000g to obtain a saturated solution of PA and to settle all unsolved particles. The PA solution was mixed for 2 h with an equal amount of the acidic (pH range from 1 to 3.5) PC (0.005 mg/ml) aqueous solution. On the second step the solution of 1.0 mg/ml of dimethylamine borane (DMAB) was added to the PA-PC aqueous solution and immediately afterward the silicon wafer was introduced in the mixture for 30 sec to adsorb the resulting products. Finally, Si-wafers were cleaned with water and dried with the argon flux.

Procedure 2. The PA solution was mixed with the equal amount of acidic (pH 2) PC (0.0005 mg/ml) aqueous solution for 15 min and then the silicon wafer was exposed to the solution for 30 sec to adsorb PC-1/2($PdCl_4$) composite. Afterward, the silica wafer was thoroughly rinsed with water and placed for 15 sec into the reduction DMAB solution. Finally, the Si-wafer was cleaned with water and dried with the argon flux.

Procedure 3. In the first step, single molecules of PE were deposited on the carefully precleaned Si-wafer or freshly cleaved mica from acidic (pH 2, HCl) aqueous solution of PC (0.0005 mg/ml) for 1 min at room temperature. Then, in the second step, the substrate was rinsed several times with water and placed into the PA solution (pH 2) for 1 min for the formation of the PC-($PdCl_4$) composite. In the third step the substrate was thoroughly rinsed with water, placed for 15 sec into reduction solution which contained 1.0 mg/ml of DMAB. Finally, the substrate was cleaned with water and dried with the argon flux.

4.3. Results and discussion

4.3.1. Development of single PE molecule templating by deposition of Pd clusters onto P2VP molecules

Figure 3.3 shows representative AFM image of P2VP chains deposited on mica from acidic aqueous solution (pH 2). The contour length of the chains evaluated from the AFM images agrees with the value calculated from degree of polymerization (Table 3.1). At these conditions more than 50% of 2-vinylpyridine monomers are protonated and polymer chain is stretched forming worm-like coils due to the electrostatic repulsion between randomly distributed positive charges along the chain. This conformation is frozen due to the interaction with the solid substrate. We performed several controlled experiments which have shown that the conformation of P2VP molecules on the solid substrates was stable at least for several hours even if they were exposed to NaCl aqueous solutions at pH 7.0 (Figure 3.15). This result assumes a slow kinetics of a conformation change of the trapped PE chains. Consequently, we assumed that flexible PE molecules in the wormlike conformation might be used as templates for mineralization in the same way as it was recently suggested for semiflexible PE, particular for DNA. Below we present different attempts to metallize single molecules of *flexible* PE.

4.3.1.1. Metallization via "*In situ*" procedure

Procedure 1 for the mineralization of PE was copied from the method developed for decoration of DNA molecules with metal clusters[123,124,125] This approach suggests to coordinate metal ions with PE and afterward to reduce metal. The product was deposited on the surface of Si-wafer. The addition of PA to P2VP solution effects a charge compensation due to the ion exchange and mutual attraction.[126] The water insoluble Pd-P2VP complex agglomerates in aqueous medium producing Pd clusters after reduction of the metal. The clusters are of a large polydispersity with the size ranging from tens to hundreds of nanometers (Figure 4.1). Molecular weight of P2VP and pH effects the cluster size only slightly. The cluster size increases with time of exposure of the Si-wafer to the solution.

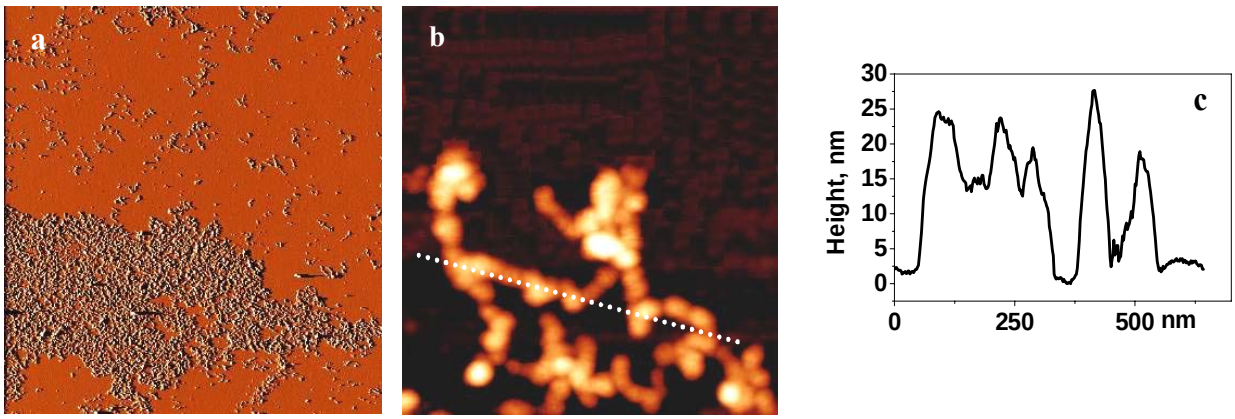

Figure 4.1 AFM images of Pd particles deposited on Si wafer by Procedure 1: 20 × 20 μm^2 – phase image (a); 0.5 × 0.5 μm^2 – topography image, Z – range = 30 nm (b) and its cross-section driven along the particle contour (c).

4.3.1.2.Metallization via two steps procedure

In the *Procedure 2* the Pd-P2VP complex was deposited on the Si-wafer in the first step and then it was reduced by exposure of the Si-wafer to the DMAB solution. The shape and the size of the obtained particles (Figure 4.2) is still far from the dimensions of elongated single PE molecules. The height of clusters equals to 3 nm and has narrow distribution. The mean long axis length is about 100 nm, width is about 50 nm. This result suggests that we mineralize collapsed PE coils. This collapse is caused by the interaction with PA.

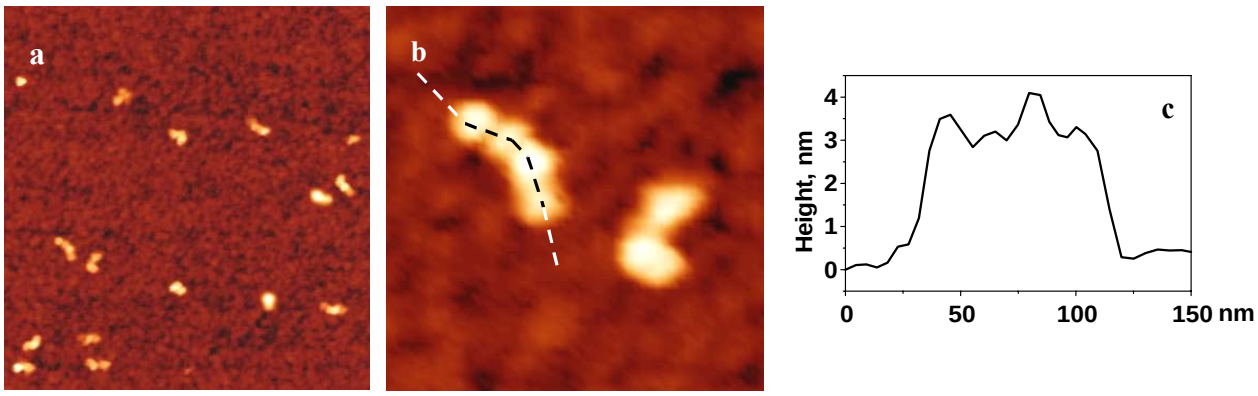

Figure 4.2 AFM topography images of Pd-P2VP composite deposited on Si-wafer by Procedure 2: 1 × 1 μm^2, Z-range 10 nm (a); 0.25 × 0.25 μm^2 Z-range 10 nm (b) and its cross-section driven along the particle contour (c).

4.3.1.3.Metallization via "step-by-step" procedure

Finally, *Procedure 3* (Scheme 4.1) consists of the P2VP deposition (step 1) from very dilute acidic (HCl, pH 2.0) aqueous solution on the surface of the Si-wafer or freshly cleaved mica. The substrate with deposited P2VP was exposed to the PA solution (step 2) to perform the ion exchange reaction. In step 3, Pd(II) was reduced by the treatment with DMAB. AFM images (Figure 4.3) document mineralization of elongated PE coils.

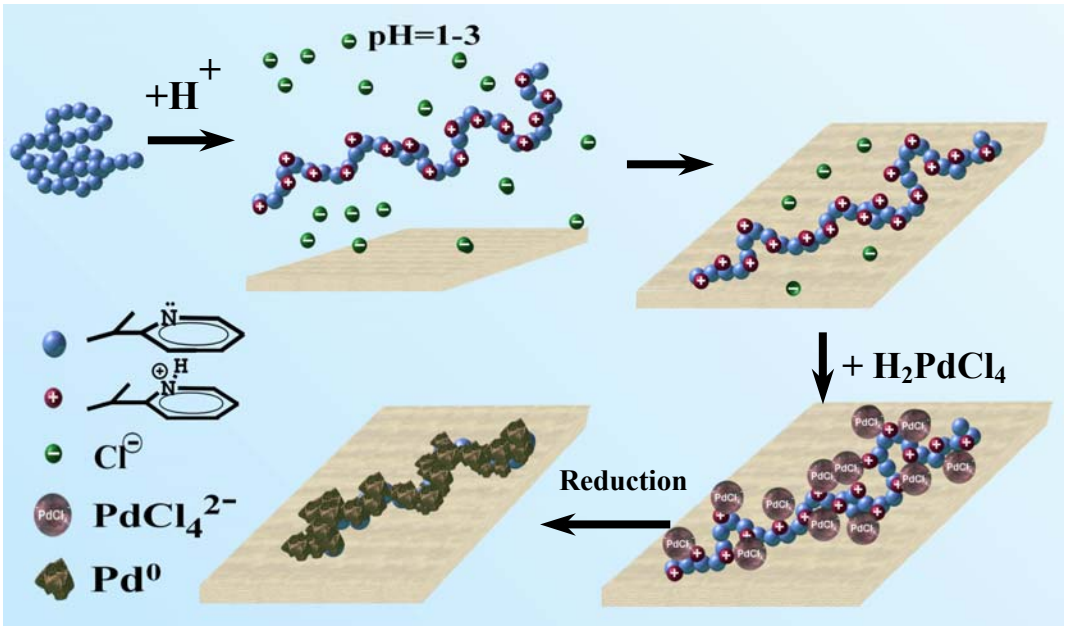

Scheme 4.1 Schematic representation of the route to metallize a single polyelectrolyte molecule via multistep procedure: dissolution of PE in acidic water when PE chains adopt wormlike conformation because of the electrostatic repulsion between positive charges, deposition of the wormlike chain on the substrate, attachment of metal ions via ion exchange reaction, and reduction of the metal.

The chemical reactions involved in this process are listed below:

$$\text{P2VP} + n\text{HCl} \leftrightarrow \text{P2VP}\cdot n\text{HCl} \quad (1)$$

$$\text{Pd(OAc)}_2 + 4\text{HCl} \leftrightarrow \text{H}_2\text{PdCl}_4 + 2\text{HOAc} \quad (2)$$

$$\text{P2VP}\cdot n\text{HCl} + (n/2)\,\text{H}_2\text{PdCl}_4 \rightarrow \text{P2VP}\cdot(n/2)\,\text{H}_2\text{PdCl}_4 + n\text{HCl} \quad (3)$$

$$2(\text{P2VP}\cdot(n/2)\text{H}_2\text{PdCl}_4) + n(\text{CH}_3)_2\text{NH}\cdot\text{BH}_3 + 3n\text{H}_2\text{O} \rightarrow 2(\text{P2VP}\cdot n\text{HCl}) + n\text{Pd}^0 + n\text{B(OH)}_3 + n(\text{CH}_3)_2\text{NH}\cdot\text{HCl} + n\text{HCl} + 2n\text{H}_2 \quad (4)$$

The obtained wire-shaped nanoparticles appear in AFM images as a 1-D sequence of the interconnected Pd clusters. This structure resembles a necklacelike morphology nicely observed in the profile of the AFM image as beads (undulations) separated by narrow strings (Figure 4.3 a,b). We performed the statistical analysis of parameters extracted from the AFM images and their profiles: height, width, contour length, and end-to-end distance (Table 4.1). For all P2VP samples of different molecular weights, we obtained the same average values of the height and the width of Pd clusters. The size distribution of the Pd clusters is presented in Figure 4.6.

The contour length of the nanowires is proportional to the molecular weight of P2VP (Figure 4.4) and it is about 3 times smaller than the contour length of the original P2VP chains (calculated from molecular weight) for all samples (Figure 4.5, Figure 4.6). This fact may be explained by conformational changes introduced by the interaction of PE with PA. This explanation is also confirmed by another fact that the biggest beads usually forms in the ends of nanowires where more pronounced conformational changes could take place. The resulting product is insoluble in water because of a decreased charge density as compared to protonated P2VP molecules.

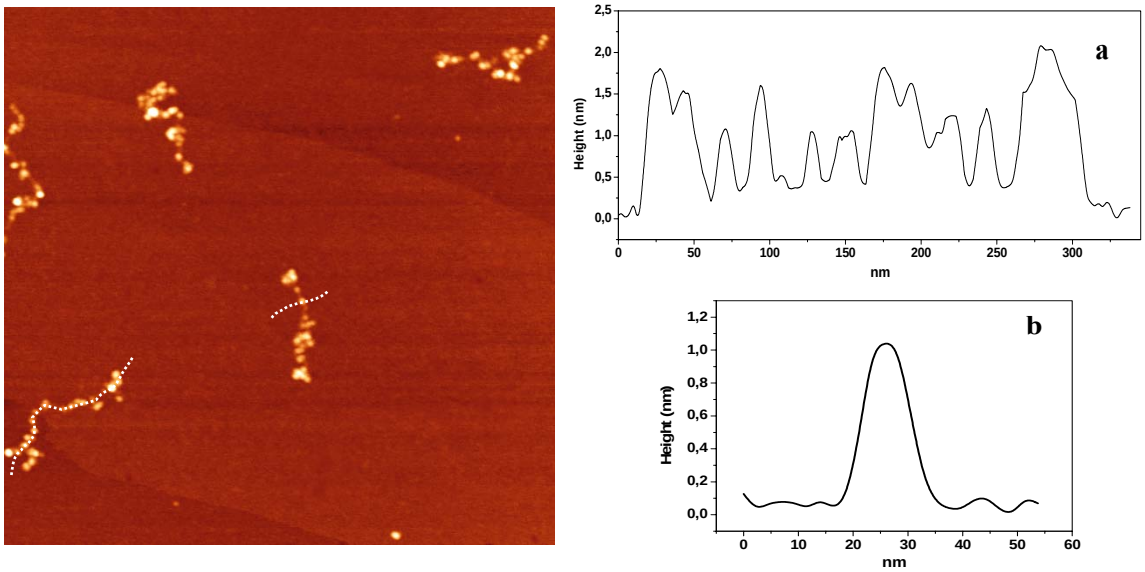

Figure 4.3 AFM images (1×1 μm^2, Z-range 5 nm) of Pd-nanowires prepared from P2VP of M_W=385 kg/mol on the surface of freshly cleaved mica by procedure 3 and cross-section profiles (original AFM-data; no deconvolution was performed) of Pd-nanowires drawn parallel (a) and perpendicular (b) to the contour.

Table 4.1 Average sizes of P2VP molecules, metallic nanowires and Pd-clusters deposited on the P2VP single molecules*

M_n (kg/mol)/ polydispersity index of P2VP	contour length of PVP, nm	average dimensions of nanowires		average size of Pd-clusters	
		contour length, nm/ polydispersity index	end-to-end distance , nm	height, nm	width, nm
59/ 1.05	143	55/1.08	44	2.5	5.1
176/ 1.4	425	132/1.2	79	2.4	5.0
385/1.08	931	346/1.03	109	2.6	5.4
735/ 1.23	1778	630/1.03	161	2.0	5.6

* polydispersity index calculated as a ratio between the second and the first moments of the Gauss distribution function.

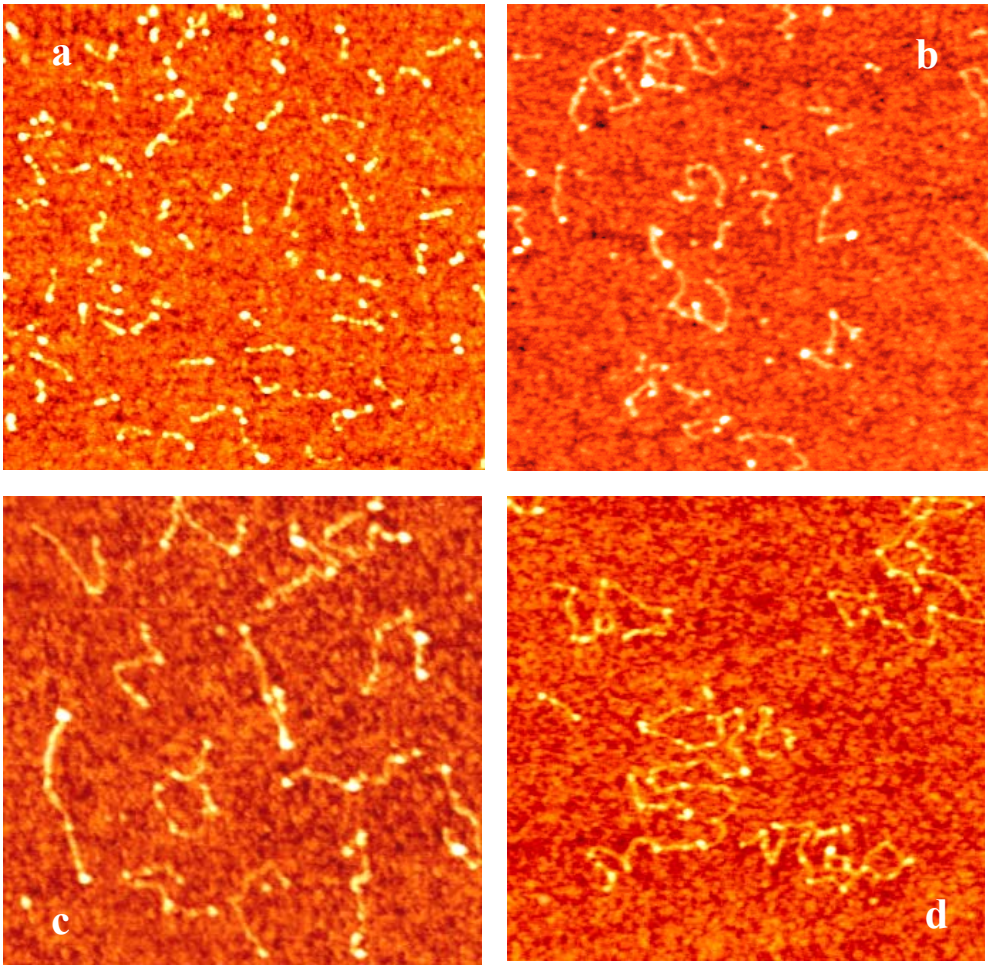

Figure 4.4 AFM images (1×1 μm2, Z-range 5 nm) of Pd-nanowires prepared on the surface of Si-wafers from P2VP of different molecular weights: 59 kg/mol (a), 176 kg/ml (b), 385 kg/mol (c), and 735 kg/mol (d).

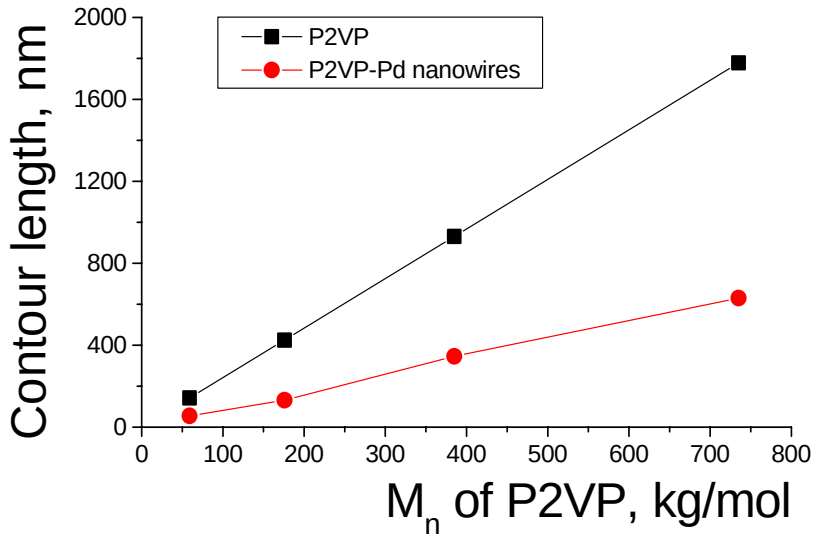

Figure 4.5 Contour length of Pd-nanowires and corresponding notmetallized P2VP chains plotted as a function of molecular weight of P2VP.

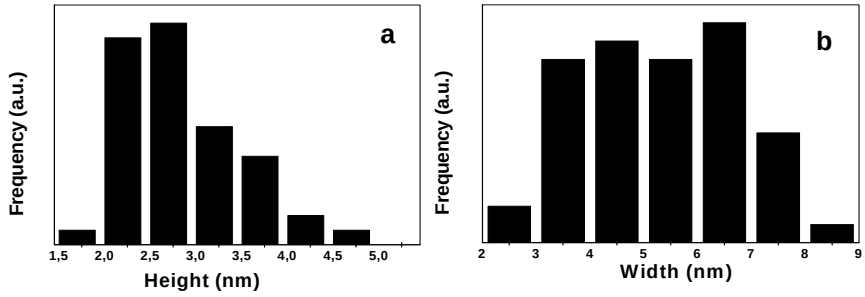

Figure 4.6 Size distribution of Pd clusters along the polymer chain: (a) height of clusters, (b) width of clusters.

The chemical composition of the nanowires was estimated using X-ray photoemission electron spectra. The atomic ratio between nitrogen of 2-vinylpyridine monomer units and Pd calculated from the XPS spectra was N:Pd = 4:1. We detected separately the charged and uncharged nitrogen with the ratio to be about 50:50 for both P2VP deposited molecules (pH 2) before metallization and for metallized wires. Consequently, we can perform a rough evaluation of size of the Pd clusters assuming that always two charged 2-vinylpyridine monomers bond 1 of the Pd atom (see step 3 in the list of chemical reactions above) and, therefore, P2VP molecules of about 400 kg/mol in average can bond about 1000 Pd atoms. The number of Pd clusters detected with AFM ranges from 10 to 20 per single structure resulting in the number of Pd atoms per cluster ranging from 50 to 100. This number of atoms corresponds to the cluster size of about 1.5-2 nm in diameter which is consistent with the cluster sizes observed in the AFM experiments.

Similar experiments were performed with P2VP chains deposited on Si-wafers from aqueous solutions at different pH values to metallize different conformations of the PE molecules. Figure 4.7 summarizes these experiments. The increase of pH values and the addition of NaCl to the PE solution result in a decrease of positive charge density of P2VP and consequently to a cascade of coil-globule transitions from wormlike coil to necklacelike coils with a different number of beads and finally to a compact globule (for more details see subchapter 3.3.1). All of these conformations are frozen on the substrate surface and metallized.

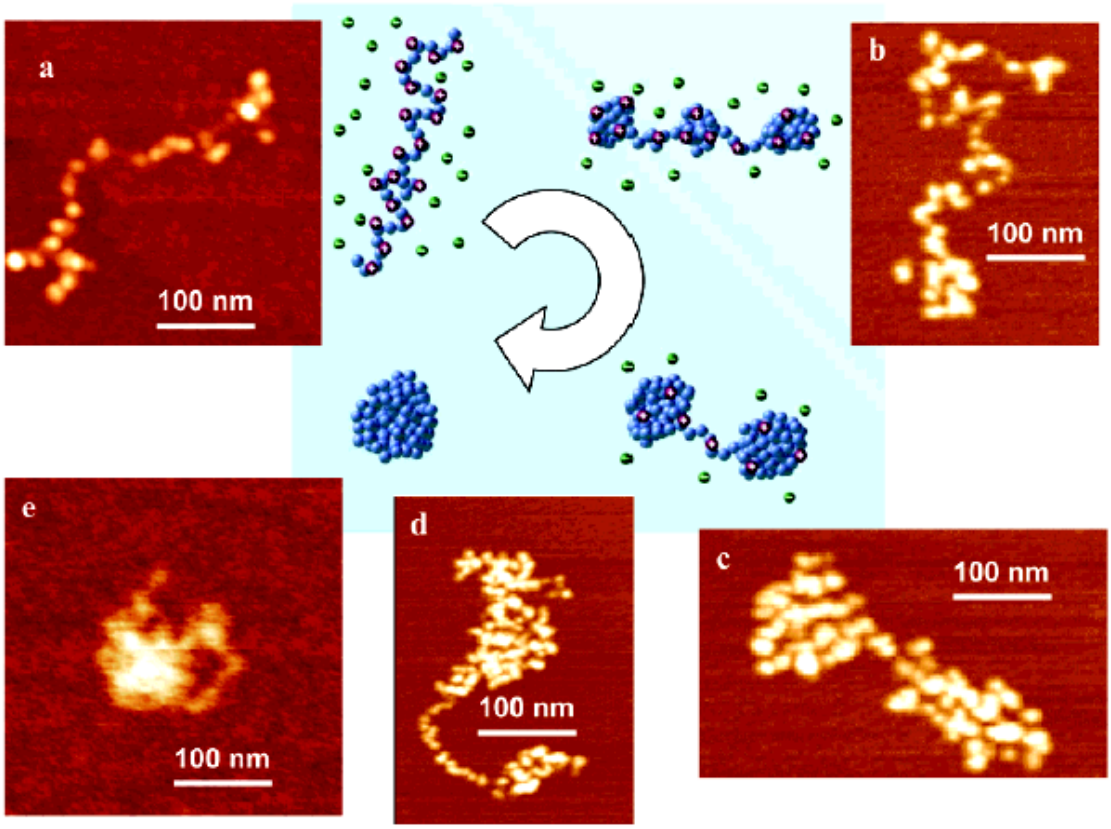

Figure 4.7 Metallized nanoparticles produced from P2VP molecules (M_n = 385 000 g/mol) adsorbed in different conformations. The polymer coils undergo a cascade of transitions from wormlike conformation to necklacelike and compact globule driven by the interplay between attractive short-range and repulsive long-range interactions. The arrow follows an increase of the ionic strength of solution: pH 2, salt free (a); pH 2.5, 0.02 mol/L NaCl (b); pH 3.5, 0.02 mol/L NaCl (c); pH 3.5, 0.1 mol/L NaCl (d); pH 3.5, 1.0 mol/L NaCl (e).

4.3.2. Metallization of PMB molecules by multy-step procedure

Metallization procedure described in previous subchapter was found to be applicable also for other polycations, in particular for poly(methacryloyloxyethyl dimethylbenzylammonium chloride) (PMB).

PMB-1 molecules adsorbed onto mica (root-mean roughness less than 0.05 nm) from extremely diluted (0.005 mg/ml) aqueous solution appear in AFM images as worm-like chains **(**Figure 4.8a, b). PMB-1 single molecules deposited on Si wafers (root-mean roughness 0.2 nm) display the same conformation but the resolution of the images is much poorer because of the larger roughness of the Si wafers (Figure 4.8c).

Metallization of PMB molecules were done by the *Procedure 3* (or "step-by-step" procedure). After Pd deposition the resulting nanowires appear in AFM images as a 1D sequence of interconnected Pd clusters (Figure 4.9a, b). The wire-shaped Pd nanoparticles are visualized in profiles of AFM images as undulations interconnected by bridging strings.

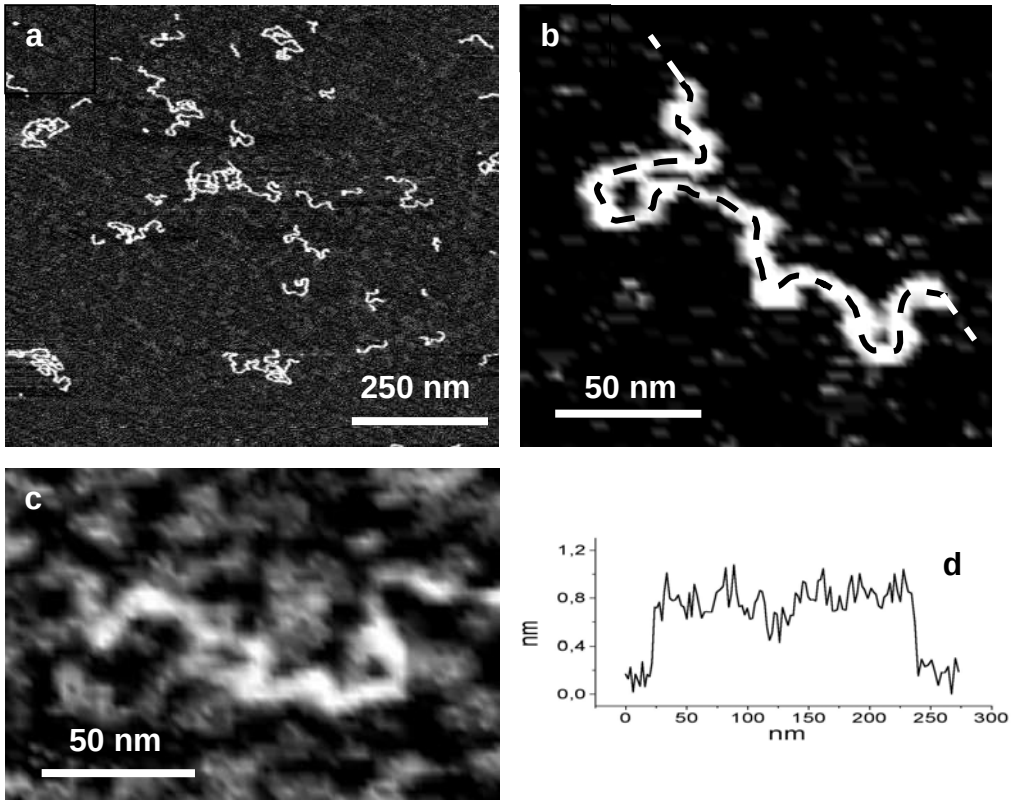

Figure 4.8 Representative AFM topography images (*Z* range 3 nm) of PMB-1: (a) on mica, (b) zoom of the image a, (c) on Si wafer, and (d) cross-section, taken along the chain as shown by the dash line in the image b. Here and below we present original AFM images (without deconvolution) in which lateral dimensions of the structures are overestimated. The dimensions of the structures corrected using the value of the tip radius are shown in Table 4.2.

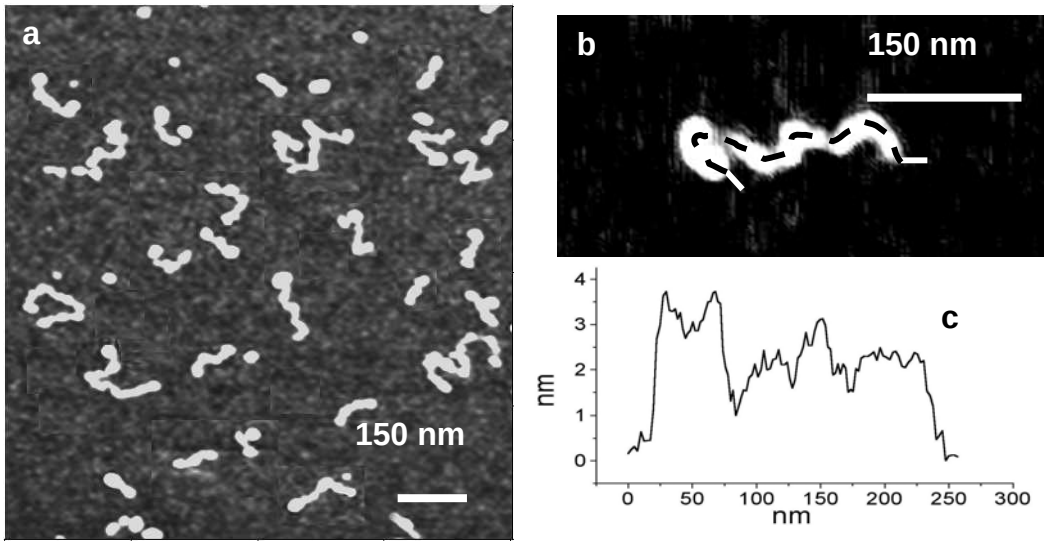

Figure 4.9 Representative AFM topography images (Z range 7 nm) of Pd-PMB-1 wire-shaped nanoparticle adsorbed on Si wafer (a, b) and cross-section along the long axis of the nanowire on image b (c)

The statistical analysis of number average (L_n) and weight average (L_w) contour length, height (H), and width (W) of bare PMB-1 molecules was done for 150 structures (Table 4.2, Appendix 5 a-c). The values of contour length were used to calculate the number average M_{nAFM} = 362 kg/mol and the weight average M_{wAFM} = 516 kg/mol molecular weights, and polydispersity index PDI = 1.42 of the polymer using the following equation (for example for number average molecular weight):

$$M_n = \frac{L_n \times m_{mon}}{2 \times l \times \sin(\theta/2)}$$

where l = 0.154 nm is the length of the C-C bond in the backbone, θ = 109°. is the valence angle between C-C bonds in the backbone, and m_{mon} = 284 g/mol is molecular mass of the monomer unit.

Table 4.2 Average sizes of PMB molecules and Pd-nanowires obtained from AFM images.

Sample	Contour length, nm L_n / L_w / PDI	Height, H, nm	Apparent width before deconvolution, W, nm	Width after deconvolution, W, nm
PMB-1	319/454/1.42	0.75 ± 0.15	17.4 ± 5	2.4 ± 0.6
Pd-PMB-1	251/368/1.47	2.6 ± 0.7	23.1 ± 8	4.1 ± 1.5

The statistical analysis of parameters of metallized structures extracted from the AFM images and profiles: height, width, and contour length of nanowires (Table 4.2, Appendix 5 d-f) have also performed. For the representative series of experiments we obtained the same average values of height (2.6 ± 0.7 nm) and width (4.1 ± 1.5 nm). The number-average contour length of metallized PMB deposited onto Si wafers ($L_{n.met}$ = 251 nm) is only slightly smaller than the length of starting PMB. The same images and quantitative characteristics of the structures were obtained before and after reduction of Pd(+2) coordinated by PMB. It suggests that morphology of the metallic nanowires is determined by the conformation of Pd-PMB hybrid worm-like chains adsorbed on Si wafers. In contrast, nanowires produced by the same procedure onto the surface of mica results in considerably more collapsed nanoparticles (Figure 4.10). An origin of this difference is still unknown, but probably, it is due to the poorer adsorption of PMB chains on mica than on Si wafers.

The lengths of the resulting Pd nanowires are determined by the length of underlying polymer chains like in case of P2VP-Pd nanowires. To prove this point, we metallized the sample of PMB2 of much larger molecular weight (M_w = 6300 kg/mol). The number average contour length of the nanoparticles fabricated from this sample was $L_{n.met}$ = 1000 nm (Figure 4.11).

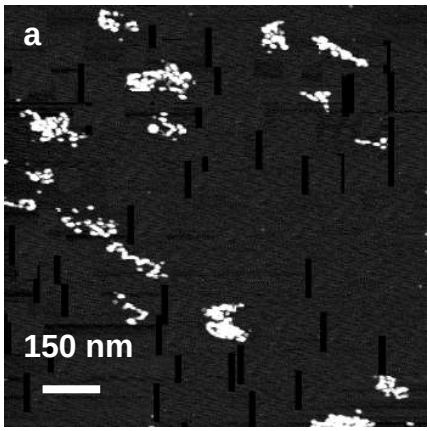

Figure 4.10 Representative AFM topography image (Z range 7 nm) of Pd-PMB-1 nanoparticles on mica.

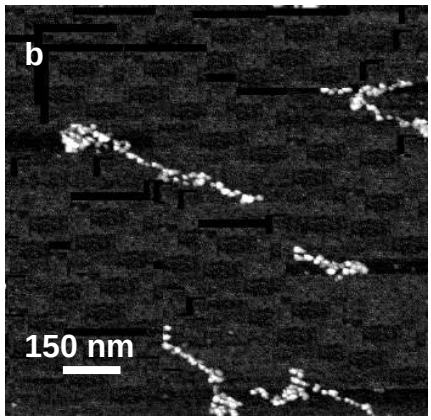

Figure 4.11 Representative AFM topography image of Pd-PMB-2 nanoparticles on Si wafer (Z range 7 nm).

Thus, the deposition of palladium clusters onto the single molecules PMB results in wire-shaped nanoparticles of about 5 nm in diameter and number-average contour length equal to 251 or 1000 nm, depending on molecular weight of PE. Those metallized nanoparticles reflect the conformation and the length of original adsorbed PE molecules.

4.4. Conclusions

Thus, the developed metallization procedure is general and can be applied for nanowires fabrication from different polycations. As a result, we have shown that molecular details of the adsorbed linear flexible polyelectrolyte molecules determine the dimensions of the nanostructures after metallization and that observed sizes are consistent with the decoration of single molecules with nanoclusters. The dimensions of the obtained nanowires are significantly smaller than those previously reported.[121,123,124,125] All of these features are of the potential benefit in applications for nanodevices and permit one to use polyelectrolyte molecules of different architectures to generate metallic nanoobjects of a desired shape.

Chapter 5.

Reconformation and Metallization of $P2VP_7$-PS_7 Star-like Block Copolymer

Single molecule conformations and associate morphologies for polystyrene/poly(2-vinylpyridine) (PS_7-$P2VP_7$) heteroarm star copolymer, formed in controlled environment and deposited onto mica or Si-wafers, have been studied by atomic force microscopy (AFM) with molecular resolution. At concentrations below 0.01mg/ml PS_7-$P2VP_7$ exists in molecularly dissolved state in both selective (acidic water, toluene) and common good (chloroform, tetrahydrofurane) solvents. In acid conditions PS_7-$P2VP_7$ forms either unimolecular or multimolecular micelles depending on concentration and pH. The core of the micelles is constituted of the collapsed PS arms surrounded by protonated P2VP shell. PS_7-$P2VP_7$ undergoes inverse intramolecular segregation upon addition of toluene. In this case, P2VP arms form the dense core of the micelles embedded in the swollen PS shell. The transition between those two inverse types of micelles is strongly modified by interaction with the mica substrate. The micelles deposited onto mica from acidic water are trapped via P2VP extended arms. Upon treatment of the trapped micelles with toluene the PS core is swollen and PS arms gradually adopt an extended conformation whereas P2VP trapped arms retain their extended conformation due to the strong interaction with the mica substrate. The obtained "squash" structures exhibit a unique conformation that is not expected to exist in any solvent and could not be obtained upon a simple adsorption procedure. Surface-supported metallization of the PS_7-$P2VP_7$ on Si-wafers improves AFM resolution due to the selective deposition of the Pd clusters along the P2VP chains. Thus the number of P2VP arms of the unimers as well as the aggregation number of the multimolecular micelles, and morphological details of the structures were directly analyzed.

5.1. Introduction

Star-shaped block copolymers have attracted much interest for the last decades due to their unique complex architecture that introduces novel properties different from those of their linear counterparts[127]. Heteroarm star copolymers constitute a specific type of star polymers where two different kinds of arms emanate from the same core (A_nB_n type)[128]. They can be viewed as a number of diblock copolymers covalently joined together at their A-B junction points. Thus, the fixed number of diblock copolymers (defined from the synthetic procedure) will remain chemically associated in solution even in non-selective solvents at extremely low concentrations. Such a molecule undergoes diverse conformational transitions in changing environment representing a very promising type of a responsive material for the fabrication of smart polymer films, micelles[129], and drug delivery systems.

We explore the AFM experiments with single molecules deposited from very diluted solution onto a solid substrate. The molecules are scanned in the tapping mode after a rapid evaporation of solvent. A correct interpretation of the obtained results requires to take care on possible changes in conformations introduced by the AFM experiment itself due to the interaction with the tip, or due to the deposition procedure. The first can be relatively easy controlled, while the second makes a real problem for the application of AFM in single polymer molecule study. We address the question how large are changes in the conformation for the deposited molecule as compared to the conformation in solution? These changes depend strongly on history of the sample and on the specific behavior of the particular system so, that there is no general answer and the interpretation of the results should be referred to each particular system. Study of the molecules with complicated architecture helps very much in solution of the problem as we show in this report.

The PS_7-$P2VP_7$ copolymer self assemble in the bulk[130] due to incompatibility of the different arms as well as they form micelles in selective solvents[131]. In the latter case it was found that the critical micelle concentration (cmc) of the copolymer is much higher than that observed for the linear block copolymers showing that the single star molecules survive (no association) at relatively low concentrations[131]. An interesting property of this copolymer is that the P2VP arms can be protonated in acidic media, and, thus, they can be transformed to a week cationic polyelectrolyte. Therefore, the copolymer is transformed to an amphiphilic state upon protonation. Since the hydrophilic part is a week polyelectrolyte, it responds to external stimuli such as pH and ionic strength.

In this chapter we describe a variety of structures formed by the copolymer due to the interplay of the van der Waals and electrostatic interactions in different environment and with the mica substrate.

5.2. Experimental Part

5.2.1. Materials

The PS_7-$P2VP_7$ heteroarm star copolymer was prepared by the group of Prof. Tsitsilianis via a three-step sequential "living" anionic polymerization procedure using divinylbenzene linkage (DVB)[132]. In the first step the polystyrene arms were prepared using *sec*butyl Lithium as the initiator at -40 ^{o}C in THF. After the consumption of the styrene monomer and sampling out, a small amount of divinylbenzene was added to the reaction medium. Star-shaped polystyrene (PS_n) was thus formed, part of which was deactivated and sampled out for the purpose of characterization. The rest "living" star polymer was used to initiate the polymerization of a chosen amount of 2-vinylpyridine that was added to the reaction medium at -75^{o}C. After complete polymerization of 2-vinyl pyridine the reaction mixture was deactivated with degassed methanol and the final product was recovered by precipitation in cold heptane, dried, redissolved in benzene and freeze-dried. The molecular characteristics of the copolymer are given in Table 5.1.

Table 5.1 Characteristic of the PS_7-$P2VP_7$ sample.

$M_w(PS_{arm})$, g/mol /number of arms	by SEC/calc.	20000/6.9
$M_w(P2VP_{arm})$, g/mol /number of arms	by LS/calc.	56500/6.9
W_{P2VP}, weight fraction of P2VP	by NMR	66(%)
$M_w(PS_7$-$P2VP_7)$, g/mol	by LS	544000

5.2.2. Sample Preparation

Samples preparation. Solution of PS_7-$P2VP_7$ in THF (0.01 g/l) was diluted by slow addition of the 10-fold excess of either acidic (pH 1, 2, 3.5, or 4.2, HCl, Aldrich) water (Milipore water, 18 MΩm × cm), or toluene, or chloroform. For experiments with salt 1 ml of PS_7-$P2VP_7$ solution in THF (0.01 g/l) was diluted by slow addition of 8 ml of acidic water (pH 2) and then 1 ml of 10mM Na_3PO_4 (Aldrich). After stirring (in the most cases for 2 h) we set a drop of the solution on the surface of freshly cleaved mica (isoelectric point at pH 3.0) for 1 minute and afterwards removed the rest of the drop with week centrifugal force. The dry samples were investigated with AFM. For reconformation-on-the-surface experiments PS_7-

$P2VP_7$ have been, firstly, adsorbed from the acid water solution and dried. In the second step, we set a drop of toluene on this sample and covered it with a Petri glass to prevent the solvent evaporation. Afterward samples taken in different periods of time were dried and investigated with AFM.

Metallization of PS_7-$P2VP_7$ on Si-wafers. Highly polished Si-wafers (obtained from Wacker-Chemitronics) were first cleaned in a ultrasonic bath three times for 5 min with dichloromethane (DCM), placed in the cleaning solution prepared from NH_4OH and H_2O_2 at 60^oC for one hour. (Note: the NH_4OH:H_2O_2 solution reacts violently with organic compounds. Caution should be used when handling this solution). Samples were finally exposed to 50% sulfuric acid for 15 min and then rinsed several times with Milipore water (18 MΩxcm). Na_2PdCl_4, dimethylamine borane (DMB) and DCM were used as received from Aldrich. Solution of PS_7-$P2VP_7$ in THF (0.01 g/l) was diluted by slow addition of the 10-fold excess of acidic water (pH 2, HCl). After stirring during 120 minutes we set a drop of the solution on the surface of the cleaned Si-wafer for 1 minute and afterwards removed the rest of the drop with a centrifugal force. Then, in the second step, the Si-wafer was rinsed several times with water and placed into the Na_2PdCl_4 solution (pH 2, HCl) for 1 min for the formation of the $P2VPH^+...(PdCl_4)^{2-}$ composite. In the third step the Si-wafer was thoroughly rinsed with water, placed for 15 sec into reduction solution which contained 1.0 mg/ml of DMB. Finally, the Si-wafer was cleaned with water and dried with an argon flux.

5.3. Results and Discussion

5.3.1. Star block Copolymer Structures Formed in Good Common Solvents

Chloroform and tetrahydrofurane (THF) are good solvents for both P2VP and PS components and PS_7-$P2VP_7$ molecules are expected to be molecularly dissolved. However, the molecules deposited on the mica surface from very dilute solutions show different conformations for those two solvents. The molecules deposited from chloroform were observed to form a hat like structures, consisting of a very flat bottom-layer about 1 nm in height, and 48 nm in diameter, and a semispherical top-layer near 2.6±0.2nm in height (H), and 18±4 nm in diameter (D) (Figure 5.1a-c,e; Table 5.2). In this case and below for simplicity in the discussion we represent all structures formed by the copolymer deposited on the mica surface as apparent core-shell structures, where the compact fragment formed by collapsed arms we take as core, while extended arms we take as shell.

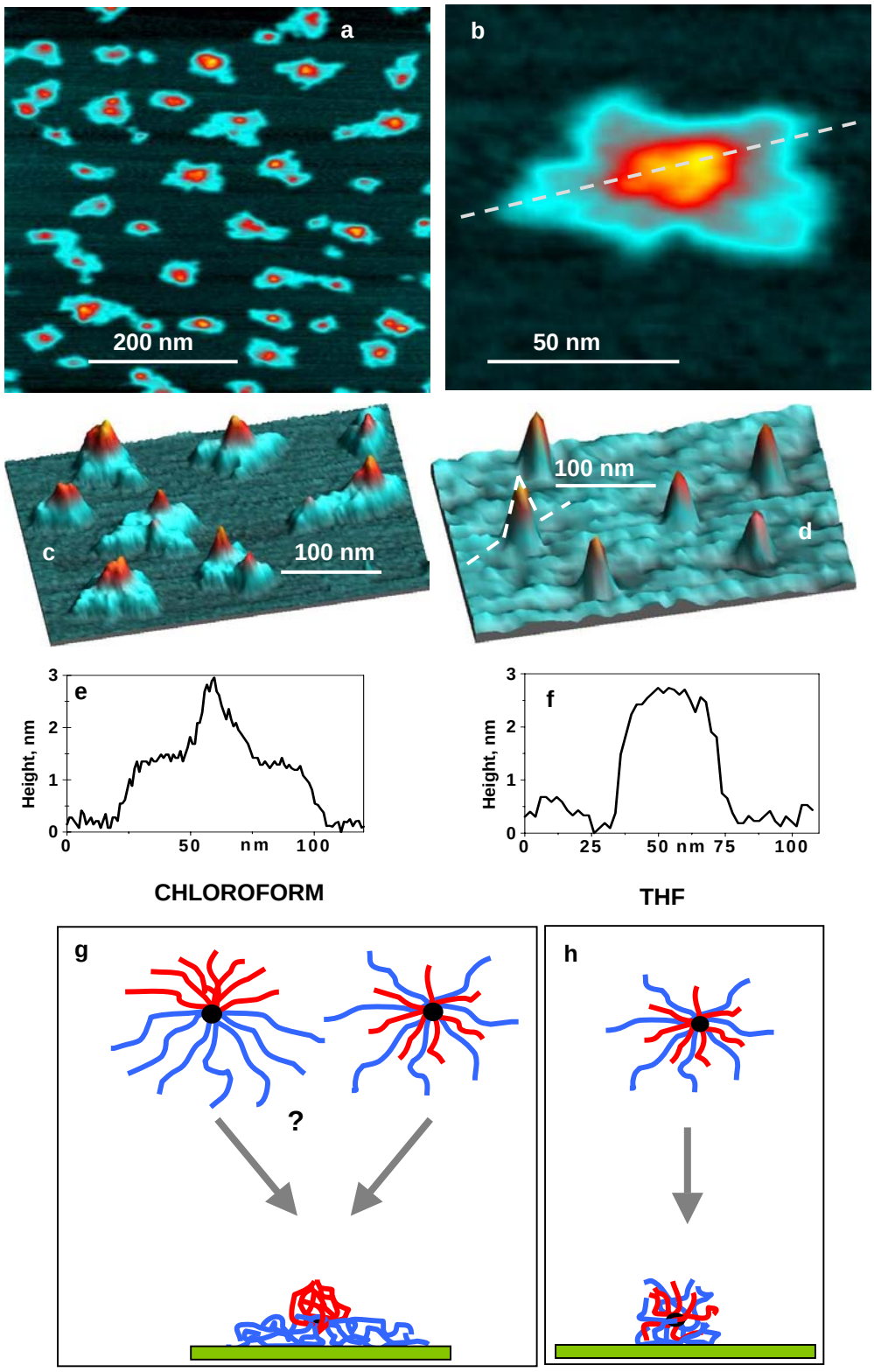

Figure 5.1 Representative AFM topographic images (a-c) and cross-section (e) of the PS_7-$P2VP_7$ adsorbed from chloroform on mica. 3D-AFM image (d) and cross-section (f) of unimers adsorbed on mica from THF. Schematic representation of the solution conformations and conformations in adsorbed dry state of the PS_7-$P2VP_7$ in chloroform (g), and THF (h), respectively (red color indicates PS arms).

Table 5.2 Average dimensions of the PS_7-$P2VP_7$ (on the base of at least 100 structures taken from 5 to 10 AFM images for each condition).

Conditions	Shell		Core	
	Diameter, nm	Height, nm	Diameter, nm	Height*, nm
$CHCl_3$**	46±8	1±0.2	18±4	2.6±0.2
THF**	36±10	2.4±0.5		
pH 2**	126±35	0.3±0.1	17±7	2.9±0.3
Pd-metallized unimolecular micelles	122±30	1±0.2	9±2	7.2±2
pH 2, Na_3PO_4, 0.2mg/ml**	99±15	0.1±0.2	15±5	5.6±0.5
pH 3.5 (unimers, 81% /micelles, 19%)	119±30	0.3±0.1	10±2/20±4	4.9±0.5/16±3
pH 4.2 (micelles) **	137±35	0.3±0.1	22±5	17±1
pH 1, 0.3g/l of PS_7-$P2VP_7$ (micelles)	-	-	34±5	15.9±3
pH 1, 0.1g/l of PS_7-$P2VP_7$ (micelles)	-	-	30±5	12.5±3
pH 1, 0.03g/l of PS_7-$P2VP_7$ (micelles)	195±40	0.4±0.1	25±5	12.1±3
Pd-metallized multimolecular micelles	151±50	1±0.2	40±10	25.4±5
Toluene 3min**	55±5	0.6±0.2	44±5	2.9±0.3
Toluene 30min**	80±10	0.5±0.2	36±10	2.4±0.3
pH 2, adsorption, then toluene 30min	129±40	0.4±0.1	41±10	2.3±0.5
pH 2, adsorption, then toluene 5h	140±50	0.8±0.5	-	-

*Measured from baseline on the mica surface.
**0.001g/l of PS_7-$P2VP_7$

To evaluate the volume (V) of the visualized structures for simplicity following formula for the cone shape was used: $V_{cone}=1/3H\times\pi(D/2)^2$, where H, and D are the height and diameter of structures observed with AFM and presented in Table 5.2. The values were compared with the calculated volume based on molecular composition of the copolymer: $V_{PS\ calc} = 7 \times N_{PS} \times M_S \times \rho_{PS}/N_A = 7 \times 190 \times 105 \times 1.05/6 \times 10^{23} = 245\text{nm}^3$, where, N_{PS} is the degree of polymerization of PS arms, M_S is the molecular mass of styrene unit, ρ_{PS} is the density of PS, and N_A is Avogadro´s number. Similar calculation for P2VP arms give $V_{P2VPcalc}=698\text{nm}^3$, and the total volume per molecule $V_{PS7\text{-}P2VP7calc}=943\text{nm}^3$.

However, when PS_7-$P2VP_7$ molecules are deposited on the surface from THF solution, approximately uniform spherical particles with D=36±10nm and H=2.4±0.5nm (Figure 5.1d,f; Table 5.2) are formed. We may speculate that this difference in morphology of the structures from THF and chloroform might be attributed to different conformations in solution. It seems that in chloroform, an intramolecular segregation occurs, leading to "Janus" like star copolymers (Figure 5.1g) whereas in THF the different arms are distributed randomly around the star core (Figure 5.1h). The phenomenon of block copolymer segregation in common good solvents, has been observed indirectly by viscometric measurements in diblock and also in star copolymer dilute solutions[133]. Also, some analogy of the heteroarm star block/copolymer to mixed polymer brushes on a flat substrate could be mentioned here. The mixed brushes demonstrate a rich phase behavior. Change of solvent selectivity results in switching between different phases, e.g from disordered state to laterally segregated or perpendicular (to the substrate) segregated phases.[134]

To support that assumption we present the solubility parameters for PS and solvents (Table 5.3) found in literature[135] and the solubility parameter for P2VP calculated from the interaction parameter $\chi_{PS\text{-}P2VP}$=0.1[136] using the equation $\chi_{PS-P2VP} = \frac{V_r(\delta_{PS} - \delta_{P2VP})^2}{RT}$, where V_r is the molar volume of P2VP (98 cm^3/mol), δ_{PS}, and δ_{P2VP} are the solubility parameters for PS and P2VP, respectively. The differences of the solubility parameters $(\delta_{Polymer} - \delta_{Solvent})^2$ presented in Table 5.3 demonstrate that chloroform is more selective solvent (for PS) than THF. Hence, chloroform may promote phase segregation in the star copolymer schematically shown in Figure 5.1g.

Once a copolymer molecule approaches the mica surface, the P2VP arms are oriented towards the substrate due to their high affinity. Such a mechanism of adsorption results in the observed structures after rapid evaporation of chloroform. Thus, the major P2VP constituent (66 wt%) is located on the surface forming the flat bottom-layer while the minor PS constituent is located on the top forming the semispherical bump (Figure 5.1g). On the other hand, in THF segregation of the arms can not be resolved in the AFM experiments indicating the formation of phases of a smaller characteristic size (Figure 5.1h).

To prove that the observed structures represent single molecules an experimental average volume of the structure was evaluated and compared with the values calculated from molecular mass of the polymers. The calculated values 698, 245, and 943 nm^3 are for P2VP arms, PS arms and total volume of the copolymer molecule, respectively. We assume that PS arms are not trapped on the surface and collapse to form structures with the bulk density.

Thus, we obtained the experimental volume for the PS core, if the copolymer is deposited from chloroform, to be 220 nm^3, that is in good agreement with the calculated value.

Table 5.3 Solubility parameters

polymer/solvent (subscripts)	solubility parameter $(cal/cm^3)^{1/2}$/ difference of solubility parameters
δ_{PS}	9.1
δ_{P2VP}	9.9
δ_{CHCl3}	9.33
δ_{THF}	9.51
$(\delta_{PS}-\delta_{THF})^2$	0.16
$(\delta_{P2VP}-\delta_{THF})^2$	0.15
$(\delta_{PS}-\delta_{CHCl3})^{1/2}$	0.32
$(\delta_{P2VP}-\delta_{CHCl3})^{1/2}$	0.05

5.3.2. Reverse $P2VP_7$-PS_7 Unimolecular Micelles in Acid Water: Effect of pH and Ionic Strength and Polymer Concentration

It was previously shown by light scattering that at a relatively high concentration (0.3 g/l) PS_7-$P2VP_7$ undergoes *intermolecular* micellization in acid water (pH 1-2) with the aggregation number equal to 8[131c]. In contrast, at extremely low concentrations (0.005 g/l of PS_7-$P2VP_7$) micellization occurs as an *intramolecular* process. In this conditions the PS_7-$P2VP_7$ star copolymer survives in non-associated state and forms stable unimolecular micelles. Figure 5.2 shows representative AFM images of mica-deposited uniform star-shaped core-shell structures formed upon dilution of PS_7-$P2VP_7$/THF solution with acid water (pH 2). Such a morphology reflects very pronounced intrasegregation of the star copolymer in acid water.[137] PS chains collapse due to hydrophobic interactions and form a compact core whereas protonated P2VP arms adopt an extended conformation due to the Coulomb repulsion and form a shell (Figure 5.2e). We may conclude that the AFM image represents an "off print" of the solution conformation when the molecules were adsorbed and trapped by the substrate. After the rapid evaporation of water the structure was formed due the collapse in Z-direction (Figure 5.2f). The experimental value of the collapsed PS core volume is about 219 nm^3 that again corresponds to the calculated value (245nm^3).

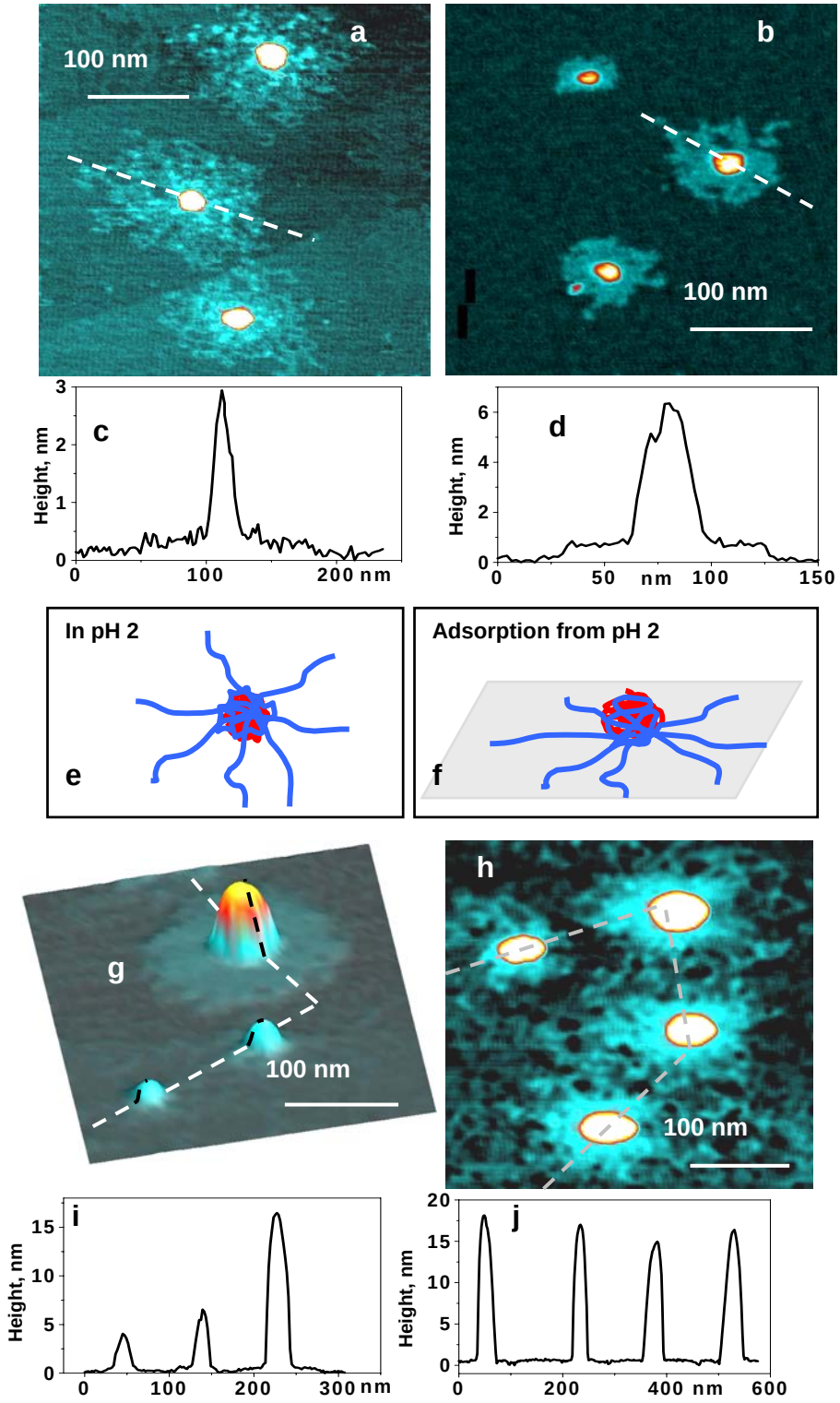

Figure 5.2 AFM topographic images (a,b,g,h) and cross-sections (c,d,i,j) of PS$_7$-P2VP$_7$ adsorbed from acid water (pH 2, HCl) onto mica: in salt free condition (a,c) and in the presence of 1mM of Na_3PO_4 (b,d). Schematic representation of the unimolecular micelle formed in acid water: in solution (e); in adsorbed state (f). 3D-image (g) and cross-section (i) of micelles with different aggregation number formed at pH 3.5. AFM images (h) and cross-section (j) of multimolecular micelles adsorbed from acid water (pH 4.2, HCl).

To improve AFM resolution of P2VP arms we employed approach to decorate polyelectrolyte chains with Pd metal clusters described in Chapter 4 (Procedure 3). After metallization PS_7-$P2VP_7$ deposited on the Si-wafer from acidic aqueous solution with fully extended P2VP arms appears in very good resolved star-shaped conformations (Figure 5.3). The P2VP arms decorated with Pd clusters are clearly observed in the AFM images and can be counted (Table 5.4).

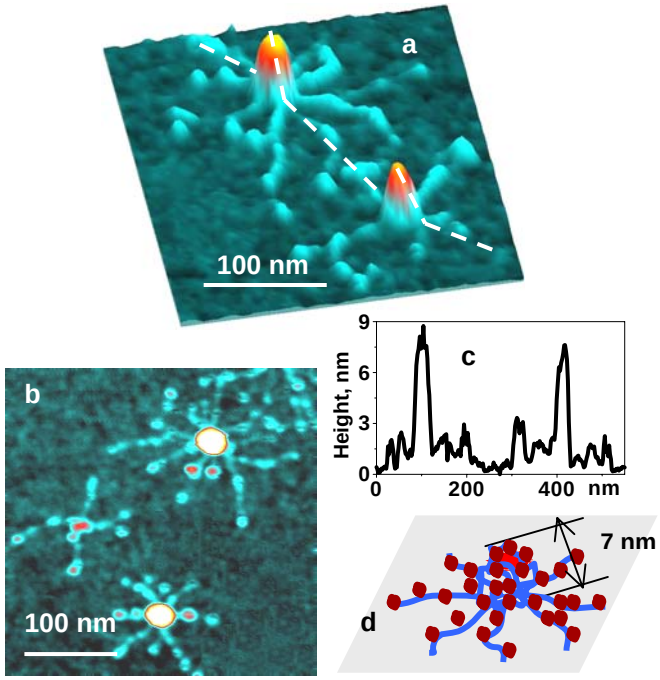

Figure 5.3 3D- (a), 2D- (b) AFM images, cross-section (c) and schematic representation (d) of Pd-metallized unimers.

Table 5.4 Dimensions of Pd...PS_7-$P2VP_7$ nanocomposites (averaged from 52 structures in 6 AFM images).

Length (L), height (H) and number (N) of P2VP arms			Diameter (D) and height (H) of PS core		Diameter (D), height (H), and number (N) of Pd clusters per arm		
L, nm	H, nm	N	D, nm	H, nm	D, nm	H, nm	N
61±15	1±0.2	7	9±3	7.2±2	3±1	2.2±1	3±1

The AFM images for the first time visualize the second generation of the P2VP arms, which were grown from the active sites located on the DVB core of the PS star polymer precursor. Although, the first generation of the PS arms was characterized (number of arms) by light scattering from the molecular weight of the star copolymer and the characterization of individual arms (sampling out before adding DVB), the characterization of the P2VP arms was now performed due to their visualization. The average number of P2VP arms was

counted directly from the AFM images to be 7±1.26 (Figure 5.4), that was in excellent agreement with the number of PS arms found by light scattering. This result gives unambiguous evidence that the number of the chemically different arms is equal. At the same time, that is very exciting example how AFM visualization can be used for analysis of polymer architecture.

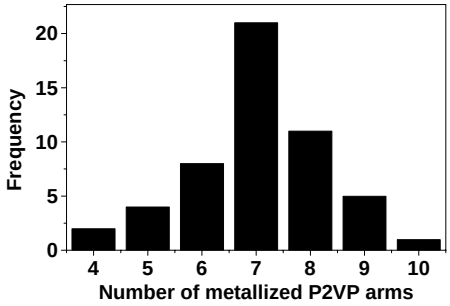

Figure 5.4 Distribution of number of metallized P2VP arms (taken from 52 structures in 6 AFM images).

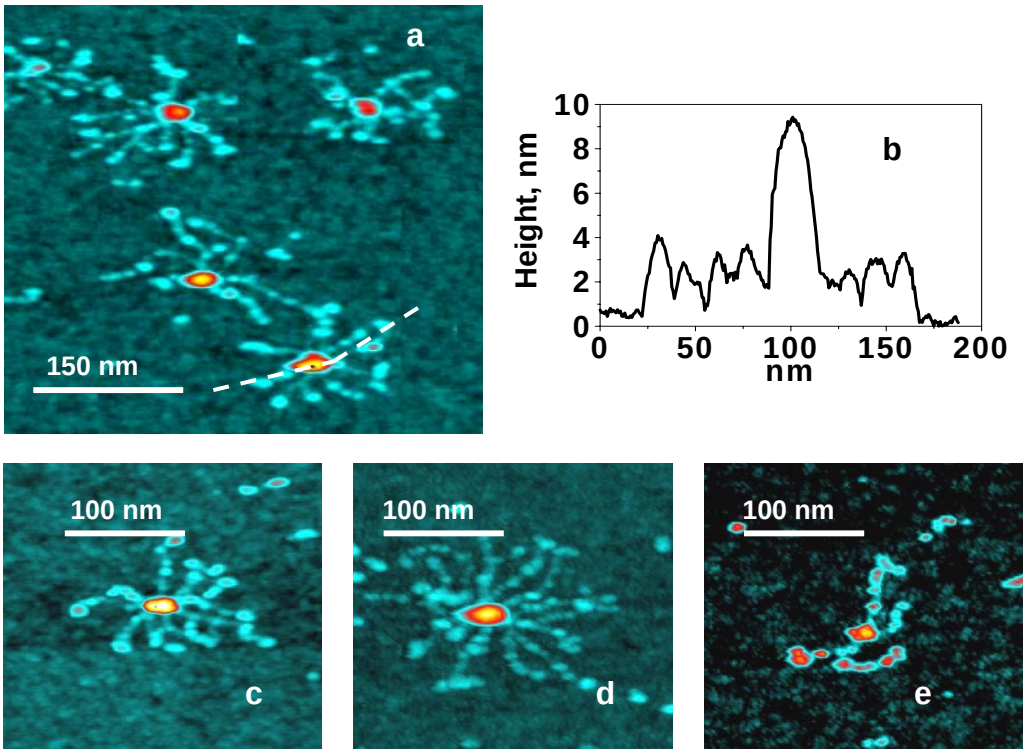

Figure 5.5 AFM topographic images of Pd...PS_7-$P2VP_7$ nanocomposites on Si-wafer: representative picture (a); cross-section taken along two arms of the star (b); molecules with different number of metallized P2VP arms: 7 (c); more then 10 (d); 4 (e).

Metallization of the adsorbed PS_7-$P2VP_7$ molecules allowed us to get better insight into the structure of the unimolecular micelles. Specifically, a considerable increase of the height of the cores was found upon metallization (from H=2.9nm before metallization to H=7-12nm

after, Table 5.2). Ion-exchange reaction of palladium tetrachloride dianion serves as a selective and efficient probe for polycations, and, thus, such an observation clearly indicates that pyridine units are localized in the shell and in the core of the micelles (Figure 5.3d).

Na_3PO_4 is a strong condensation agent for PE. A coil-globule transition for a cationic PE was documented at 10-15 mM of Na_3PO_4 (see chapter 3.3.2). A full precipitation of PS_7-$P2VP_7$ from acid water (pH 2) solution at even lower concentration of Na_3PO_4 (5mM) was observed. However at 1mM Na_3PO_4, PS_7-$P2VP_7$ molecules survive in non-associated state with a contracted shell (D=99±15nm instead of D=126±35nm in salt-free conditions; Table 5.2; Figure 5.2b). On the other hand, the size of the hydrophobic core increases (H=5.6±0.5nm instead of H=2.9±0.3nm in salt-free conditions) indicating that uncharged P2VP arms condense on the core. This confirms the suggestions deduced indirectly from light scattering and fluorescence measurements reported previously[131c]. On the other hand this experiment gives the additional evidence that the deposited structures analyzed with AFM precisely reflect the prehistory in the solution.

Unimolecular micelles were found to be stable in dilute solutions at pH 2 during at least several days. At pH 3.5 about 20% of PS_7-$P2VP_7$ molecules undergo association leading to multimolecular micelles, whereas most of molecules remain unassociated (unimers) with slightly compressed shells (Table 5.2). Figure 5.2g,i shows clearly the coexistance of micelles and unimers with significant differences on their size. At pH 4.2, the association phenomena lead to multimolecular micelles (Figure 5.2h,j). The size of the PS cores (H = 17±1; D = 22±5) is increased significantly as compared to unimolecular micelles. The association is also reflected in an increase of the diameter of the shell (D = 137±35) if more P2VP chains are accumulated in the corona resulting in larger stretching due to the volume exclusion effect. The formation of micelles at pH 4.2 (Figure 5.2h,j) may be attributed to the fact that a considerable part of P2VP exists in non-protonated state altering the hydrophobic-hydrophilic balance of the copolymer, and therefore destabilizing the unimers inducing association.

At the concentration higher then 0.01 g/l in acid water (pH 1) PS_7-$P2VP_7$ forms aggregates. As expected, the increase of the polymer concentration leads to the increase of the aggregation. Although most of structures formed at concentration 0.03 g/l are unimolecular micelles, ten-times more concentrated solution demonstrates a comparable amount of multimolecular micelles and unimers (Figure 5.6).

Metallization by Pd improves the AFM contrast and allows to estimate the aggregation number by the direct counting of the metallized arms (Figure 5.7b). As in the case of unimers,

metallization of the multimolecular micelles leads to the increase of the height of the core from 10-20 nm before metallization to 25-35 nm after metallization.

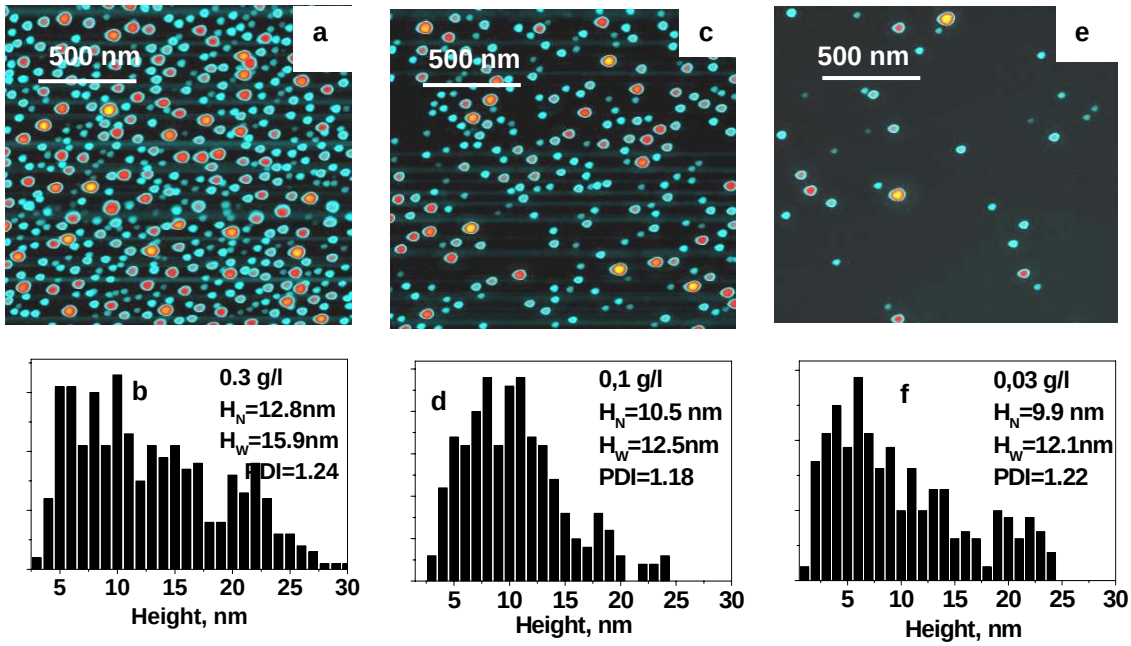

Figure 5.6 AFM images and height distribution diagrams of micelles obtained in acid water (HCl, pH 1) at different concentration of PS_7-$P2VP_7$: 0.3g/l (a,b); 0.1g/l (c,d); 0.03g/l (e,f). All structures with the height larger as 10 nm we consider as associates.

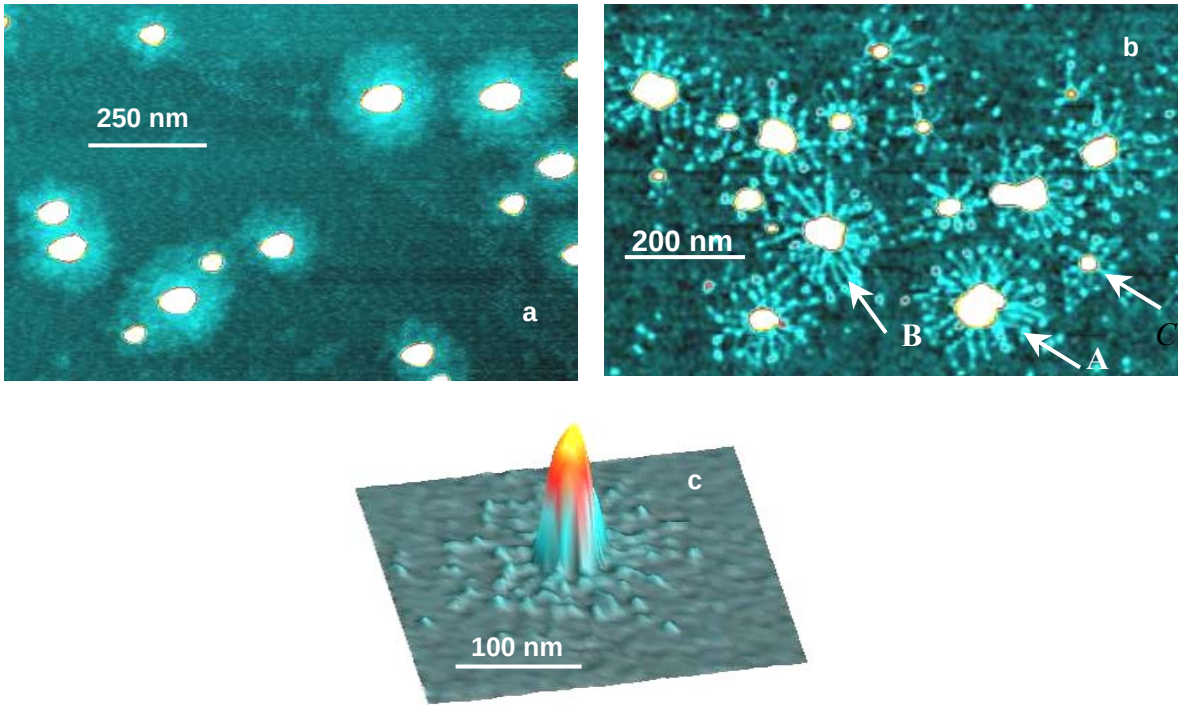

Figure 5.7 Coexistence of uni- and multimolecular micelles at concentration of PS_7-$P2VP_7$ 0.03g/l (HCl, pH 1) before (a) and after metallization with Pd (b,c). Metallization improves AFM contrast and thus aggregation number can be directly estimated. For example, the structure marked as A corresponds to tetramer with about 28 P2VP arms, as B corresponds to trimer with about 21 P2VP arms, and C marks unimer with seven P2VP arms.

5.3.3. Unimolecular Micelles of $P2VP_7$-PS_7 Adsorbed From Selective Solvent for Polystyrene

It is well documented that the critical micelle concentration (*cmc*) of similarly designed PS_6-$P2VP_6$ star copolymers in toluene is near 0.7 mg/ml and that at concentrations below *cmc* PS_6-$P2VP_6$ forms inverse unimolecular micelles[131a]. AFM experiments confirm these results for PS_7-$P2VP_7$. Immediately after addition of toluene (good solvent for PS arms and bad solvent for P2VP arms) into the PS_7-$P2VP_7$/THF solution, intramolecular segregation occurs rather than aggregation. Unimers initially formed upon addition of toluene are poorly segregated particles consisting of swollen cores (D = 44±5nm) and small shells (D=55±5nm, Table 5.2; Figure 5.8a,c). A full reconformation of the unimers in toluene solution occurs within 1 hour. After subsequent adsorption star-like structures with well-definite PS arms (about 30 nm in length) in the shell and P2VP arms collapsed in the core were observed (Figure 5.8b,d).

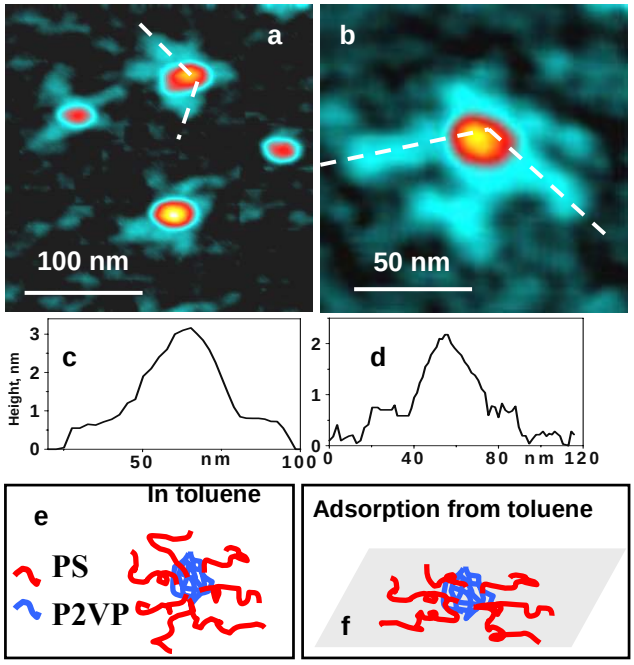

Figure 5.8 AFM images (a, b) and cross-section (c, d) of reverse unimolecular micelles formed upon addition of toluene in THF solution: after 3 minutes (a,c); after 30 minutes (b,d). Schematic representation of the reverse unimolecular micelle formed in toluene: in solution (e); in adsorbed state (f).

The core diameter is D=36±10nm, about twice of the PS core that is observed for the unimolecular micelles in water. The latter is consistent with the composition of the copolymer ($W_{P2PV}/W_{PS}\approx2$). Moreover, the P2VP core volume calculated from AFM data is V_{AFM}= 813 nm^3 which is slightly higher than the volume of P2VP blocks calculated from the degree of

polymerization ($V_{P2VPcalc}$= 698 nm^3).[138] That provides the evidence for the formation of the inverse unimolecular micelles upon addition of toluene.

5.3.4. Reconformation on the Surface

Above we declare that protonated single P2VP chains can be frozen in extended conformation upon adsorption onto the mica surface (chapter 3.3.3). Such adsorbed polycation molecules retain their initial conformation for a long period of time even after the exposure to solutions of a high ionic strength. This effect has been attributed to strong attractive interactions between P2VP chains and mica. On the other hand, we have found that adsorbed hydrophobic polymers interact weekly with the mica surface and alter their conformation responding to environmental changes. Exploring this different behavior of P2VP and PS chains on the mica surface we may produce a unique conformation of the block copolymer, which may not exist in any solvent and could not be obtained upon an adsorption procedure. Firstly, PS_7-$P2VP_7$ molecules were adsorbed onto mica from acid water in the star-shaped conformation with collapsed PS blocks and extended P2VP chains (Figure 5.2a). Thereafter, the mica substrate with the deposited copolymer was placed into toluene. The absorbed PS_7-$P2VP_7$ molecules gradually changed their conformation (Figure 5.9a-f) via swelling and extension of the PS arms. The P2VP arms retained their conformation unchanged. Finally, the PS_7-$P2VP_7$ molecules formed very flat “squash” structures. Multimolecular micelles deposited onto the mica surface undergo similar reconformation (Figure 5.9g-h). During the transformation the height of the core decreases (from 10-20 nm to 2-3 nm) whereas the diameter of the core increases several times (up to 100 nm).

Similar experiments were performed for the metallized structures. Initially, the unimers and multimolecular micelles were deposited on the Si-wafer. Afterward, we metallized the structures and exposed them to toluene. In contrast, the *metallized structures* (unimers and multimolecular micelles) *only partially decreased* their height upon exposure to toluene during several hours (from 7-12 nm to 4-6 nm for unimers and from 25-35 nm to 15-30 nm for multimolecular micelles, Table 5.2). Obviously, such a decrease is due to the reconformation of PS blocks from a collapsed into the more extended state. The remained material located in the center of the micelles, most likely, corresponds to the Pd clusters in the core of the micelles.

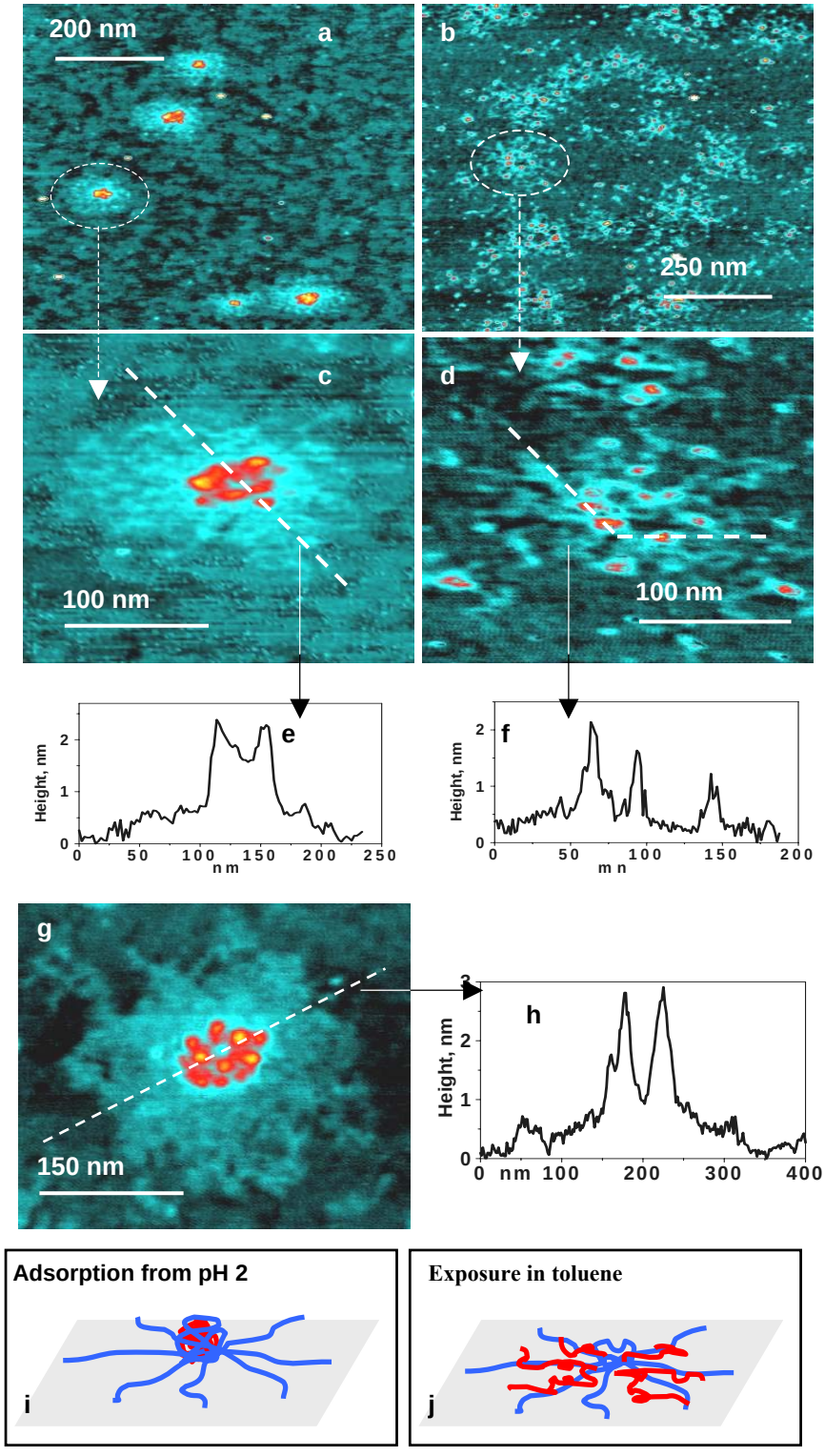

Figure 5.9 AFM images (a-d) and cross-sections (e and f) of the PS_7-$P2VP_7$ unimers (a-f) and multimolecular micelles (g-h) adsorbed from acid water (pH 2, HCl) onto the mica and then placed in toluene for 30 minutes (a, c and e) and 5 h (b,d-h). Schematic representation of the unimolecular micelle adsorbed from acid water (i), and formed upon exposure to toluene (j).

5.3.5. Comparison of the Molecular Dimensions on the Surface and in Solution

The chapter is focused on the possibility to reconstruct the molecular structure in solution based on the visualized with AFM single molecules deposited on the mica surface. Thus, we study the rapidly deposited molecules in the state which is far from equilibrium conformation. Adsorption can strongly modify the conformation, however the kinetics of the reorganization process can be relatively slow. At the same time, we may indeed expect changes in conformation of the molecules even during relatively short time of contact with the substrate. In Table 5.5 we compare sizes of single molecules evaluated with different methods in solution with the size of the shell obtained in the AFM experiments. The quite good agreement proved evidence that in this case the change of conformation on the surface is slow and the molecular size is not strongly changed during the deposition time.

Table 5.5. Comparison of the molecular radius (R) of unimers in solution and onto the mica surface after the rapid deposition.

Solvent	Radius, nm		
	Dynamic light scattering, R_h	Gel permeation chromatography* R_{GPC}	AFM R_{AFM}
THF	-	15[139]	18±5
toluene	31[131b]		40±5
water, pH 2	85[131c]		97±20

* approximation

The above mentioned experiments provide very nice example how the interplay between different interactions at solid-liquid interface may help to study behavior of polymer chain and how the interaction with substrate may help in single molecule experiment.

5.4. Conclusions

We found that PS_7-$P2VP_7$ block copolymers undergo diverse conformational transitions responding to external stimuli. At concentrations below 0.01g/l, PS_7-$P2VP_7$ exists in molecularly dissolved state in both selective (acid water, toluene) and common good (chloroform, tetrahydrofurane) solvents. In the latter case the obtained structures on mica show that a “Janus” like segregated structure is likely to exist in chloroform.

In acid conditions PS_7-$P2VP_7$ forms either unimolecular or multimolecular micelles depending on pH and ionic strength. PS_7-$P2VP_7$ undergoes the inverse intramolecular segregation upon addition of toluene. In this case, the inverse unimolecular micelles are constituted of the P2VP dense core and the PS swollen shell.

The PS core of unimers, adsorbed from acid water, *adopts* an extended conformation upon exposure to toluene whereas P2VP chains *retain* their extended conformation during this procedure. Thus the obtained "squash" structures present a unique conformation which does not exist in any solvent and could not be obtained upon simple adsorption procedure.

Metallization of the PS_7-$P2VP_7$ improves AFM resolution due to the selective deposition of Pd clusters along the P2VP chains. Thus, number of P2VP arms of the unimers as well as aggregation number of the multimolecular micelles can be directly estimated.

The conclusions from the most single molecule AFM experiments are in very good agreement with the results obtained from different methods exploring physical properties of molecule assembly. In our discussion we employed only few speculations. Finally, it gives evidence that, although the deposition of single molecule on a solid substrate may strongly alter the conformation in a general case, in the particular system the careful AFM experiment is indeed a powerful tool for the study of conformations of single polymer molecules.

Chapter 6.

Single Polycation Molecules Contrasted with Cyanide-Bridged Compounds

In this chapter we report on a simple contrasting procedure to improve AFM visualization of single positively charged polymer chains deposited on substrates of relatively high roughness via counterion exchange between Cl^- anions and bulky hexacyanoferrate anions or negatively charged nanoclusters of Prussian Blue. This method allowed us to increase the thickness of the resulting structures up to 10 nm, and consequently, to provide visualization of isolated polymer chains on glass surfaces with root-mean square roughness of about 1 nm. In contrast, the deposition of the relatively large PB clusters (more than 10 nm in size) distorts conformation and even eventually leads to a fragmentation of polymer chains.

6.1. Introduction

Atomic force microscopy (AFM) is broadly used for the characterization of polymer surfaces[140] as well as for investigation of isolated (single) polymer molecules.[101] In contrast to conventional physical and chemical methods which provide an information refereed to ensemble of molecules, AFM observation of individual members provides the direct information about properties of individual members as well as allows for the estimation of distribution. Most of experiments were performed with relatively "thick" macromolecules if the diameter of the chain was larger then 1 nm: dendronized polymers,[141] "molecular brushes"[142] and some naturally occurred polymers.[143] However, most of synthetic polymers and many natural polymers have much thinner chains.[144] In Chapter 3 we describe a successful visualization of several synthetic polycations (PC) and block copolymers of different architecture with AFM operating in the tapping mode. These polymers were deposited onto an atomically flat mica surface (root-mean square roughness, RMS less than 0.05 nm). However, they are "invisible" or very poor recognized on Si-wafers due to the higher roughness of the substrate surface (RMS = 0.2 nm). Several methods to improve the detection of polymer chains via chemical modification of tips[145] or by applying special AFM modes[146] has been proposed. Nevertheless, the development of new approaches for the investigations of *isolated chains with molecular resolution* on rough surfaces is still a challenging task.

We suggest that the selective deposition of appropriate materials along PC molecules (such as bulky counterions or nanoclusters) could be very promising method to increase the thickness of the PC chains and thus make them well-recognizable even on rough surfaces. Such a staining strategy is schematically represented in Figure 6.1. For a successful visualization the grain size of the contrasting agent should be larger than a mean size of surface features.

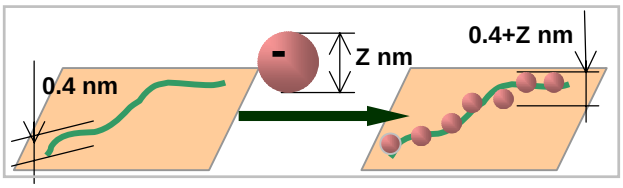

Figure 6.1 Schematic representation of the contrasting of adsorbed PC: 0.4 nm thick polymer chain becomes AFM-visible onto the rough surface due to deposition of bulky HCF-anions or nanoclusters with the grain size Z nm.

In the chapter 4.3.1.3 we have described an approach to produce *wire-shaped* Pd nanoparticles via metallization of flexible synthetic PC. The metallized molecules are nicely resolved on the Si-wafer with the TM AFM and the location of the Pd clusters clearly reflects

the contours of the underlying PC chains (Figure 6.2). Nevertheless, the interaction of PC molecules with the bivalent $PdCl_4^{2-}$ anions causes a strong contraction of polymer chains even if the chains are trapped by the surface. The observed worm-shaped metallized PC molecules can be considered as structures reflecting the substantially alternated PC conformations due to building the PC-Pd molecular composite (Figure 6.2c).

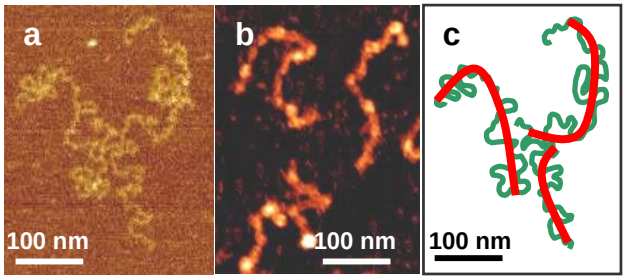

Figure 6.2 AFM topography images of P2VP molecules on mica(a); P2VP chains on Si-wafer decorated with Pd clusters (b). Schematic representation of a possible reconfomation of P2VP molecules affected by the deposition of Pd clusters (c).

Thus, an improvement of the staining procedure would be very important for the further development of AFM single polymer molecule experimental methods. The list of the characteristics to be improved for the staining method is as follows: a) high density of deposited contrasting clusters along the polymer chain; b) high selectivity of the staining material deposition; c) persistence of the polymer conformation in the staining procedure (upon reaction with the contrasting agents); d) reversible binding of the contrasting substances (a possibility to remove the staining material with no distortion of the polymer chain conformation).

6.2. Experimental Section

6.2.1. Materials

Samples of PMB (M_W = 6130 Kg/mol, polydispersity index (PDI) = 1.6) (see also chapter 3.2.1) were obtained from Dr. Werner Jaeger (Fraunhofer-Institut für Angewandte Polymerforschung, Golm, Germany). The synthesis is described elsewhere.[93] Poly(2-vinylpyridine) (P2VP) of molecular weight 385 kg/mol was purchased from Polymer Sources Inc. (synthesized by anionic polymerization, PDI of about 1.1).

6.2.2. Substrates

The following substrates were used: freshly cleaved mica, highly polished Si-wafers (obtained from Wacker-Chemitronics), Si-wafers with deposited by lithography gold stripes (electrodes), or microscope glass slides (Menzel-Glaser, Nr. 01 1101). Before experiments the substrates were first cleaned in an ultrasonic bath initially three times for 5 min with

dichloromethane (DCM), and then in the cleaning solution prepared from NH_4OH and H_2O_2 at 60°C for one hour. (Note: the NH_4OH:H_2O_2 solution reacts violently with organic compounds. Caution should be used when handling this solution). Samples were finally exposed to 50% sulfuric acid for 15 min and then rinsed several times with Milipore water (18 MΩ×cm).

6.2.3. Sample preparation

PMB or P2VP were deposited onto the respective substrate from the 0.0005 g/l acid water (pH 2, HCl, Aldrich) solutions by dipping of the substrates into corresponding solution or by drop casting. To deposit PC chain in stretched conformation we used a spin-coater and placed several drops of a PC solution onto the substrate rotating at 10000 rpm. The dry samples were investigated with AFM.

Contrasting with Pd clusters. The substrate with deposited PC was then dipped into Na_2PdCl_4 solution (0.005 g/l) in acidic (HCl, pH 2.0) water for 1 min at ambient temperature and afterward rinsed in water. In the final step Pd(+2) was reduced by the treatment with 1.0 mg/ml aqueous solution of dimethylamine borane (DMB, Aldrich). Finally, the substrate was cleaned with water and dried with an argon flux. (for more details see also chapter 0)

Contrasting with HCF anions. The substrate with deposited PC was dipped into either $K_4Fe(CN)_6$ or $K_3Fe(CN)_6$ (Aldrich) solution (5 g/l) in acidic (HCl, pH 2.0) water for 3 min at ambient temperature and afterward rinsed in water. Finally, the substrate was dried with the argon flux.

Contrasting with PB clusters. To prepare a dispersion of Prussian Blue nanoclusters, the solutions of $K_4Fe(CN)_6{\cdot}3H_20$ (0.5 g/l, 1.18 mMol/l) in acid water (HCl, pH 2.0) and equal volume of the $FeCl_3$ solution in acid water (HCl, pH 2.0) were extensively mixed together for several minutes. We used three different concentrations of $FeCl_3$ 0.024 g/l (0.148 mMol/l), 0.048 g/l (0.296 mMol/l), and 0.127 g/l (0.79 mMol/l) for the preparation of three samples PB1, PB2, and PB3, respectively. The substrate with deposited PC was then dipped into the freshly prepared dispersion of PB clusters for 3 min at ambient temperature and afterward rinsed in water. Finally, the substrate was dried with the argon flux.

UV-vis measurements. The spectroscopic measurements were carried out using Perkin Elmer UV/vis Spectrometer Lambda 19.

6.3. Result and discussion

6.3.1. Deposition of hexacyanoferrate (II) anions

Negatively charged HCF anions was found to bind strongly to the positively charged PC. A relatively big size of the HCF-anion guarantees an efficient improvement of the AFM contrast as schematically shown in Figure 6.1. AFM images of PMB and P2VP molecules adsorbed onto the Si-wafer and then stained with HCF acid solution (pH 2, HCl) are shown in Figure 6.3.

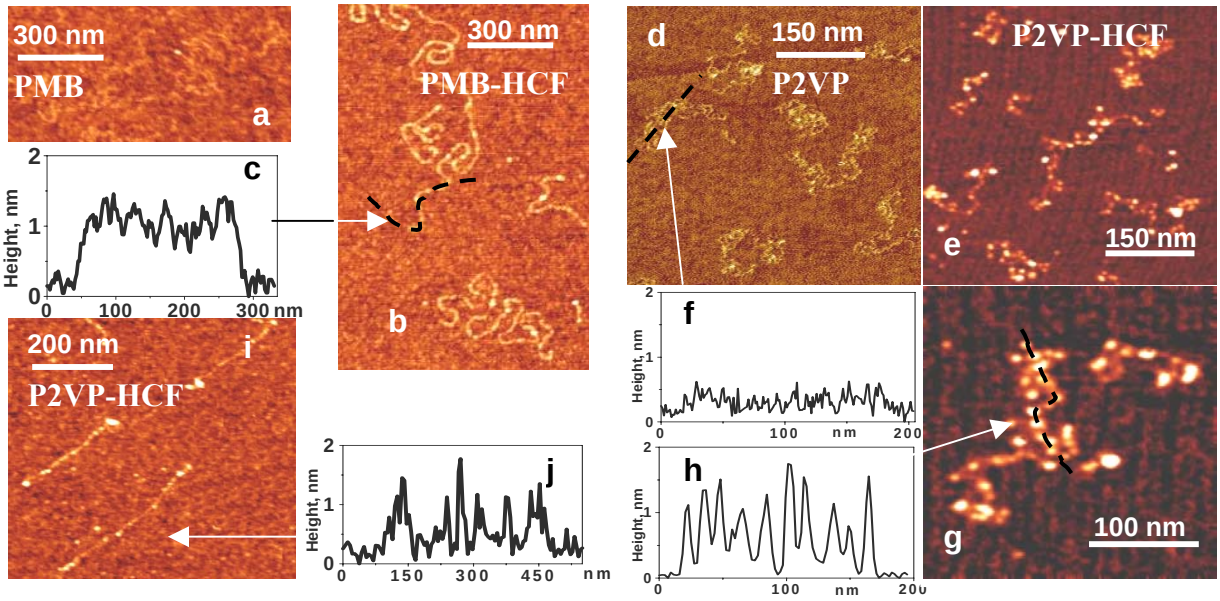

Figure 6.3 AFM topography images (Z-range 5 nm) and a cross-sections of PC molecules (bare and contrasted with HCF). PMB molecules adsorbed on the Si-wafer before (a) and after (b) contrasting with HCF; the cross-section is made along the chain axis marked by the arrow (c). P2VP molecules adsorbed on mica before (d) and after (e,g) contrasting with HCF and the cross-section (f and h). P2VP molecules deposited by ultra-fast spin-coating onto the Si-wafer and contrasted with HCF (i), and their cross-sections (j).

In all cases we observe an increase of the height of resulting structures approximately on 0.6-0.7 nm that is consistent with the dimension of HCF-anion. To demonstrate that the shape of molecules decorated with HCF reflects the initial conformation of PC chains we contrasted P2VP molecules deposited by two different methods. For the first method we deposited the protonated P2VP chains in extended coil conformation (pH2 aqueous solution) onto the mica and the Si-wafer by drop-casting. For the second method the P2VP molecules were aligned in stretched conformations by ultra-fast (10000 rpm) spin-coating. AFM images of PMB molecules (Figure 6.3) clearly depict differences in structures prepared by these two methods. Comparing the images 6.3 a and 6.3 d with 6.3 b and 6.3 e, respectively, demonstrates the

well recognized improvement of the contrast for the molecules deposited by both methods in coiled (Fig. 6.3 a-e) and stretched by ultra-fast spin-coating (Fig. 6.3i) conformations. The cross-section of the structures as deposited (Fig. 6.3 f) and stained (Fig. 6.3 c, h, j) explains that the contrast improvement is due to the increase of height of PC molecules decorated with HCF anions.

Figure 6.4 present AFM images of PS_7- $P2VP_7$ molecules contrasted with HCF. Although PS_7- $P2VP_7$ molecules adsorbed onto mica from acid water (pH 2) solution display a clear core-shell morphology (Fig. 6.4a), only the core of unimers with height of 5 nm can be resolved on the Si-wafer (Fig. 6.4b)

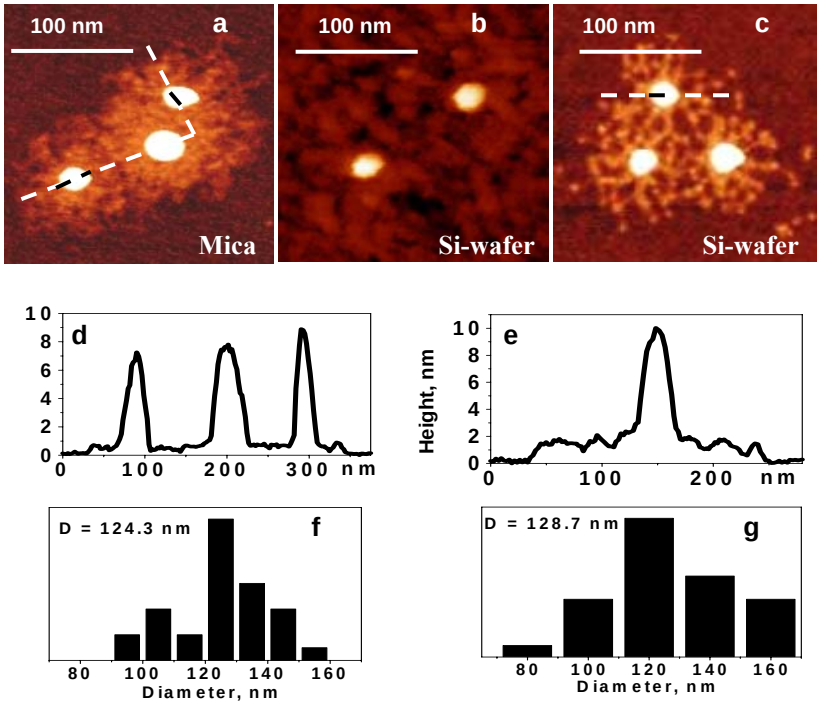

Figure 6.4 AFM images of PS_7-P2VP (a-c) molecules before (a,b), and after (c) contrasting with HCF (Z-range 5 nm). All images on Si-wafers, but (a) on mica. Histograms of molecular diameter distribution for PS_7-$P2VP_7$ adsorbed onto the mica, no contrasting (f), and onto the Si-wafer after contrasting with HCF (g).

Figure 6.4c shows PS_7- $P2VP_7$ molecules adsorbed onto Si-wafer and then stained with HCF acid solution (pH 2, HCl). Also in this case we observed an 0.6-0.7 nm increase of heights of resulting structures. The statistical analysis of the molecular diameter from AFM images of the PS_7-$P2VP_7$ unimers before the contrasting on mica and after the contrasting on the Si-wafer provides evidence that the contrasting procedure introduces no changes in the conformation (Fig 6.4d,e).

We performed a special experiment to precisely monitor the effect of the staining on the PC conformations deposited onto the lithography-labeled Si-wafer with relatively roughness (0.5 nm) by scanning always the one place and visualizing the one molecule before and after

the contrasting. As a representative example, Figure 6.5 shows images of several PMB molecules taken before and after the staining with HCF-anions. Although "as deposited" PMB molecules are poorly resolved on AFM images (Figure 6.5a,c), they are clearly observed after the contrasting with $K_4Fe(CN)_6$ (Figure 6.5b,d). Long molecules (A and F) and short chains (B, D and E) deposited by ultra-fast (10000 rpm) spin-coating adapt stretched conformations and their contour length can be easily measured: L_A = 3339 nm; L_B = 275 nm; L_D =247nm; L_E =376; nm and L_F = 2727 nm. Although contour length of several molecules (marked "C" in Figure 6.5), can not be measured due to the coiled conformation, the detailed analysis of the AFM data clearly indicates that increase of the chain thickness from few tens of nanometer to 1.5 nm (Figure 6.5e,f) upon treatment with $K_4Fe(CN)_6$ occurs virtually without remarkable changes of their location, contour length, and visible fine details of the conformations.

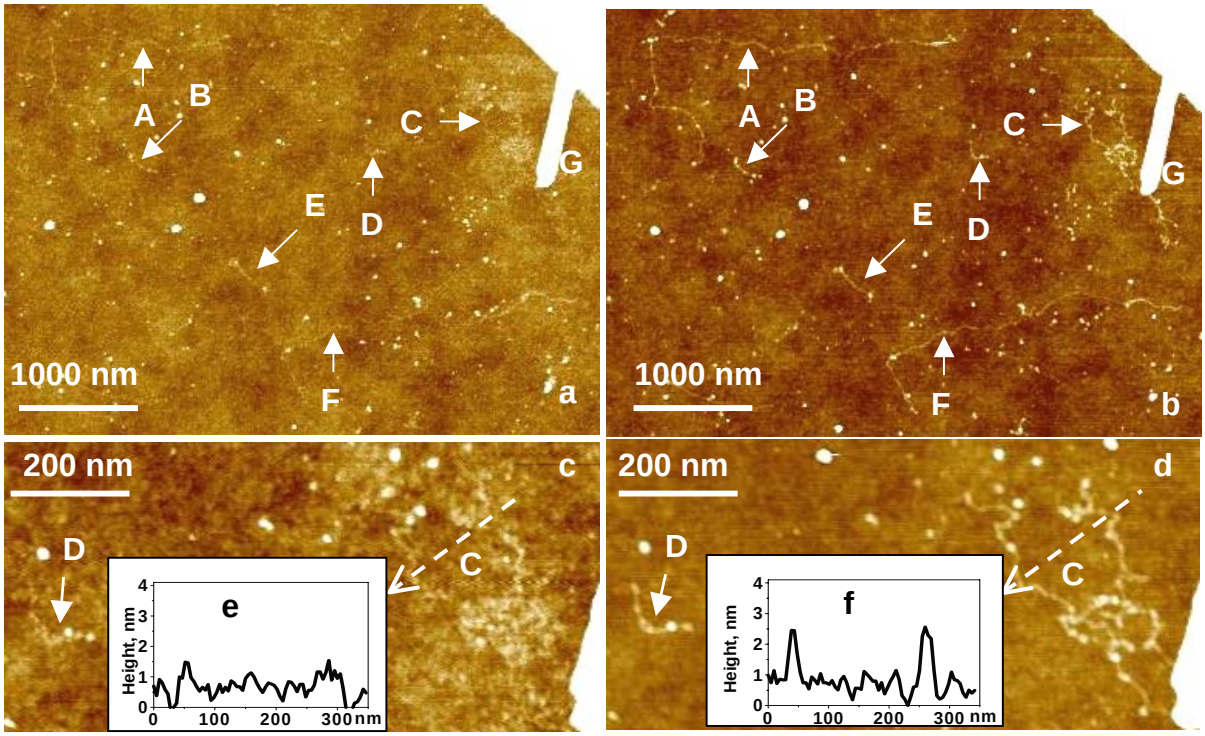

Figure 6.5 AFM topography images of the PMB molecule deposited on the lithography-labeled Si-wafer (RMS=0.6±0.4 nm) before (a,c), and after (b,d) contrasting with HCF (Z-range 5nm). The cross-sections (e,f) made on the same place of the Si-wafer before and after the contrasting reflect the 1nm-increase of the height of PMB molecules. Letters A-F mark several PMB molecules distinguished on the surface.

We also found that minor part of molecules appears to be partially distorted during the procedure. A "negative" example is shown in Figure 6.6. The 2.2 μm long PMB molecule deposited on the Si-wafer in the stretched conformation is visualized before (Fig. 6.6a) and after (Fig. 6.6b) staining. After the contrasting with $K_4Fe(CN)_6$ it is thicker and nicely visible.

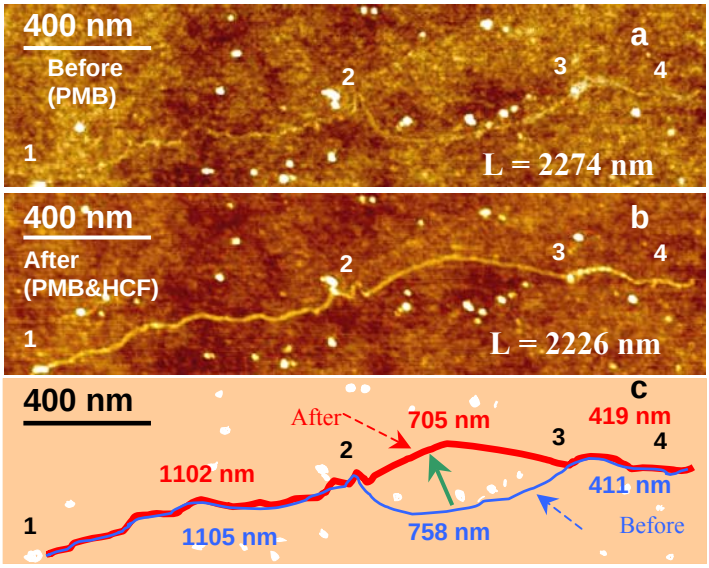

Figure 6.6 AFM topography images of the PMB molecule on Si-wafer (RMS=0.6±0.4 nm) before (a), and after (b) contrasting with HCF (Z-range 5nm). Snapshot (c) demonstrates the transition of the 2-3 segment induced by the contrasting procedure (see explanations in the text).

Although the segments **1-2** and **3-4** of the molecule with the length of 1100 nm and 410 nm, respectively, remained unchanged, the central part **2-3** with the initial length of 758 nm has been moved up for about 250 nm, as it is shown by the green arrow on the snapshot (Fig. 6.6c). The transformation is accompanied with about 7% collapse of the **2-3** fragment. Thus, we see the important role of the attractive interaction between the surface and PC molecule. If a PMB chain (or its fragment) bearing HCF-anions loses the contact with the surface it collapses due to the counter ion condensation effect.

Thus, we showed that the deposition of HCF-anion (the diameter about 0.7nm) improved the visualization of PC deposited onto the surfaces with the RMS less then 0.5 nm. The visualization of PC chains onto surfaces with a higher roughness needs to apply contrasting agents of a larger size.

6.3.2. Deposition of Prussian Blue nanoclusters

It is well known that mixing of stoichoimetric amounts of $K_4Fe(CN)_6$ and $FeCl_3$ leads to synthesis of microscopic particles of $Fe_4[Fe(CN)_6]_3$ (PB) which precipitates from the solution:[147] $3K_4Fe(CN)_6 + 4FeCl_3 = Fe_4[Fe(CN)_6]_3 + 12KCl$. Several methods to fabricate well-defined surfactant- or polymer-protected Prussian Blue (PB) nanoclusters have been recently reported.[148] Here we described a simple method to produce surfactant-free water-soluble negatively charged PB nanoclusters stabilized by excess of HCF-anions. Specifically, we found out that mixing of diluted solution of $FeCl_3$ with an excess of $K_4Fe(CN)_6$ solution in

acid conditions (pH 2) leads to clear deep-blue dispersions stable during several months. The characteristic blue color and the broad signal in the UV-vis spectra at λ_{max} = 695 nm are consistent with the intermetal charge-transfer from Fe^{2+} to Fe^{3+} band and gives evidence for the formation of PB (Figure 6.7).[149]

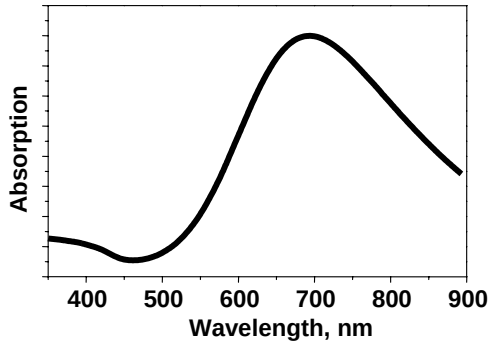

Figure 6.7 UV-vis spectra of Prussian Blue dispersion (prepared at molar ratio $K_4Fe(CN)_6/FeCl_3$ - 4/1, PB2).

A range of PB dispersions at different mixing ratios and stirring time was prepared and studied. To characterize the PB clusters a drop of the suspension onto the Si-wafer with the pre-adsorbed PMB molecules was set and washed out excess of the unattached material. PB clusters selectively bind to the PC deposited onto the Si-wafer. In the reference experiment no adsorption of PB clusters onto bare substrates (without pre-adsorbed PC molecules) neither at neutral pH nor in acid conditions was found (as confirmed by AFM and ellipsometry).

Figure 6.8 shows typical AFM images of PMB-PB nanoparticles with the beads-on-string morphology obtained upon deposition of PB clusters of the spin-stretched PMB molecules. Statistical treatment of the data was performed. At least, three images for each dispersion were collected and ,at least, 150 clusters of each type of dispersion were analyzed by defining the height of clusters form cross-sections.

We assume a near spherical geometry of PB clusters, and, hence, their height is taken as diameter of the spherical clusters. It should be noted that lateral dimensions of the clusters extracted from cross-sections of AFM images are overestimated due to the well-known tip-broadening effect (see subchapter 2.1.3). Therefore only height of the clusters was analyzed. As seen in Figure 6.8l,m, all PB clusters have narrowly distributed sizes (PDI = 1.1-1.2) (see also Appendix 6). We found that stabilization of the size of PB clusters occurs within 10 minutes: mixing of $K_4Fe(CN)_6$ and $FeCl_3$ solutions at molar ratio - 8/1 leads to PB particles of diameter about 2.7 nm (PB1, Figure 6.8a-e) whereas mixing at molar ratio - 4/1 leads to PB2 clusters with diameter near 4.8 nm (Figure 6.8i-k) (Appendix 6, Appendix 7). Obviously, the stability of the PB clusters is due to negative charges provided by the excess of HCF-anions located on the clusters surface. That explains why PB clusters of a smaller diameter are formed from solutions with higher $K_4Fe(CN)_6$ content.

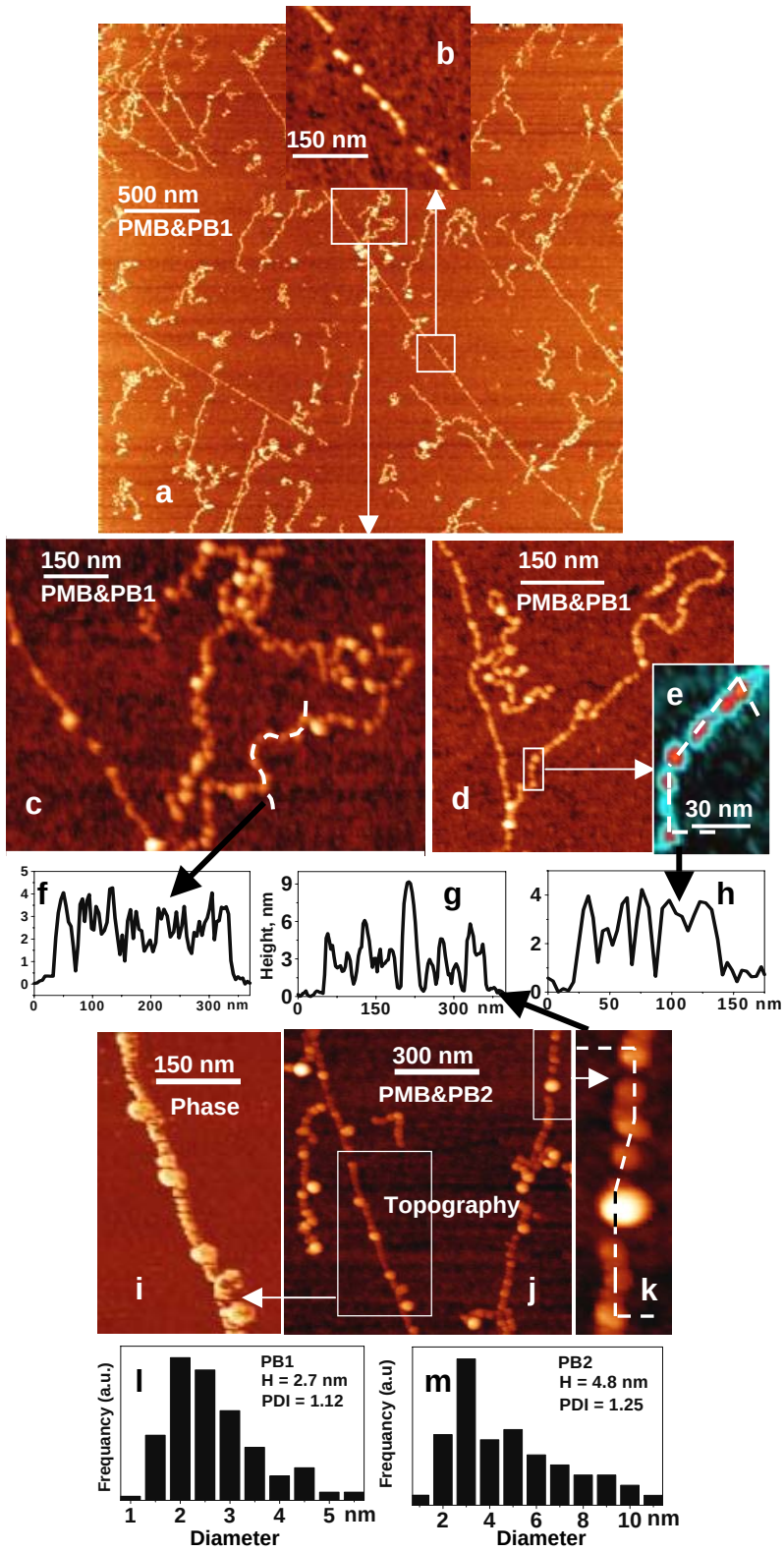

Figure 6.8 AFM phase (i) and topography (all other, Z-range 10nm) images of the PMB molecules deposited onto the Si-wafer by the spin-stretching and then contrasted with PB nanoparticles (prepared at molar ratio $K_4Fe(CN)_6/FeCl_3$ - 8/1, PB1 for images (a-e) and 4/1, PB2 for images (i-k)). The dash line in (c,e,k) indicates the locus of the cross-sections (f,h,g, respectively). Histogram (l,m) present the size distribution of the PB clusters.

The PB clusters bind PC selectively and homogeneously along PC chains. This modification significantly improves both the topography (Figure 6.8a-e, j-k) and the phase contrast in AFM images (Figure 6.8i). The distance between adjacent clusters depends on the

diameter of PB clusters and it is in the range from 10 to 20 nm. The high binding density of the PB clusters is sufficient for the visualization of molecular details of PC conformations on rough surfaces with the RMS larger then 0.5 nm.

We again address the question if the deposition of the PB nanoclusters can alternate conformation of the PC molecules. Figure 6.8a presents the PMB molecules deposited on the Si-wafer by spin-coating and then stained with PB1 clusters (D=2.7nm).

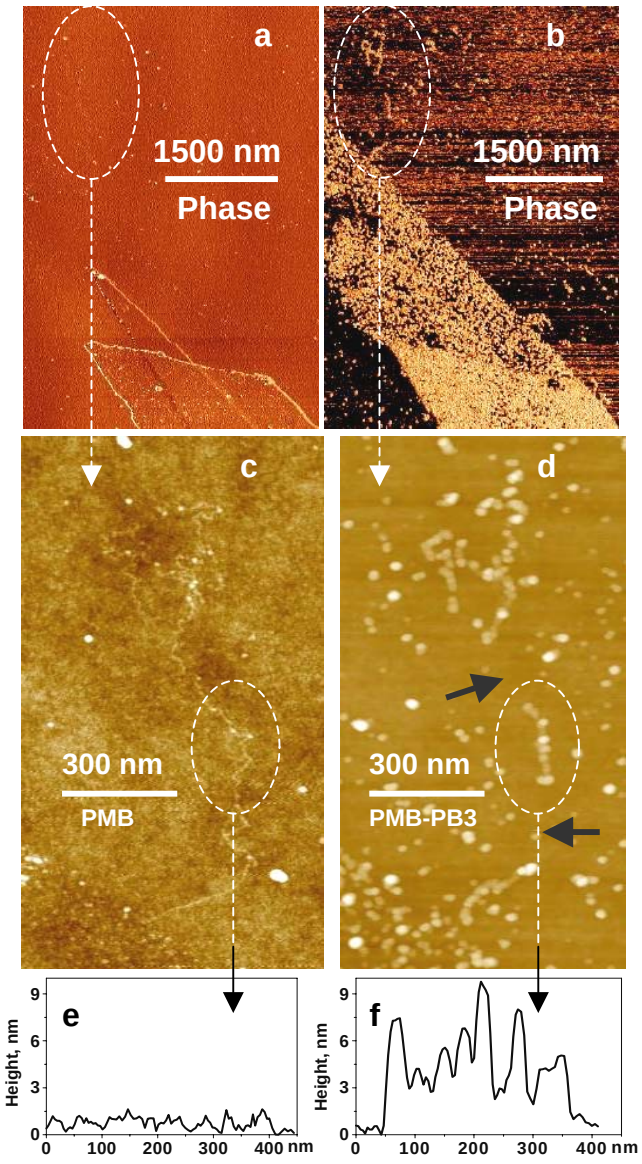

Figure 6.9 AFM phase (a-b) and topography (c-d) images (Z-range 20nm) of the PMB molecules deposited onto the lithographically labeled Si-wafer before (a,c), and after (b,d) contrasting with PB clusters (prepared at molar ratio $K_4Fe(CN)_6/FeCl_3$ - 3/1). Cross-sections (e,f) are made on the same place of the Si-wafer before and after the contrasting.

As seen from the zoom-image (Figure 6.8b) some of stretched PMB chains contain 10-30 nm gaps. It is important, these gaps remain unchanged even upon repeating of the staining procedure. These gaps mean either fracture of the chain or that there are no deposited PB clusters on it because of some reasons.

Even larger defects were observed when PMB molecules were decorated with the larger PB clusters. Figure 6.9 shows PMB chains deposited on lithographically labeled surface and decorated with PB clusters by the treatment with $K_4Fe(CN)_6/FeCl_3$ solution (molar mixing ratio – 1.5/1, PB3). PMB molecules with attached PB clusters display considerably distorted conformations and contain large gaps (up to 200 nm, marked by thick arrows).

The selectivity of the binding of HCF anions and PB nanoclusters along PC molecules should be especially emphasized. The AFM images (Fig. 6.3-6.6 and 6.8) prove that the contrasting materials preferentially bind to PC chains but not to the bare surface of the substrates.

Finally, we demonstrate that the staining procedure allows for the visualization of single polymer molecules deposited onto microscope glass slides with RMS about 1 nm. The contrasting of PMB molecules with PB3 clusters results in a quite remarkable contrast so that PMB chains can be easily visualized (Figure 6.10).

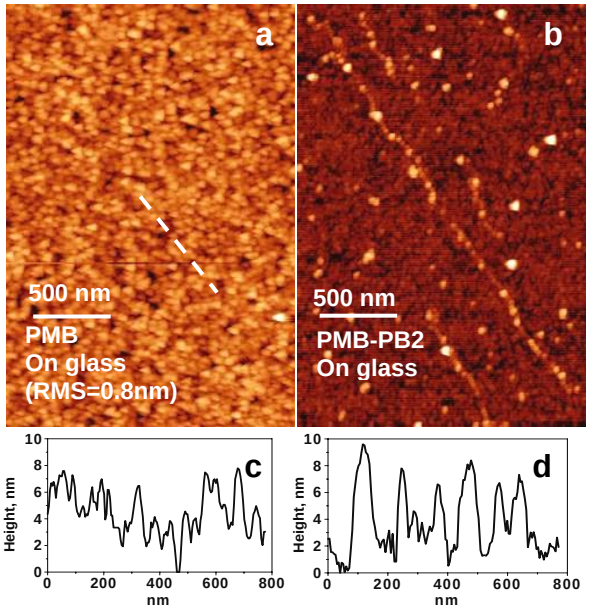

Figure 6.10 AFM topography images (Z-range 15nm) and cross-sections (c, d) of the PMB molecules deposited onto the microscope glass slide before (a,c) and after (b,d) the contrasting with PB2 clusters (prepared at molar ratio ($K_4Fe(CN)_6/FeCl_3$ - 4/1).

6.4. Conclusions

We developed the simple contrasting procedure to improve AFM visualization of positively charged polymer chains deposited on the substrates of relatively high roughness. The staining mechanism is based on the counter ion exchange between Cl^- counter anions and bulky HCF anions or negatively charged nanoclusters of Prussian Blue. This method allowed us to increase the thickness of the resulting structures up to 10 nm, and, consequently, to provide visualization of polymer chains on rough surfaces. In contrast, the deposition of the

relatively large PB clusters (more than 10 nm) considerably distorts the initial polymer conformation and even leads to a fragmentation of polymer chains. We believe, that our innovation is important for the development of single molecule experiments with polymer chains. The reaction of HCF-anion could be used for recognition of polycation molecules, when polycations, polyanions and neutral molecules coexist on the surface. Recently, the study was strongly restricted to atomically smooth surfaces. The contrasting procedure extends the range of substrates (Si-wafers, chemically modified or patterned Si-wafers, polished glasses, polymer films, etc) appropriate for the experiments. That is very useful for study of numerous processes involving the interaction of synthetic and biomacromolecules with various surfaces.

Summary

For the first time, synthetic “normal-sized” polymers of various architecture adsorbed on solid substrates have been visualized with molecular resolution by AFM in different conformation.

This finding allowed us to study largely discussed problem, a coil-to-globule transition of PEs. Particularly, it was found that PE molecules undergo conformational transitions from stretched worm-like coil to compact globule via set of necklace-like globules, as the fraction of charged monomers decreases with an increase of pH and ionic strength. These results are in good agreement with recently developed DRO theory for weakly charged flexible polyelectrolytes in poor solvent.

The size of the deposited single molecules correlates very well with molecular dimensions in solution obtained in light scattering experiments.

PE single molecules of various architectures can be mineralized in different confirmations that constitutes the route to nanoparticles with desired shape (including wire-shape and star-shaped), size, and composition (including metallic, magnetic and semiconductive nanoparticles). It was shown that molecular details of the adsorbed linear flexible polyelectrolyte molecules determine the dimensions of the nanostructures after metallization and that observed sizes are consistent with the decoration of single molecules with nanoclusters. Thus those metallized nanoparticles (cluster assembles) reflect the conformation of original adsorbed polyelectrolyte molecules. The dimensions of the obtained nanowires are significantly smaller than those previously reported. All of these features are of the potential benefit in applications for nanodevices and permit one to use polyelectrolyte molecules of different architectures to generate metallic nanoobjects of a desired shape.

It was found that PS_7-$P2VP_7$ block copolymers undergo diverse conformational transitions responding to external stimuli. At low concentration PS_7-$P2VP_7$ exists in molecularly dissolved state in both selective (acid water, toluene) and common good (chloroform, tetrahydrofurane) solvents.

In acid conditions PS_7-$P2VP_7$ forms either unimolecular or multimolecular micelles depending on pH and ionic strength. PS_7-$P2VP_7$ undergoes the inverse intramolecular segregation upon addition of toluene. In this case, the inverse unimolecular micelles are constituted of the P2VP dense core and the PS swollen shell.

The PS core of unimers, adsorbed from acid water, adopts an extended conformation upon exposure to toluene whereas P2VP chains retain their extended conformation during this

procedure. Thus the obtained "squash" structures present a unique conformation which does not exist in any solvent and could not be obtained upon simple adsorption procedure.

Metallization of the PS_7-$P2VP_7$ improves AFM resolution due to the selective deposition of Pd clusters along the P2VP chains. For the first time, the number of the P2VP second generation arms of the heteroarm block/copolymer was directly counted in the single molecule AFM experiment.

Simple contrasting procedure was developed to improve AFM visualization of positively charged polymer chains deposited on the substrates of relatively high roughness. The staining mechanism is based on the counter ion exchange between Cl^- counter anions and bulky HCF anions or negatively charged nanoclusters of Prussian Blue. This method allows increasing the thickness of the resulting structures up to 10 nm, and, consequently, provide visualization of polymer chains on rough surfaces. In contrast, the deposition of the relatively large PB clusters (more than 10 nm) considerably distorts the initial polymer conformation and even leads to a fragmentation of polymer chains.

This innovation is important for the development of single molecule experiments with polymer chains. The reaction of HCF-anion could be used for recognition of polycation molecules, when polycations, polyanions and neutral molecules coexist on the surface. Recently, the study was strongly restricted to atomically smooth surfaces. The contrasting procedure extends the range of substrates (Si-wafers, chemically modified or patterned Si-wafers, polished glasses, polymer films, etc) appropriate for the experiments. That is very useful for study of numerous processes involving the interaction of synthetic and biomacromolecules with various surfaces.

Thus, polymer single molecules can be considered not only as representative of the ensemble molecules, but also as *individual nanoscale objects* which can be used for future nanotechnology for the fabrication of single molecule electronic devices. Also these findings are important from fundamental point of view, since developed approach can be successfully applied for investigation of various "classical" problems in polymer science, such as polymer reconformation, interpolyelectrolyte complex formation, polymer diffusion, adsorption, etc.

Appendix

Appendix 1. Histograms representing distribution of the length of necklaces of PMB-2 deposited on mica from aqueous solutions at pH 3 and different concentration of Na_3PO_4.

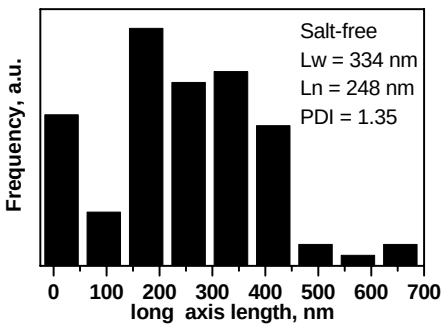

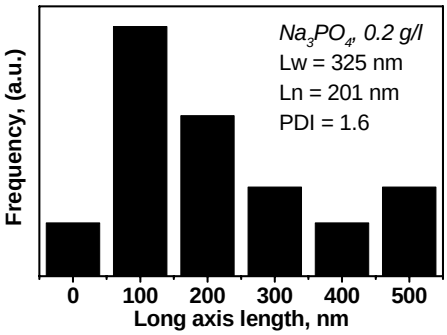

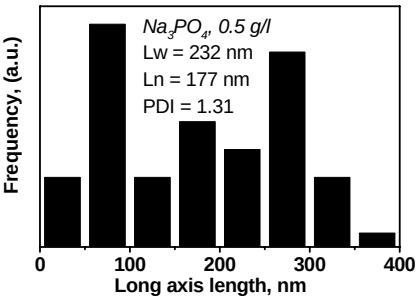

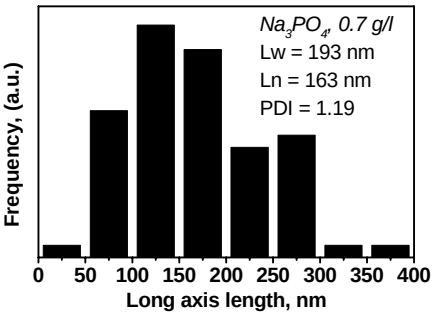

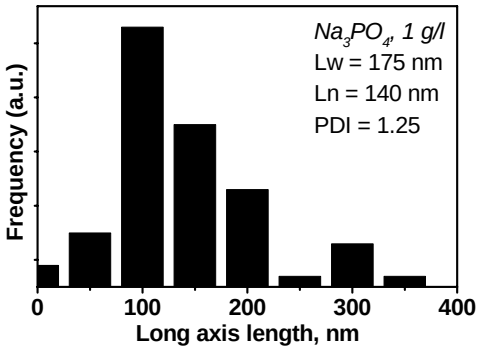

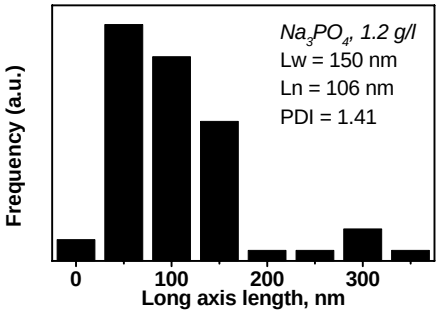

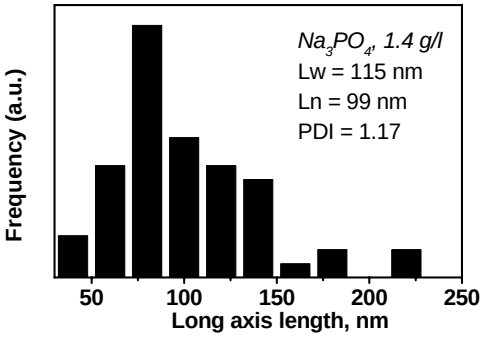

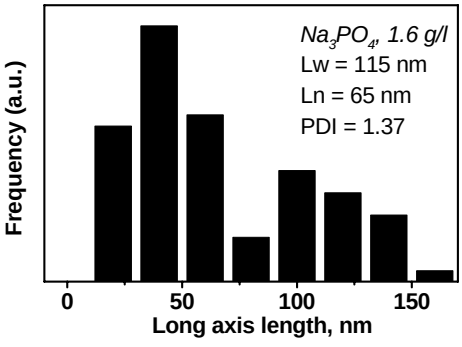

Appendix 2. AFM images of PMB-1 molecules deposited on mica from aqueous solutions at pH 3 with added NaCl: salt free solution (referance) (a and b); 0.005 M (c); 0.02 M (e); 0. 2 M (d and f); 1 M (g).

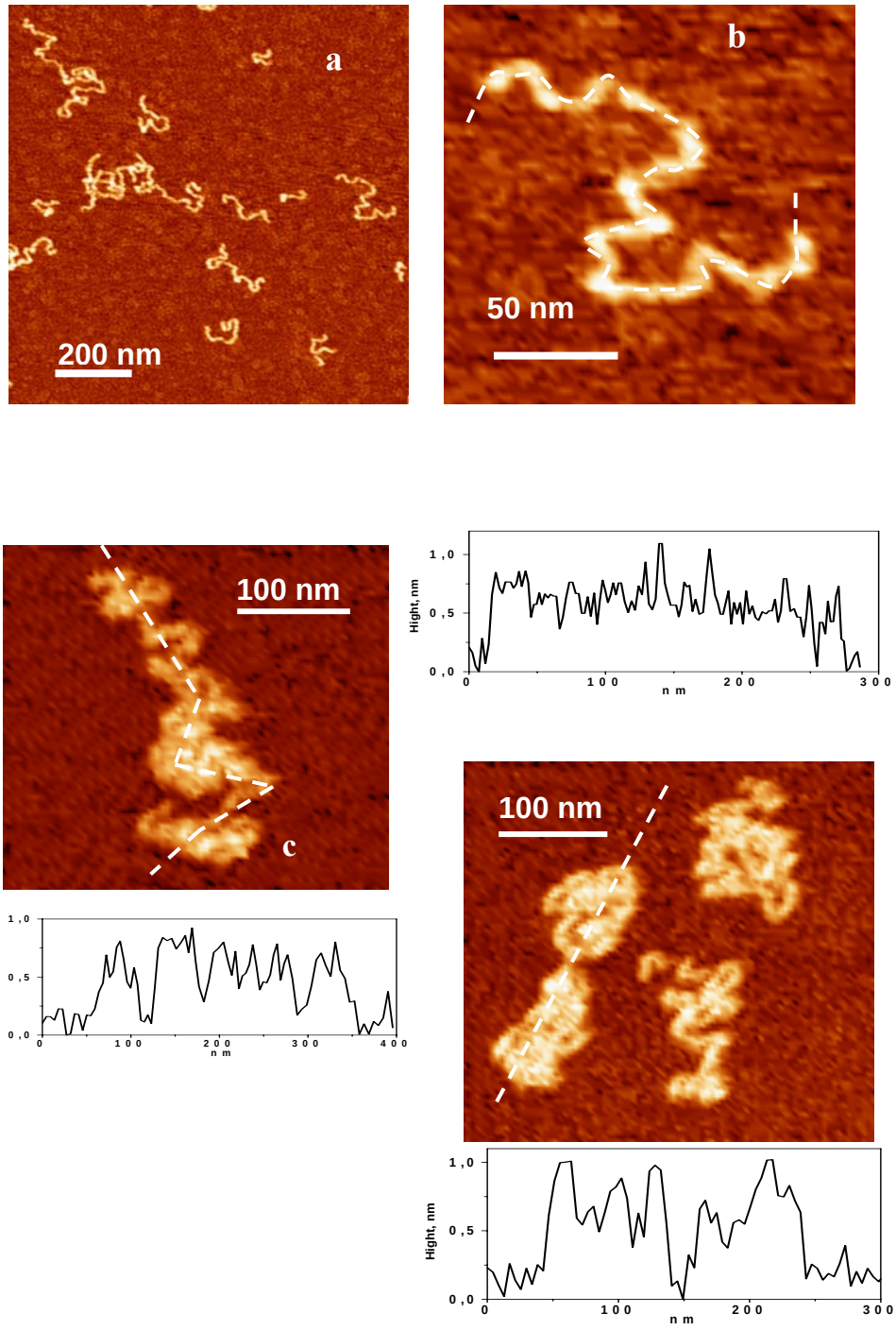

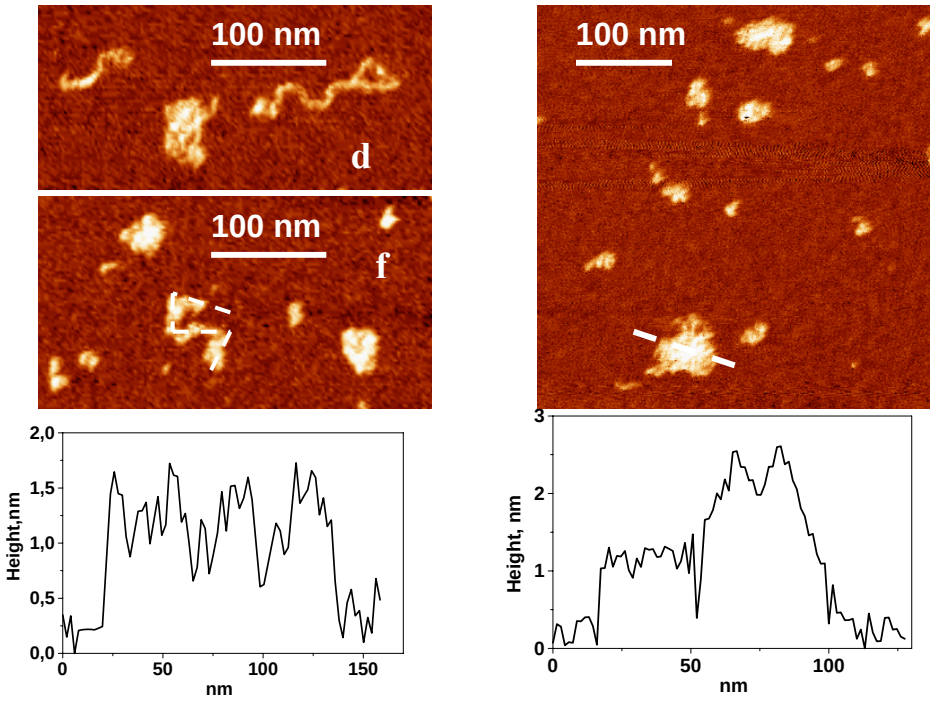

Appendix 3. Histograms representing distribution of the length of necklaces of PMB-1 deposited on mica from aqueous solutions at pH 3 and different concentration of NaCl.

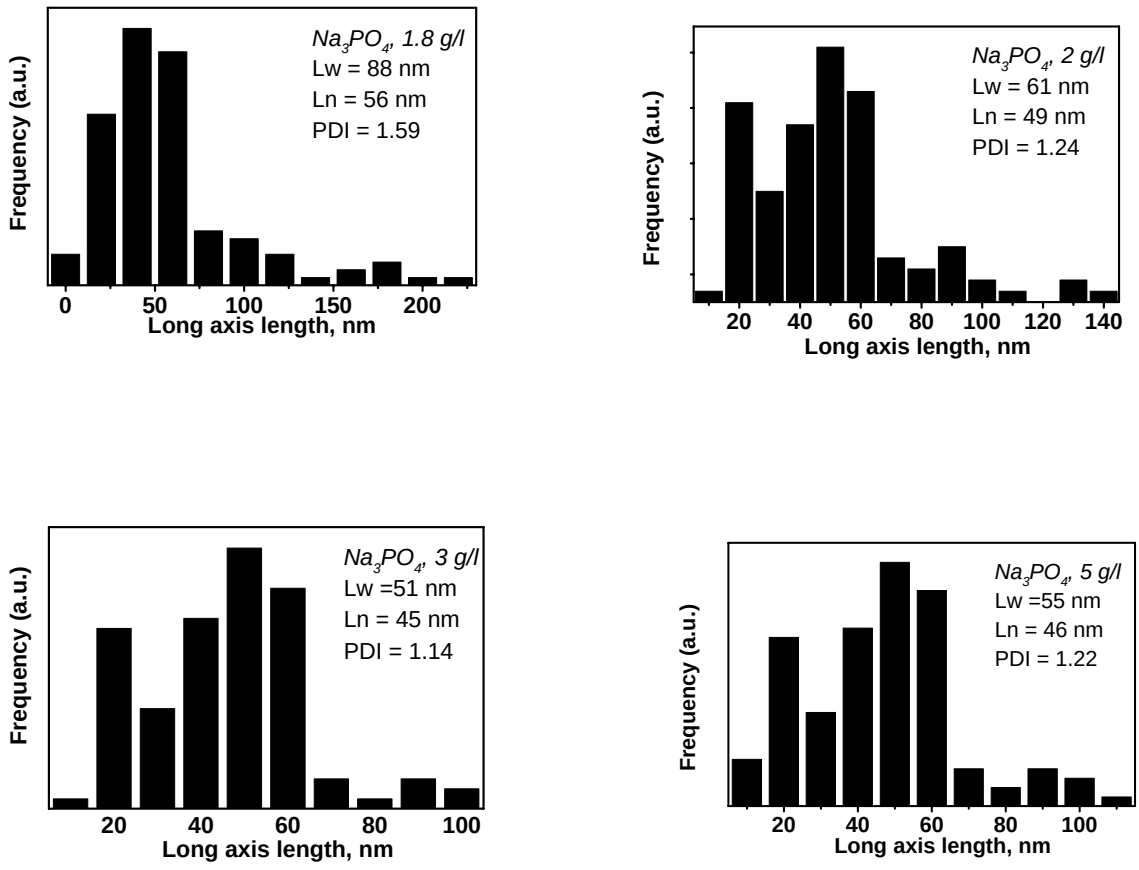

Appendix 4. ζ-potential of mica surface vs. pH at 0.001 M KCl aqueous solution

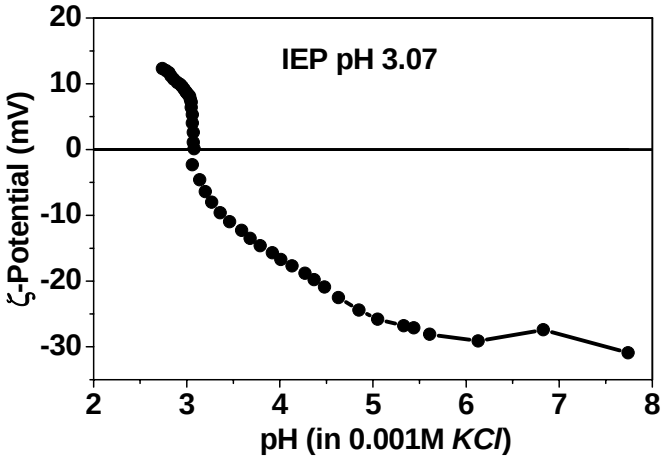

Appendix 5 Distribution of contour lengths (a, d), heights (b, e) and widths (c, f): (left – a, b, c) for PMB chains; (right – d, e, f) for Pd- PMB wire-shaped nanoparticles.

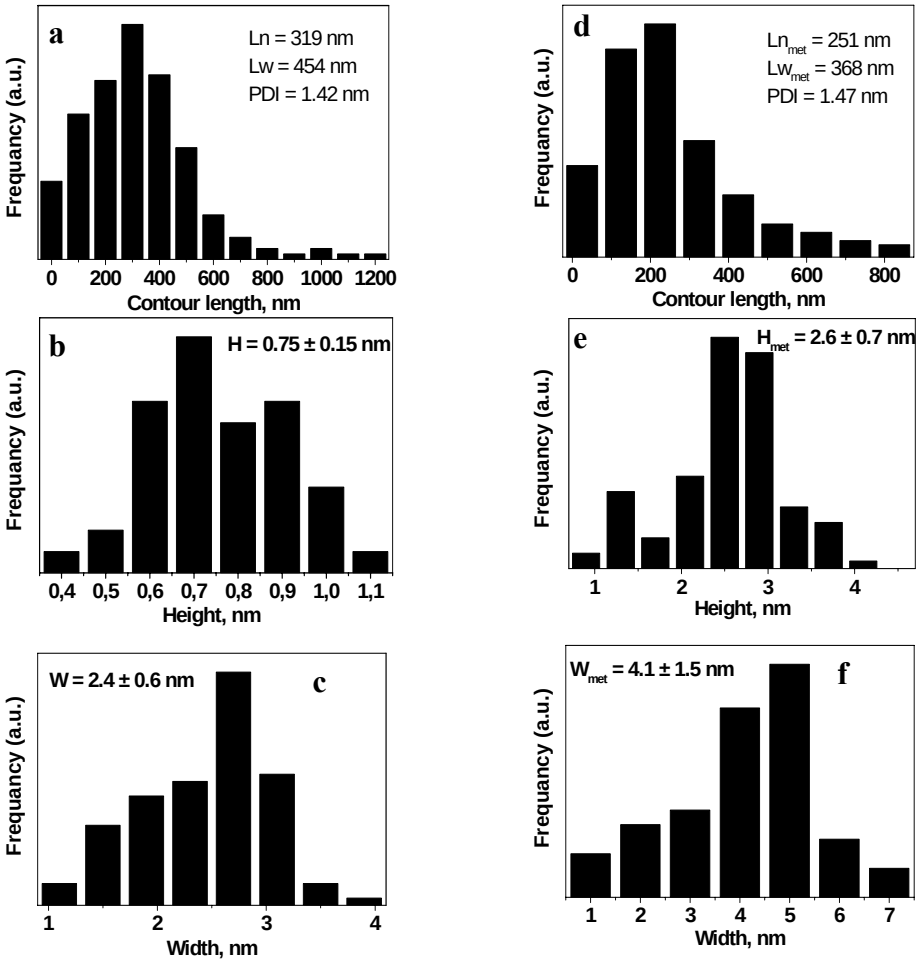

Appendix 6 Histograms presents the size distribution of the PB clusters stirred before the deposition during corresponding time.

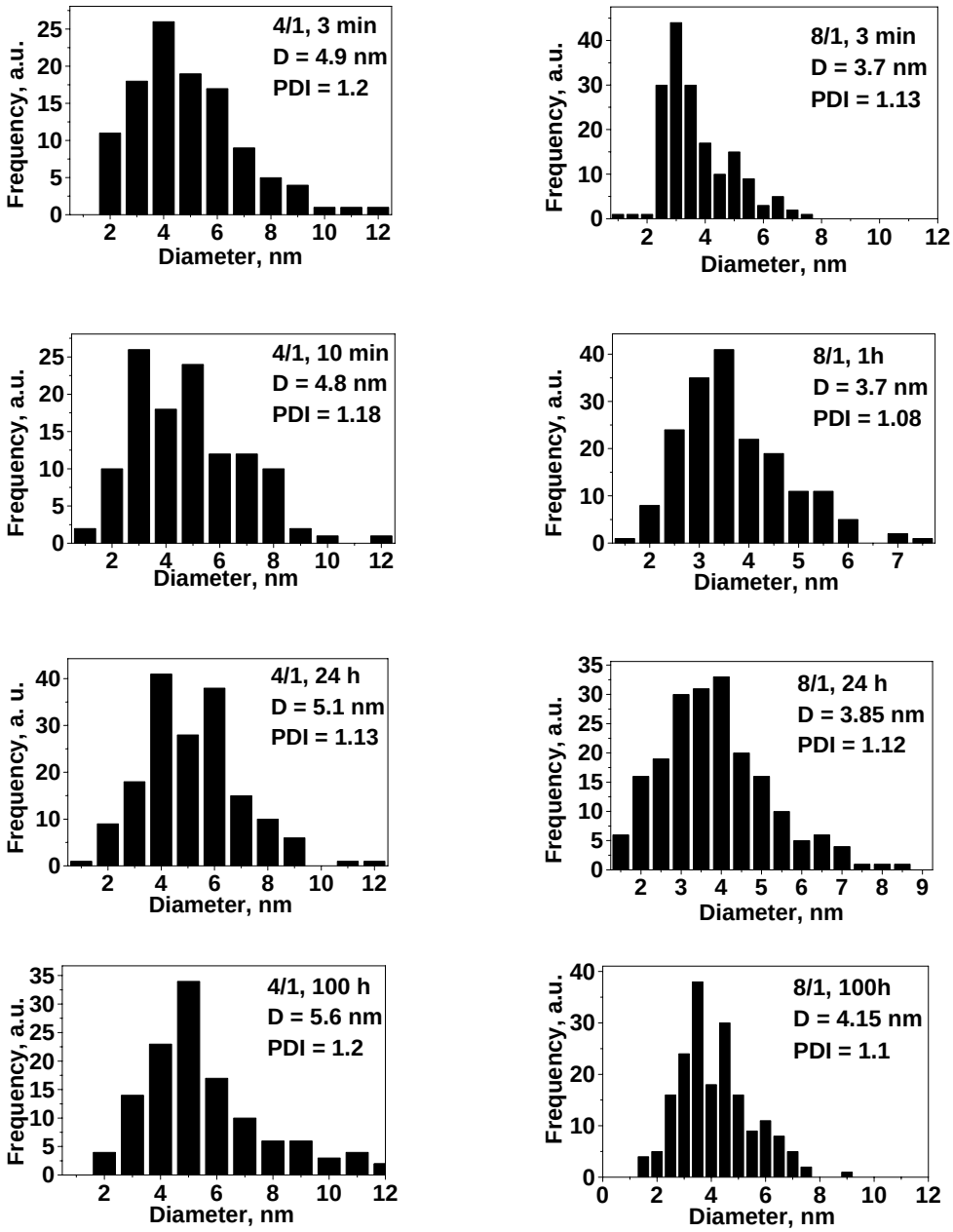

Appendix 7 Dependence of the size of the PB clusters as a function of stirring time.

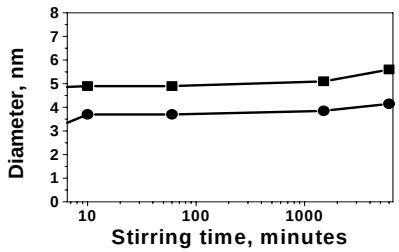

- PB 1 – molar ratio 8/1
- PB 2 – molar ratio 4/1

Bibliography

[1] Chou S. Y., Keimel C. and Gu J. *Nature,* **2002,** *417***,** 835.
[2] Bezryadin A. and Dekker C. *J.. Vac. Sci. Technol.* B **1997,** *15***,** 793.
[3] Whitesides G. M., Mathias J. P. and Seto C. T. *Science* **1991,** *254***,** 1312; Jackman R. J., Brittain S. T., Adams A., Prentiss M. G. and Whitesides G. M. *Science* **1998,** *280,* 2089
[4] Quake S. and Scherer A. *Science* **2000,** *290*, 1536.
[5] *Polyelectrolytes;* Hara, M.Ed.; Marcel Dekker: New York, 1993. Dautzenberg, H.; Jaeger, W.; Kötz, B. P. J.; Seidel, C.; Stscherbina D. *Polyelectroytes: Formation. characterization and application.* Hanser Publishers: Munich, Vienna, New York, 1994.
[6] G. C. Eastmond. Comprehensive polymer sciences. Pergamon Press,**1989**.
[7] Kuhn, W.; Kuhn, H. *Helv. Chim. Acta*, **1943**, *26*, 1394.
[8] Flory, P. J. „ Principles of Polymer Chemistry" Cornell University Press, Ithaca, **1953**.
[9] de Gennes, P.-G. *Scaling Concepts in Polymer Physics*; Cornell University Press: Ithaca, NY, 1985.
[10] Kratky, O.; Porod, G. *Recueil Trav. Chim. Pays-Bas,* **1949**, *68*, 1106.
[11] T. J. Odijk. *Polym. Sci. Polym.Phys. Ed.,* **1977**, *15*, 477.
[12] J. Skolnick and M. Fixman. *Macromolecules*, **1977**, *10*, 944.
[13] Fisher, L. W.; Sochor, A. R.; Tan, J. S. *Macromolecules* **1977***, 10,* 949. Tricot, M. *Macromolecules* **1984**, *17,* 1698. Ghosh, S.; Li, X.; Reed, C. E.; Reed, W. F. *Biopolymers* **1990,** *30,* 1101.
[14] Manning D.S. *J. Chem. Phys.,* **1969,** *51,* 924.
[15] Zimm, B. H. and Le Bret, M. *J. Biomol Struc. Dynamics,* **1983,** *1,* 461.
[16] Khokhlov, A. R. *J. Phys. A* **1980,** *13,* 979.
[17] Raphael, E.; Joanny, J.-F. *Europhys.Lett.* **1990,** *13,* 623.
[18] Higgs, P.G.; Raphael, E. *J. Phys. I* **1991,** *1,* 1.
[19] Kantor, Y.; Kardar, M.; *Europhys. Lett.* **1994,** *27,* 643; *Phys. Rev. E* **1995***, 51,* 1299.
[20] Dobrynin, A. V.; Rubinstein M.; Obukhov S. P. *Macromolecules,* **1996,** *29,* 2974-2979.
[21] for examlpe: Binder, K., *Monte Carlo Methods in Statistical Physics,* Ed.; Springer: New York, 1979. Roe, R. J. *Computer Simulations of Polymers.* Prentice Hall:Englewood Cliffs, NJ, 1991.
[22] Baumgarner, A. *J. Chem. Phys.* **1980,** *72,* 871; *ibid.* **1980,** *73,* 2483.
[23] Hooper, H. H.; Beltran, S.; Sassi, A. P.; Blanch, H. W.; Prausnitz, J. M. *J. Chem. Phys.* **1990**, *93*, 2715.
[24] Higgs, P. G.; Orland, H. *J. Chem. Phys.* **1991**, *95*, 4506.
[25] Micka, U.; Holm, C.; Kremer, K. *Langmuir* **1999,** *15,* 4033.
[26] Wiegel, F.W. *J. Phys. A,* **1976,** *10*, 299.
[27] Muthukumar, M. *J. Chem. Phys.* **1987,** *86*, 7230; Varoqui, R. *J. Phys. II* **1993,** *3*, 1097. Chatellier, X.; Joanny, J.-F. *J. Phys. II* **1996,** *6*, 1669. Borukhov, I.; Andelman, D.; Orland, H. *Macromolecules* **1998,** *31*,1665.
[28] Joanny, J.-F. *Eur. Phys. J. B* **1999,** *9*, 117.
[29] a) Borisov, O.V.; Birshtein, T.M.; Zhulina, E.B. *J. Phys. II,* **1994**, *4*,913. b) Yamakov, V.; Dünweg, B.; Borisov, O.V.; Milchev, A. *J.Phys. Condens. Matter,* **1999,** *11*, 9907. c) Zhulina, E.B.; Borisov, O.V.; van Male, J.; Leermakers, F.A.M. *Langmuir*, **2001,** *17*, 1277.
[30] Napper, D.H. *Polymeric Stabilization of Colloidal Dispersions*, Academic Press, London, 1985.
[31] Fleer, G.J.; Cohen Stuart, M.A.; Scheutjens, J.M.H.M.; Cosgrove, T.; Vincent, B. *Polymers at Interfaces,* Chapman& Hall, London, 1993.

[32] Borisov, O.V.; Zhulina, E.B.; Birshtein, T.M. *Macromolecules,* **1994**, *27*, 4795.
[33] Borisov, O.V.; Hakem F.; Vilgis T.A.; Joanny, J.-F.; and Johner, A. *Eur. Phys. J. E,* **2001,** *6,* 37
[34] Johner, A.; Joanny, J.-F. *J. Phys. II* **, 1991,** *1*, 181.
[35] J.N. Israelachvili, *Intermolecular and Surface Forces,* Academic Press, London, 1985.
[36] de Gennes, P.-G. *J. Phys. (Paris)*, **1976,** *37,*1445.
[37] de Gennes, P.-G.; Pincus, P.; Velasco, R.M.; Brochard, F. *J. Phys. (Paris)*, **1976,** *37,*1461.
[38] Joanny, J.F.; deGennes, P.G.; *C. R. Acad. Sci. II,* **1984,** *299*, 279.
[39] Binning G., Roher H., Gerber C., Weibel E., "Surface Studies by Scanning Tunneling Microscopy," *Phys Rev Lett.* **1982,** *49,* 57.
[40] Binning G. B., Quate C. F., and Gerber Ch., "Atomic Force Microscope," *Phys Rev Lett*, **1986,** *12,* 930.
[41] Digital Instruments, Veeco Metrology Group, *Training Notebook*, rev. 3.0, 1999.
[42] Seiko S.S. *Advances in Polymer Science*, 2000, vol.151, 61-174.
[43] Magonov, S. N.; Elings, V.; Whangbo, M.-H. *Surf Sci* **1997**, *375*, L385-L391.
[44] Zhong Q.; Inniss, D.; Kjoller, K.; Elings, V. B. *Surf Sci* **1993**, *290*, L688.
[45] Quist, A. P.; Ahlbom, J.; Reimann, C. T.; Sundqvist, B. U. R. *Nucl Instrum Methods B* **1994**, *88*, 164
[46] Radmacher M., Tillmann R.W., Gaub H.E. *Biophys J*, **1993**, *64*, 735
[47] Bar G., Thomann Y., Brandsch R., Cantow H.-J., Whangbo M.-H. *Langmuir,* **1997**, *13*, 3807
[48] Noy A., Sanders C.H., Vezenov D.V., Wong S.S., Lieber C.M. *Langmuir,* **1998**, *14*, 1508.
[49] Tamayo, J.; García, R. *Langmuir* **1996**, *12*, 4430-4435.
[50] Weisenhorn A. L., Hansma P. K., Albrecht T. R., Quate C. F. *Appl Phys Lett,* **1989**, **54,** 2651
[51] Ducker W. A., Senden T. J., Pashley R. M. *Langmuir*, **1992**, *8*, 1831
[52] Senden T. J., Drummond C. J., Kékichef P. *Langmuir,* **1994**, *10*, 358
[53] Meyer E., Howald L., Overney R. M., Heinzelmann H., Frommer J., Güntherodt H.-J., Wagner T., Schier H., Roth S. *Nature,* **1991**, *349*, 398
[54] Butt H.-J., Downing K. H., Hansma P. K. *Biophys J*, **1990**, *58*, 1473
[55] Ohnesorge F., Binnig G. *Science,* **1993**, *260*, 1451
[56] Lee G. U., Chrisey L. A., Colton R. J. *Science*, **1994**, *266*, 771
[57] Putman C. A. J., van der Werf K. O., de Grooth B. G., van Hulst N. F., Greve J. *Appl Phys Lett*, **1994**, *64*, 2454
[58] Hansma P. K., Cleveland J. P., Radmacher M., Walters D. A., Hilner P. E., Bezanilla M., Fritz M., Vie D., Hansma H. J., Prater C. B., Massie J., Fukunada L., Gurley J., Elings V. *Appl Phys Lett*, **1994**, *64*, 1738
[59] Walters D. A., Cleveland J. P., Thomson N. H., Hansma P. K., Wendman M. A., Gurley G., Elings V. *Rev Sci Instrum,* **1996**, *67*, 3583-3590.
[60] Elmer F. J., Dreier M. *J Appl Phys,* **1997**, *81*, 7709-7714
[61] Tolksdorf C., Revenko I. "Choosing AFM probes for Biological Applications", www.di.com, application note 44.
[62] Digital Instruments, Veeco Metrology Group, Support Note 290, "Fluid operation: overview for contact and TappingMode with a MultiMode microscope".
[63] Colton R. J., Engel A., Frommer J. E., Gaub H. E., Gewirth A. A., Guckenberger R., Rabe J., Heckl W. M., Parkinson B. (eds) Procedures in scanning probe microscopies. **1998** Wiley, Chichester
[64] Bar G., Brandsch R. and Whangbo M.-H., *Surface Sci.* **1999**, *422*, L192
[65] Grütter P., Zimmermann-Edling W., Brodbeck D. D. *Appl Phys Lett*, **1992**, *60*, L2741.

[66] Sheiko S.S., Möller M., Reuvekamp E.M.C.M., Zandbergen H.W. *Ultramicroscopy,* **1994**, *53*, L371.
[67] Schwartz D.U., Haefke H., Reimann P., Güntherodt H.-J. *J Microsc,* **1994**, *173*, L183.
[68] Reiss G., Brückl H., Vancea J., Lecheler R., Hastreiter E. *J Appl Phys*, **1991**, *70*, L523.
[69] Paik S.M., Kim S., Schuller I.K. *Phys Rev Lett B*, **1991**, *44*, L3272.
[70] Vesenka J., Miller R., Henderson E. *Rev Sci Instrum,* **1994**, *65*, 2249.
[71] Carpick R.W., Agrait N., Ogletree D.F., Salmeron M. *J Vac Sci Technol B,* **1996,** *14,* 1289.
[72] Gracias D.H., Somorjai G.A. *Macromolecules,* **1998**, *31,* 1269
[73] www.mikromasch.com, www.spmtips.com
[74] www.nanosensors.com
[75] www.budgetsensors.com
[76] www.veecoprobes.com
[77] Xu, S.; Arnsdorf, M. F. *J. Microscopy* **1994**, *173*, 199-210. Vesenka, J.; Manne, S.; Giberson, R.; Marsh, T.; Henderson, E. *Biophysical J.* **1993**, *65*, 992-997
[78] Dautzenberg H., Jaeger W., Kötz J., Philipp B., Seidel Ch., Stscherbina D., *Polyelectrolytes: formation, characterization and application,* Nanser Pb., **1994.**
[79] Chu B., *Laser Light Scattering*, 2nd Edition, Academic Press, **1991**.
[80] Tanaka, T. *Phys. Rev. Lett.* **1978,** *40*, 820.
[81] Lifshitz, I.M; Grosberg, A. Yu.; Khokhlov, A. R. *Rev. Mod. Phys.* **1978,** *50*, 683-713.
[82] Vasilevskaya, V.; Khokhlov, A. R.; Matsuzawa, Y.; Yoshikawa, K. *J. Chem. Phys.* **1995**, *102*, 6595-6602. Vasilevskaya, V.; Khokhlov, A. R.; Kidoaki, S.; Yoshikawa, K. *Biopolymers* **1997**, *41,* 51-59. Kuznetsov, Y. A.; Timoshenko, E, G, *J, Chem, Phys,* **1999**, *111*, 3744-3752.
[83] For example, Cosule, L. C.; Schellman, J. A. *Nature* **1976**, *259*, 333. Widom, J.; Baldwin, R. L. *J. Mol. Biol.* **1980**, *144*, 431. Post, C.B.; Zimm, B. H. *Biopolymers* **1982,** *21*, 2123. Park, I.H.; Wang, Q. W.; Chu, B. *Macromolecules* **1987**, *20*, 1965-1969.
[84] Yoshikawa, K.; Takahashi, M.; Vasilevskaya, V.; Khohlov A. R. *Phys. Rev. Lett.* **1996**, *76*, 3029-3031. Vasilevskaya, V.; Khokhlov, A. R.; Matsuzawa, Y.; Yoshikawa, K. *J. Chem. Phys.* **1996**, *102*, 6595-6602. Takahashi, M.; Yoshikawa, K.; Vasilevskaya, V.; Khokhlov, A. R. *J. Phys. Chem. B* **1997**, *101*, 9396-9401. Starodubtsev, S. G.; Yoshikawa, K. *Langmuir* **1998**, *14*, 214-217. Sergeev, V.; Mikhailenko, S.; Pyshkina, O.; Vaminsky, I.; Yoshikawa, K. *J. Am. Chem. Soc.* **1999**, *121*, 1780-1785. Iwataki, T.; Yoshikawa, K.; Kidoaki, S.; Umeno, D.; Kiji, M.; Maeda, M. *J. Am. Chem. Soc.* **2000**, *122*, 9891-9896.
[85] Sheiko, S. S.; Prokhorova, S. A.; Beers, K. L.; Matyjaszewski, K.; Potemkin, I. I.; Khokhlov, A. R.; Möller, M. *Macromolecules* **2001**, *34*, 8354-8360.
[86] Yoshikawa, Y.; Yoshikawa, K.; Kanbe, T. *Langmuir* **1999,** *15,* 4085-4088. Ono, M. Y.; Spain, M. *J. Am. Chem. Soc.* **1997**, *121*, 7330-7334.
[87] Yoshikawa, K.; Yoshikawa, Y.; Koyama, Y.; Kanbe, T. *J. Am. Chem. Soc.* **1997**, *119*, 6473-6477. Starodubtsev, S. G.; Yoshikawa, K. *J. Phys. Chem*. **1996**, *100*, 19702-19705.
[88] Hill, D. J.; Mio, M. J.; Prince, R. B.; Hughes, T. S.; Moore, J. S. *Chem. Rev.* **2001,** *101,* 3893-4011.
[89] Grosberg, A. Yu.; Khokhlov, A. R. *Statistical physics of macromolecules*. AIP Press, New York, 1994.
[90] Khokhlov, A. R. *J. Phys. A* **1980**, *13*, 979-987.
[91] (a) Kantor, Y.; Kardar, M. *Phys. Rev. E.* **1995**, *51*, 1299. (b) Dobrynin, A. V.; Rubinstein, M.; Obukhov, S. P. *Macromolecules* **1996**, *29*, 2974-2979. (c) Dobrynin, A. V.; Rubinstein, M. *Macromolecules* **1999**, 32, 915-922. (d) Dobrynin, A. V.; Rubinstein, M. *Macromolecules* **2001**, *34*, 1964-1972. (e) Dobrynin, A. V.; Rubinstein, M. *Macromolecules* **2002**, *35*, 2754-2768. (f) Solis, F. J.; de la Cruz, M. O. *Macromolecules* **1998**, *31*, 5502-5506. (g) Lyulin, A. V.; Dünweg, B.; Borisov, O. V.; Darinskii, A. A. *Macromolecules* **1999**, *32*, 3264-3278. (h) Mica, U.; Holm, C.; Kremer, K. *Langmuir* **1999**, *15*, 4033-4044.

[92] Aseyev, V. O.; Klenin, S.; Tenhu, H.; Grillo, I.; Geissler, E. *Macromolecules* **2001**, *34*, 3706-3709. Wang, X.; Qiu, X.; Wu, C. *Macromolecules* **1998**, *31*, 2972-2976. Lee, M.-J.; Green, M. M.; Morawetz, H. *Macromolecules* **2002**, *35*, 4216-4217.
[93] Zimmermann, A., Jaeger, W., Reichert, K.-H. *Polymer News* **1997**, 390-392. Jaeger, W.; Paulke, B.-R.; Zimmermann, A.; Lieske, A.; Wendler, U.; Bohrisch, J. *Polymer Prepr.* **1999**, *40*, 980-981.
[94] Jacobash, H-J.; Simon, F.; Werner, C., Belmann, C. *Tech. Messen* **1966**, *63*, 447.

[95] (a) Förster, S.; Schmidt, M.; Antonietti, M. *J. Phys. Chem* **1992**, *96*, 4008. (b) Beer, M.; Schmidt, M.; Muthukumar, M. *Macromolecules* **1997**, *30*, 8375-8385.

[96] Pefferkorn, E.; Elaissari, A. *J. Colloid Interface Sci.* **1990,** *138,* 187.
[97] Schiessel, H.; Pincus, P. *Macromolecxules* **1998**, *31*, 7953-7959.
[98] Franz, P.; Granick, S. *Phys. Rev. Lett.* **1991**, *66*, 899.
[99] Pefferekorn, E.; Carroy, R.; Varoqui, R. *J. Polym. Sci. Polym. Phys. Ed.* **1985**, *23*, 1997. Pefferkorn, E.; Haouam, A.; Varoqui, R. *Macromolecules* **1989**, *22*, 2667. Johnson, H. E.; Granick, S. *Macromolecules* **1990**, *23,* 3367. Johnson, H. E.; Granick, S. *Science* **1992**, *255*, 966.
[100] Voronov, A., Pefferkorn, E., Minko, S. *Macromol. Rapid. Commun*., 1999, **20**, 85-87. Minko, S., Voronov, A., Pefferkorn, E. *Langmuir*, **2000**, *16*, 7876-7878.
[101] Sheiko, S. S.; Möller, M. *Chem. Rev*. **2001**, *101*, 4099-4123.
[102] Rivetti, C.; Guthold, M.; Bustamante, C. *J. Mol. Biol.* **1996**, *264*, 919.
[103] Fredericks, J. R.; Hamilton, A. D. *Comprehensive Supramolecular Chemistry*; Lehn, J.-M., Ed.; Pergamon: New York, 1996; Chapter 16.
[104] Lehn, J.-M. In *Supramolecular Polymers*; Ciferri, A., Ed.; Marcel Dekker: New York, 2000. Brunsveld, L.; Folmer, B. J. B.; Meijer, E. W.; Sijbesma, R. P. *Chem. Rev.* **2001**, *101*, 4071-4097.
[105] Niemeyer, C. M. *Angev. Chem. Int. Ed. Engl.* **2001,** *40*, 4128; Mirkin, C. A. *Inorg. Chem.* **2000**, *39,* 2258; Storhoff, J. J., Mirkin, C. A. *Chem. Rev.* **1999**, *99,* 1849.
[106] Ball, P. *Nature* **2000**, *406,* 118.
[107] Heath, J. R.; Kuekes, P. J.; Snider, G. S.; Williams, R. S. *Science* **1998**, *280*, 1716-1721.
[108] Collier, C. P.; Wong, E. W.; Belohradský, M.; Raymo, F. M.; Stoddart, J. F.; Kuekes, P. J.; Williams, R. S.; Heath, J. R. *Science* **1999**, *285*, 391-394.
[109] Huang, M. H.; Mao, S.; Feick, H.; Yan, H.; Wu, Y.; Kind, H.; Weber, E.; Russo, R.; Yang, P. *Science* **2001**, *292*, 1897-1899.
[110] Liang, W.; Yokojima, S.;. Ng, M; Chen, G.; He, G. *J. Am. Chem. Soc*. **2001**, *123*, 9830-9836.
[111] Cao, H.; Xu, Z.; Sang,H.; Sheng, D.; Tie, C. *Adv. Mater*. **2001**, *13*, 121-123.
[112] Andres, R. P.; Bielefeld, J. D.; Henderson, J. I.; Janes, D. B.; Kolagunta, V. R.; Kubiak, C. P.; Mahoney, W. J.; Osifchin, R. G. *Science* **1996**, *273*, 1690-1693.
[113] Zhang, D.; Qi, L.; ma, J.; Cheng, H *Chem. Mater.* **2001,** *13,* 2753. Song, J.H.; Wu, Y.; Messer, B.; Kind, H.; Yang, P. *J. Am. Chem. Soc.* **2001,** *123,* 10397. Han, Y.J.; Kim, J.M.; Stucky G.D. *Chem. Mater*. **2000**, *12*, 2068. Thurn-Albrecht, T.; Schotter, J.; Kästle, G.A.; Emley, N.; Shibauchi, T.; Krusin-Elbaum, L.; Guarini, K.; Black, C.T.; Tuominen, M.T.; Russell, T.P. *Science,* **2000,** *290,* 2126. Fukuoka, A.; Sakamoto, Y.; Guan, S.; Inagaki, S.; Sugimoto, N.; Fukushima, Y.; Hirahara, K.; Iijima, S.; Ichikawa, M. *J. Am. Chem. Soc.* **2001,** *123,* 3373.
[114] Zach, M. P.; Ng, K. H.; Penner, R. M. *Science* **2000**, *290*, 2120
[115] Morales, M.; Lieber, C. M. *Science* **1998**, *279*, 208.
[116] Zhang, D.; Qi, L.; Ma, J.; Cheng, H. *Chem. Mater.* **2001**, *13*, 2753.
[117] Govindaraj, A.; Satishkumar, B. C.; Nath, M.; Rao, N. R. *Chem. Mater*. **2000**, *12*, 202.

[118] Jana, N. R.; Gearheart, L.; Murphy, C. J. *Chem. Commun.* **2001**, *7*, 617.
[119] Mössmer, S.; Spatz, J.; Möller, M.; Aberle, T.; Schmidt, J.; Burchard, W. *Macromolecules* **2000**, *33*, 4791.
[120] Tsutsumi, S.; Funaki, Y.; Hirokawa, Y.; Hashimoto, T. *Langmuir* **1999**, *15*, 5200.
[121] Quarke, S. R. ; Scherer, A. *Science* **2000**, *290*, 1536.
[122] Borochov, N.; Eisenberg, H.; Kam, Z. *Biopolymers* **1981**, *20*, 231.
[123] Braun, E.; Eichen, Y.; Sivan, U.; Ben-Yoseph, G. *Nature* **1998**, *391*, 775.
[124] Richter, J.; Seidel, R.; Kirsch, R.; Mertig, M.; Pompe, W.; Plaschke, J.; Schackert, H. K. *Adv. Mater.* **2000**, *12*, 507-510.
[125] Ford, W. E.; Harnack, O.; Yasuda, A.; Wessels, J. M. *Adv. Mater.* **2001**, *13*, 1793-1797.
[126] Liu, J.; Cheng, L.; Song, V.; Dong, S. *Langmuir* **2001**, *17*, 6747-6750.
[127] Hadjichristidis, N.; Pispas, S.; Pitsikalis, M.; Iatrou, H.; Vlahos, C. *Adv. Polym. Sci.* **1999**, *142*, 71. Hadjichristidis, N.; Pitsikalis, M.; Pispas, S.; Iatrou H. *Chem. Rev*. **2001**, *101*, 3747-3792.
[128] Tsitsilianis, C.; Chaumont, P.; Rempp, P.; *Makromol. Chem.* **1990**, *191*, 2319.
[129] Liu, S.; Armes S. P. *Angew. Chem.* **2002**, 114, 1413-1416.
[130] (a) Werts, M.P.L.; Van der Vegte, E.W.; Grayer, V.; Esselink, E.; Tsitsilianis, C.; Hadziioannou, G. *Adv. Mater.* **1998**, *10(6)*, 452. (b) Grayer, V.; Dormidontova, E.; Hadziioannou, G.; Tsitsilianis, C. *Macromolecules* **2000,** *33,* 6330.
[131] (a) Voulgaris, D.; Tsitsilianis, C.; Esselink, F.; Hadziioannou, G. *Polymer* **1998**, *39*, 6429. (b) Voulgaris, D.; Tsitsilianis, C.; Grayer, V.; Esselink, F.; Hadziioannou,; G. *Polymer* **1999**, 40, 5879. (c) Tsitsilianis, C.; Voulgaris, D.;M. Štěpánek, Podhájecká , K.; Procházka, K.; Tuzar, Z.; Brown, W. *Langmuir* **2000,** *16,* 6868.
[132] Tsitsilianis, C.; Voulgaris D. *Macromol. Chem. Phys.* **1997**, *198*, 997.
[133] (a) Tsitsilianis**,** C.; Staikos, G.; Dondos, A.; Lutz, P.; Rempp, P.; Benoit H. *Makromol.Chem.* **191,** 2309-2318, (1990). (b) Dondos, A.; Papanagopoulos, D. *J Polym. Sci. Polym.Phys.Ed.* **1996**, *34*, 1281. (c) Tsitsilianis**,** C.; Kouli, O. *Macromol. Rapid Commun.* **1995**, *16*, 591.
[134] Minko, S.; Müller, M.; Usov, D.; Scholl, A.; Froeck, C.; Stamm, M. *Phys. Rev. Lett.* **2002**, *88*, 0355502.
[135] Brandrup, J., Immergut, E.A., Grulke, E.A. *Polymer Handbook*, 4th Edition, Wiley-Interscience, New York, 1999.
[136] Shull, K.R., Kramer, E.J., Hadziioannou, G., Tang, W. *Macromolecules* 1990, *23*, 4780-4787.
[137] Wolterink, J.; Leermakers, F.; Fleer, G.; Koopal, L.; Zhulina, E.; Borisov, O. *Macromolecules* **1999**, *32,* 2365-2377.
[138] Grayer, V.; Esselink, F.; J.; Hadziioannou, G.; Tsitsilianis, C.; 4th Panhellinio Conference on Polymers, Proceedings **1997**, p267.
[139] Tsitsilianis, C.; Voulgaris, D. *Polymer* **2000**, *41,* 1607.
[140] Magonov, S. N.; Reneker, D. H. *Annu. Rev. Mater. Sci*. **1997**, *27*, 175; Tsukruk, V. V.; Reneker, D. H. *Polymer* **1995**, *36*, 1791.
[141] L. Shu, A.D. Schlüter, C. Ecker, N. Severin, J.P. Rabe, *Angew. Chem.* **2001**, 113, 4802.
[142] Djalali, R.; Li, S.-Y.; Schmidt M. *Macromolecules* **2002,** *35,* 4282.
[143] Hansma, H. G.; Vesenka, J.; Siegerist, C.; Kelderman, G.; Morrett, H.; Sinsheimer, R. L.; Elings, V.; Bustamante, C.; Hansma, P. K. *Science* **1992**, *256*, 1180; S. Gao, L. Chi, S. Lenhert, B. Anczhykowski, C.M. Niemeyer, M. Adler, H. Fuchs, *ChemPhysChem* **2001**, *6*, 384.
[144] Kumaki, J.; Hashimoto. T. *J. Am. Chem. Soc.* **2003**, *125*, 4907.
[145] Frisbie, C. D.; Rozsnyai, L. F.; Noy, A.; Wrighton, M. S.; Lieber, C. M. *Science* **1994**, *265*, 2071.

[146] Zhu, M.; Akari, S.; Möhwald, H. *Nano Letters*, **2001**, *1*, 569.
[147] Keggin, J. F.; Miles, F. D. *Nature (London)* **1936**, *137*, 577.
[148] Vaucher, S.; Li, M.; Mann, S. *Angew. Chem.* **2000**, *112*, 1863. Catala, L.; Gacoin, J.-P. B.; Rivere, E.; Paulsen, C.; Lhotel, E.; Mallah, T. *Adv. Mater.* **2003**, *15*, 826. Uemura T.; Kitagawa S. *J. Am. Chem. Soc.* **2003**, *125,* 7814.
[149] Robin, M. B. *Inorg. Chem.* **1962**, *1*, 337.

Acknowledgment

The realization of the work presented in this thesis was possible thanks to the invaluable contribution and support of a significant amount of people.

First of all I would like to thank Prof. Dr. Manfred Stamm for being my “Doktorvater”. I thank him for the opportunity he gave me to make my Ph.D. work in Dresden and for useful discussions.

I would like to say big thanks to Prof. Dr. Sergij Minko for being a critical guide and for his support.

I’m really grateful to Dr. Anton Kiriy for his readiness to help, for his great contribution to planning and realization of the experiments, elucidative discussions, the help in understanding and interpretation of the results, and proof-reading of this work.

I would like to express my gratitude to everybody supporting me during my Ph.D. and in particular to:

Andres Janke, Nicole Petong, Dr. Alexander Sydorenko and Dr. Christian Froek for help and sharing their experience concerning the AFM measurements;

Dr. Frank Simon and Dieter Pleul for X-ray Photoelectron Spectroscopy (XPS) measurements;

Dr. Cornelia Bellmann for advice and help in ζ-potential measurements;

Dr. Volodymyr Senkovskyy for the help in computer-related problems.

I would like to acknowledge Dr. Petr Štěpánek and Dr. Zdeněk Tuzar, (Institute of Macromolecular Chemistry, Prague) for their warm hospitality during my stay in Prague and for the work performed with the Dynamic Light Scattering measurements and assistance in data evaluation.

I would like to thank Dr. Werner Jaeger (Fraunhofer-Institut für Angewandte Polymerforschung, Golm) for providing the samples of poly(methacryloyloxyethyl dimethylbenzylammonium chlorid) (PMB).

I am grateful to Prof. Dr. Constantinos Tsitsilianis and members of his group at University of Patras, Greece for collaboration and providing of PS_7-PVP_7 star-like block copolymers.

A particular thanks goes to all the present and past colleagues Vera Bocharova, Dr. Denis Usov, Nikolay Houbenov, Igor Tokarev, Michael Motornov, Leonid Ionov, Alla Synytska, Pylyp Volodin, Radim Krenek, Nataliya Kiriy, Marco Amici, Amir Fahmi, Giso Pfütze, Dr. Valery Luchnikov, Vyacheslav Gruzdev, Nataliya Khanduyeva, Pagra Truman, Magda Goncalves-Miskiewiscz for helping me with the everyday problems in the lab and for extremely pleasant and stimulating environment between not just colleagues but friends. We spend a really nice time together during which I have been learning more than only science.

I thank Dr. Jurgen Piontek and all co-workers of the IPF for their friendliness that make sometimes the life of a foreigner more joyous.

Last but not least I want to thank my parents, my sister Lena and my friends in Kiev for always being there for me.

I am grateful to DFG and EGK “Advanced polymeric materials” for financial support.

PUBLICATIONS

1. Gorodyska G., Kiriy A., Minko S., Stamm M. Metallic Nanoparticles from Single Polyelectrolyte Molecules. Organic/Inorganic Hybrid Materials Q6.33 Editors: R.M. Laine, C. Sanchez, S. Yang, C.J. Brinker *MRS Proceedings*, V. 726, 187-192, **2002**.

2. Minko, S.; Kiriy, A.; Gorodyska, G.; Stamm, M.; Single Flexible Hydrophobic Polyelectrolyte Molecules Adsorbed on Solid Substrate: Transition between a Stretched Chain, Necklace-like Conformation and a Globule J. Am. Chem. Soc.; 2002; 124(13); 3218-3219.

3. Minko, S., Gorodyska G., Kiriy, A.; W. Jaeger G., Stamm, M. Visualization of Single Polyelectrolyte Molecules. *Polym. Mater. Sci. Eng*, **2002**, *87*, 185-186.

4. Kiriy, A.; Minko, S.; Gorodyska, G.; Stamm, M.; Jaeger, W.; Palladium Wire-Shaped Nanoparticles from Single Synthetic Polycation Molecules Nano Lett.; 2002; 2(8); 881-885.

5. Minko, S.; Kiriy, A.; Gorodyska, G.; Stamm, M.; Mineralization of Single Flexible Polyelectrolyte Molecules J. Am. Chem. Soc.; 2002; 124(34); 10192-10197.

6. Kiriy, A.; Gorodyska, G.; Minko, S.; Jaeger, W.; Stepanek, P.; Stamm, M.; Cascade of Coil-Globule Conformational Transitions of Single Flexible Polyelectrolyte Molecules in Poor Solvent J. Am. Chem. Soc.; 2002; 124(45); 13454-13462.
   The paper have been highlighted as the "Editor's Choice" in 8/10/02 issue of *Science* (Washington): **2002**, *298*, 1139.

7. Gorodyska, G.; Kiriy, A.; Minko, S.; Tsitsilianis, C.; Stamm, M. Reconformation and Metallization of Unimolecular Micelles in Controlled Environment. *Nano Letters*, **2003**, 3(3), 365-368.

8. Kiriy, N.; Jähne, E.; Adler H.-J.; Schneider, M.; Kiriy, A.; Gorodyska, G.; Minko, S.; Jehnichen, D.; Simon, P.; Fokin, A. A.; Stamm, M. One-dimensional aggregation of regioregular polyalkylthiophenes. *Nano Letters* **2003**, *3*, 707-712.

9. Kiriy, A.; Gorodyska, G.; Minko, S.; Tsitsilianis, C.; Stamm, M. Atomic force microscopy visualization of single star copolymer molecules. *Polym. Mater. Sci. Eng* **2003**, *88*, 233-234.

10. Kiriy, A.; Gorodyska, G.; Minko, S.; Tsitsilianis, C.; Jaeger, W., Stamm, M. Chemical Contrasting in a Single Polymer Molecule AFM Experiment. *J. Am. Chem. Soc.* **2003**, *125*, 11202 – 11203.

11. Kiriy, A.; Gorodyska, G.; Minko, S.; Tsitsilianis, C.; Stamm, M. Single Molecules and Associates of Heteroarm Star Copolymer Visualised by Atomic Force Microscopy. *Macromolecules* **2003,** *36,* 8704-8711.

12. Tsitsilianis, C.; Bossard, F.; Sfika, V.; Stavrouli, N.; Kiriy, A.; Gorodyska, G.; Stamm, M.; Minko, S.; Multifunctional Double Hydrophilic Triblock Copolymer in Solution and on Surface. *Polym. Mater. Sci. Eng*. **2004**, *90*, 368-369.

13. Kiriy, A.; Bocharova, V.; Gorodyska, G.; Minko, S.; Stamm, M. Assembling of Prussian Blue Nanoclusters Along Single Polyelectrolyte Molecules. *Polym. Mater. Sci. Eng*. **2004**, *90*, 593-594.Kiriy, A.; Gorodyska, G.; Minko, S.; Stamm, M. Cyanide-Bridged Compounds As Contrasting Agents For Afm Imaging Of Single Polycation Molecules. *Polym. Preprint*. **2004**, *45*, 486-487.

15. Minko, S.; Kiriy, A.; Gorodyska, G.; Lupitskyy, R.; Tsitsilianis, C.; Stamm, M. Conformational transitions visualized in single polyelectrolyte molecule afm experiments. *Polym. Preprint*. **2004**, *45*(2), 258.

16. Kiriy, A.; Gorodyska, G.; Sheparovych, R.; Lupytsky, R.; Minko, S.; Kiriy, N.; Stamm, M. Cyanide-Bridged Compounds as Contrasting Agents for AFM Imaging of Single Polycation Molecules. *Macromolecules.* Accepted**.**

17. Sfika, V.; Tsitsilianis, C.; Kiriy, A.; Gorodyska, G.; and Stamm M. pH-Responsive heteroarm star-like micelles from double hydrophilic ABC terpolymer with ampholitic A and C blocks. *Macromolecule,* ASAP.

18. Bocharova, V.; Simon, P.; Gorodyska, G.; Kiriy, A.; Stamm, M; Lou, X; Stoffelbach, F.; Detrembleur, C.; Jérôme, R. Negatively Charged Water Soluble Prussian Blue Nanocrystals and Carbon Nanotube-Polyelectrolyte-Prussian Blue Heterostructures. *Nanoletters*, submitted.

CONFERENCES

March 11-15, 2002 *DPG - Frühjahrstagung (Spring Conference of German Physical Society)*, Regensburg, Germany
poster "Nanowires from Single Synthetic Polyelectrolyte Molecules via Metallization",
Gorodyska, G.; Kiriy, A.; Minko, S.; Stamm M.

March 20-21, 2002 *8th Veeco Usermeeting,* Saarbrücken, Germany
oral presentation "Visualization of Single Synthetic Polyelectrolyte Molecules"
Gorodyska, G.; Kiriy, A.; Minko, S.; Stamm M.

May 5-8, 2002 *11 Rolduc Polymer Meeting*, *Crossing Length-Scales and Disciplines from Macromolecular Structures to Functional Polymeric Systems*, Kerkrade, Holland.
poster "Direct visualization of the transition between stretched chain and globule conformations of single flexible hydrophobic polyelectrolyte molecules".
Gorodyska, G.; Kiriy, A.; Minko, S.; Stamm M.

Nov. 14 - 15, 2002 *5th IPF Colloquium "Theory and Experiment"* , Dresden, Germany
2 posters "Metallic nanoparticles from single polyelectrolyte molecules" andSingle polyelectrolyte molecules: transition between wormlike, necklace and globular conformations".
Gorodyska, G.; Minko, S.; Kiriy, A.; Stamm M.

Febr. 15 – 20, 2003 *Discussion Meeting on "Multi-Level Ordering - Molecular Organization for Nanosystems"* Kloster Banz, Germany
poster "Bloomed unimolecular stimuli-responsive micelles from star-shaped block copolymer"
Gorodyska, G.; Kiriy, A.; Minko, S.; Tsitsilianis, C.; and Stamm M.

March 16-19,.2003 *9th Dresden Polymer Discussion: POLYELECTROLYTES*, , Meißen, Germany
poster "Cascade Of Coil-Globule Conformational Transitions Of Single Flexible Polyelectrolyte Molecules In Poor Solvent"
Gorodyska, G.; Kiriy, A.; Minko, S.; Stamm M.

March 24-28,.2003 *DPG - Frühjahrstagung*, Dresden, Germany
poster “Conformational transitions of single polyelectrolyte molecules”
Gorodyska, G.; Kiriy, A.; Minko, S.; Tsitsilianis, C.; and Stamm M.

June 3, 2003 International Seminar About Polymers, Gliwice, Poland
poster "Metallic nanoparticles from single polyelectrolyte molecules″
Gorodyska, G.; Kiriy, A.; Minko, S.; Tsitsilianis, C.; and Stamm M.

Oct 6-8, 2003 9^{th} *Veeco Usermeeting,* Potsdam, Germany
talk “Chemical Contrasting in Single Polymer Molecule AFM Experiment”
Gorodyska, G.; Kiriy, A.; Minko, S.; and Stamm M.

Lebenslauf

Ganna Gorodyska	7.03.1977 in Kiew, Ukraine ledig
Schulausbildung	
09/1984 – 06/1994	Schule – Gymnasium № 143 in Kiew mit Auszeichnung (Goldmedaille)
Hochschulausbildung/ Promotion	
09/1994 – 06/2000	National Technische Universität der Ukraine “Kiewer Polytechnische Hochschule” Fach: Biomedizinische Elektronik Diplom des Magisters mit Auszeichnung
seit 02/2001	Promotion an dem Leibniz-Indtitut für Polymerforshung Dresden Arbeitsgruppe Herr Prof. Stamm

Versicherung

Hiermit versichere ich, dass ich die vorliegende Arbeit ohne unzulässige Hilfe Dritter und ohne Benutzung anderer als der angegebenen Hilfsmittel angefertigt habe; die aus fremden Quellen direkt oder indirekt übernommenen Gedanken sind als solche kenntlich gemacht. Die Arbeit wurde bisher weder im Inland noch im Ausland in gleicher oder ähnlicher Form einer anderen Prüfungsbehörde vorgelegt.

Die vorliegende Arbeit wurde unter der wissenschaftlichen Betreuung von Prof. Dr. M. Stamm an dem Leibniz-Institut für Polymerforschung Dresden angefertigt.

Keine frühere erfolglose Promotionsverfahren stattgefunden haben.

Die Promotionsordnung der Technischen Universität Dresden der Fakultät Mathematik und Naturwissenschaft vom 16.04.2003 erkenne ich an.

Ganna Gorodyska